

Nicola Sophie Caroline Altenhuber, BSc

Multi Layer Optical Sensor Systems Prepared by Microdispensing Technology

MASTER'S THESIS

to achieve the university degree of

Diplom-Ingenieurin (Dipl.-Ing.)

Master's degree programme: Technical Chemistry

submitted to

Graz University of Technology

Supervisor

Torsten Mayr, Assoc.Prof. Dipl.-Chem. Dr.rer.nat.

Institute of Analytical Chemistry and Food Chemistry

Graz, May, 2017

“There are a whole lot of things in this world of ours you haven’t started wondering about yet.”
Roald Dahl, *James and the Giant Peach*

Abstract

The goal of this thesis was to develop, prepare and evaluate optical glucose sensors using microdispensing technology. Working principle of the sensors is the consumption of oxygen through the enzymatic conversion of glucose and oxygen to gluconolactone.

The sensors consist of three different layers. The inner layer is an oxygen sensor spot. The oxygen sensor spot measures the consumption of oxygen in presence of glucose. The middle layer is an enzyme glucose oxidase layer, where oxygen is used in the conversion of glucose. The outer layer is a diffusion layer composed of a Hydrogel. Through this layer oxygen can pass unhindered but the diffusion of glucose takes place at a controlled rate. With this layer, it is possible to run the reaction diffusion limited and not dependent on the enzyme activity. The diffusion layer consists of polyHEMA or ethylcellulose.

The layers were printed on support slides using a microdispenser which works with a piezoelectrically controlled tappet which presses fluid droplets through a nozzle.

Profiles of all sensors were established by measuring with a profilometer. The prepared sensors had a diameter of about 3 mm and were up to 50 μm thick. The sensor slides were integrated in two kinds of microfluidic chips. The first one had a volume of 250 μL and the second one had a volume of 120 μL . Both chips had a rhombic chamber design.

The changes in the phosphorescence lifetime of the sensors were measured by flushing the chips with different glucose buffer solutions.

Improving the different layers of the sensors was one of the main tasks. By printing with different methods and on different support slides surface inhomogeneities, like the coffee ring effect, were minimised. The sensors showed good adherence on all tested slides, such as glass, silanised glass, PS, plasma etched PS, PMMA, plasma etched PMMA, Topas, plasma etched Topas, PC and plasma etched PC.

The dynamic range was tuned by varying the thickness of the diffusion layer. Sensors with a thin polyHEMA diffusion barrier layer had dynamic ranges of 0 to 1 mM glucose. Sensors with a thick polyHEMA diffusion layer showed a change in the phase angle up to a glucose concentration of 12.5 mM glucose. Sensors with polyHEMA as diffusion barrier layer were reproducible regarding the sensor production. However, after 10 days the measured signal changed. Using a different diffusion barrier material, for example ethylcellulose, is also possible, but prepared sensors turned out to be non-reproducible. Furthermore, the influence of different flow velocities on the dynamic range of the sensors was investigated and also steady state measurements were possible.

Kurzfassung

Das Ziel dieser Arbeit war es, optische Sensoren mittels eines Mikrodosiergerätes zu entwickeln, herzustellen und zu evaluieren. Das Arbeitsprinzip der Sensoren ist die Messung des Sauerstoffverbrauchs aufgrund enzymatischer Umsetzung von Glucose und Sauerstoff zu Gluconolaktone. Die Sensoren sind aus drei verschiedenen Schichten zusammengesetzt. Die unterste Schicht ist ein Sauerstoff-Sensor-Spot bestehend aus einem Porphyrin Farbstoff in PS. Die Lumineszenz-Lebenszeit eines Fluorophor wird in Anwesenheit von Sauerstoff gelöscht. Die mittlere Schicht ist eine Glukose Oxidase Enzymschicht, in der Glukose mit Sauerstoff reagiert und in der Sauerstoff verbraucht wird. Die äußerste Schicht ist eine Diffusionsschicht. Durch diese Schicht passiert Sauerstoff ungehindert, jedoch Glukose wird diffusionsgehindert. Dadurch ist es möglich, die Reaktionsgeschwindigkeit von der Diffusion und nicht von der Enzymaktivität abhängig zu machen. PolyHEMA und Ethlycellulose fungierten als Diffusionsbarriere.

Die einzelnen Schichten wurden auf Platten mittels Mikrodosiergeräts aufgetragen. Bei dem Mikrodosiergerät wird ein piezoelektrischer Stößel so gesteuert, dass er Flüssigkeitstropfen durch eine Düse presst. Profile aller Sensoren wurden unter Verwendung eines Profilometers gemessen. Die hergestellten Sensoren hatten einen Durchmesser von etwa 3 mm und waren bis zu 50 μm hoch. Die Sensoren wurden in einen mikrofluidischen Chip integriert. Zwei verschiedene Arten von Chips wurden verwendet. Der erste hatte ein Volumen von 250 μL and der zweite ein Volumen von 120 μL . Beide Chips bestanden aus rhombischen Kammern.

Änderung in der Phosphoreszenzlebenszeit der Sensoren wurde gemessen, indem die Chips mit verschiedenen gepufferten Glucoselösungen gespült wurden. Die Verbesserung der verschiedenen Schichten war eine der Hauptaufgaben. Durch unterschiedliche Druckmethoden auf verschiedenen Materialien wurde der Kaffeering-Effekt, der sich durch eine inhomogene Oberfläche zeigt, verringert. Die Sensoren hafteten gut auf den getesteten Materialien: Glas, silanisiertes Glas, PS, plasmageätztes PS, PMMA, plasmageätztes PMMA, Topas, plasmageätztes Topas, PC und plasmageätztes PC. Der dynamische Bereich wurde eingestellt, indem die Dicke der Diffusionsschicht variiert wurde. Sensoren, die polyHEMA als Diffusionsschicht hatten, und solche mit einer geringen Anzahl an Diffusionsschichten übereinander hatten einen dynamischen Bereich von 0 bis 1 mM Glukose. Eine Veränderung im Phasenwinkel konnte bei Sensoren mit mehreren Diffusionsschichten bis zu 12 mM Glukose beobachtet werden. Sensoren mit polyHEMA als Diffusionsschichten waren in der Produktion reproduzierbar, sie wurden sie nach 10 Tagen wieder vermessen, jedoch änderte sich das Signal. Die Verwendung verschiedener Diffusionsschichten, zum Beispiel Ethylcellulose, ist auch möglich, aber die produzierten Sensoren waren nicht reproduzierbar. Die Abhängigkeit von der Fließgeschwindigkeit wurde bewiesen und Messungen in stehender Flüssigkeit waren möglich.

EIDESSTATTLICHE ERKLÄRUNG

Ich erkläre an Eides statt, dass ich die vorliegende Arbeit selbstständig verfasst, andere als die angegebenen Quellen/Hilfsmittel nicht benutzt, und die den benutzten Quellen wörtlich und inhaltlich entnommenen Stellen als solche kenntlich gemacht habe. Das in TUGRAZonline hochgeladene Textdokument ist mit der vorliegenden Masterarbeit identisch.

AFFIDAVIT

I declare that I have authored this thesis independently, that I have not used other than the declared sources/resources, and that I have explicitly indicated all material which has been quoted either literally or by content from the sources used. The text document uploaded to TUGRAZonline is identical to the present master's thesis.

Datum/Date

Unterschrift/Signature

Danksagung

Lange habe ich nicht gewusst, wie ich diese Danksagung verfassen sollte. Meine Mama fing schon an, Anekdoten aus meiner Kindheit zu erzählen, wie ich als kleines Kind alleine durch die Küche turnte und mir selbst das Frühstück richtete, meine Kochversuche, die meistens funktionierten und bei denen ich nicht wie mein Papa die Zimmerdecke mit Rotwein neu färbte. Vergessen hat sie dabei wohl, dass ich vor dem Frühstück auch hin und wieder den supertollsten Legoturm, der vom Boden bis zur Zimmerdecke reichte, gebaut habe! All das hat mich wohl irgendwie dazu gebracht, Chemie zu studieren.

An dieser Stelle würde ich gerne allen Menschen danken, die mich bei meiner Masterarbeit und vor allem auf meinem Weg dorthin begleitet haben.

Als Erstes möchte ich meiner Mama und meinem Papa danken, nicht nur für die finanzielle Unterstützung, sondern auch dass sie mir immer jeden meiner Wünsche erfüllt haben und mir immer tatkräftig bei Seite gestanden sind, sei es bei meinem Australien-Aufenthalt, meinem Erasmus-Semester in Finnland, meinem Chemiestudium oder dem Korrekturlesen mancher Arbeit. Natürlich danke ich auch Cathi, Jan und Müsli, obwohl sie mich nicht in ihrer Danksagung erwähnten und ich ewig beleidigt sein werde, für die schöne Zeit neben dem Studium, dem Frühstück, dem Abendessen, den Spieleabenden, den Spritzersonntagen und dem gemeinsamen Frisbeebringen!

Ich möchte mich auch bei meinen besten Freunden in Graz und auf der ganzen Welt für die gemeinsame Zeit, die ich mit euch verbringen darf, bedanken. Es war immer ein Vergnügen mit euch spontan auf ein Bier ins Sägewerk zu gehen, einen Filmabend zu machen, abendlang zu ratschen oder Lasertag zu spielen. Unvergesslich sind da natürlich auch unsere gemeinsamen Trips nach München, Kreta, Barcelona und Prag, dabei darf man unsere neuen Freunde Louis, Gianni und die Taube nicht vergessen.

Ein riesengroßes Dankeschön geht auch an Fips, der wohl der beste Masterarbeitsbetreuer überhaupt ist. Ich konnte mit jeglichen Fragen und Problemen zu ihm kommen, wie dumm die Fragen auch teilweise waren. Außerdem hat er nie geschimpft wenn ich etwas kaputt gemacht habe oder etwas spontan einfach so, ziemlich grundlos, zu rauchen anfang.

Ich möchte mich auch bei Torsten bedanken, der mir diese Arbeit ermöglicht hat, der mir wertvollen Input gab, mich bei jedem aufkommenden Problem unterstützte, Anregungen zu weiteren Versuchen gab, interessante Varianten aufzeigte und Resultate objektiv diskutierte.

Danke auch an das supertolle Institut, in dem ich die letzten Monate verbringen durfte. Ihr habt mir immer weitergeholfen und es war ein Spaß mit euch Zeit zu verbringen, nicht nur bei

der Arbeit, sondern auch bei verschiedenen Aktivitäten.

Zu guter Letzt möchte ich auch Dominik danken, der mich in den letzten Jahren auf meinem Weg begleitet hat. Danke, dass du die letzten Jahre mit mir verbracht hast, mich stundenlang abgeprüft hast, immer für mich da warst, manchmal das Mädchen warst (vor allem beim Werwolfspielen) und alle meine Launen meistens toleriert hast.

Nicola Sophie Caroline Altenhuber, BSc

Graz, May, 2017

Contents

1	Introduction	1
2	Theoretical Background	2
2.1	Printing Techniques	2
2.1.1	Knife Coating	2
2.1.2	Screen Printing	3
2.1.3	Spraying	4
2.1.4	Spin Coating	4
2.1.5	Inkjet Printing	5
2.1.6	Aerosol Jet Printing	8
2.1.7	Microdispenser	8
2.1.8	Microcontact Printing	10
2.1.9	Probe-Based Techniques	11
2.2	Optical Sensors	13
2.2.1	Luminescence in General	13
2.2.2	Luminescence Lifetime and Quenching	15
2.2.3	Luminescence Measurement Techniques	17
2.3	Glucose Sensors	18
2.3.1	Electrochemical Glucose Sensors	19
2.3.2	Optical Glucose Sensors	21
2.3.3	Glucose Sensors Using Synthetic Boronic Acids	22
2.3.4	Glucose Sensors Using Glucose-Binding Proteins	23
2.4	Glucose	23
2.5	Enzymes	24
3	Materials and Methods	25
3.1	Devices	25
3.2	Chemicals	26
3.3	Polymer Slides	27
4	Experimental	29
4.1	Preparation of the Sensor Cocktails	29
4.1.1	Oxygen Sensor Cocktail	29
4.1.2	Glucose Oxidase Enzyme Layer Cocktail	29

4.1.3	Diffusion Barrier Cocktails	30
4.2	Profilometer Measurements	30
4.3	Assembling the Sensor Chips	31
4.4	Glucose Buffer	33
4.5	Primary Sensors	33
4.5.1	The Microdispenser Spraying Add-On	34
4.5.2	Influence of the Substrate Materials and Properties of the Morphology of the Enzyme Layers	35
4.6	Final Sensors	35
4.7	Sensor Reproducibility	36
4.8	Flow Velocity Dependency	36
4.9	Bulk Measurements	37
4.10	Oxygen Calibration	37
5	Results and Discussion	38
5.1	The Glucose Sensors Prepared in this Thesis	38
5.2	Optimisation of the Printing Parameters	38
5.2.1	Evaluation of the Microdispenser Spraying Add-On for the Application of Diffusion Barrier Layer	39
5.2.2	Influence of the Substrate Materials and Properties on the Morphology of the Enzyme Layers	43
5.2.3	Diffusion Barrier Height Variation	49
5.3	Final Printed Sensors	51
5.3.1	Performance of the Oxygen Sensor Spot	52
5.3.2	Response of Printed Sensors to Glucose	53
5.4	Glucose Sensors Printed on Different Support Materias	54
5.5	Influence of Diffusion Layer Height on Dynamic Range	57
5.6	Reproducibility of the Sensors	59
5.7	Flow Velocity Dependency of the Sensors	64
5.8	Measurements of Glucose in Bulk	67
6	Conclusion and Outlook	68
7	References	70
8	List of Figures	75
9	List of Tables	78
10	List of Abbreviations	79

11 Appendix	80
11.1 CNC Control	81
11.2 Phase Angle Measurements of the Different Sensors	83

1 Introduction

The quantification of glucose is amongst the most important analytical tasks. The glucose concentration has to be determined in blood measurements, especially of diabetes patients, food analysis or in bioprocess monitoring. Various types of glucose sensors already exist. The most common ones are electrochemical glucose sensors.

Optical sensors are based on the measurement of photons and, therefore, have some advantages in comparison to electrochemical glucose sensors. The main advantage is that optical glucose sensors do not require a reference electrode.

In this thesis optical glucose sensors were prepared by measuring the consumption of oxygen. Oxygen is a good quencher for various luminophores. By measuring the oxygen concentration the glucose concentration can be determined.

The goal of this work was to prepare optical glucose sensors for the application in microfluidic systems and microreactors. For this reason a microdispenser was utilised as sensor printer. The microdispenser is an inkjet system and the advantages of such systems are the motive customisation and the printing speed.

A major part of this work was printing different layers of the glucose sensors, fine tuning them, decreasing the coffee ring effect, investigating the reproducibility and the dependency on the flow velocity of the sensors.

2 Theoretical Background

2.1 Printing Techniques

Sensors prepared in this thesis consist of 3 different layers on top of each other. To achieve precise and homogenous layers a microdispenser has been used. In this chapter different printing techniques will be pointed out. Different principles of printing methods are summarised in a comprehensive report by Gonzalez et. al. [1].

The printing techniques described in this master thesis are the following:

- Knife Coating
- Screen Printing
- Spraying
- Spin Coating
- Inkjet Printing
- Aerosol Jet Printing
- Microcontact Printing
- Probe Based Techniques

2.1.1 Knife Coating

Knife coating is a rather fast printing technique because of the simple and fast application of the ink and the fast spreading of the ink. Here the ink is applied on a substrate and spread with a knife. The height of the knife gives the thickness of the layer. The width and the moving distance give the area of ink on the substrate. A substrate can be knife-coated with or without a mask. Printing with a mask is very similar to screen printing, where you just print your desired features using a mask. Knife coating is mostly used for laboratory tests and research. It is affordable and can produce prototypes fast. During the process of knife coating the substrate has to be flat and cannot have a structural surface. The resolution is restricted by the mask and realizing small features is therefore hardly possible.

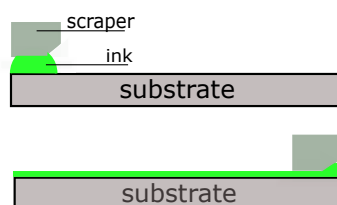


Figure 2.1: Scheme of a Knife Coating Printer

Organic photovoltaic cells have been prepared using knife coating [2]. Multilayer potassium sensors consisting of an lipophilic layer containing the carrier valinomycin and a hydrophilic layer containing anionic fluorophore sulforhodamin B were prepared using a home-made knife coating device [3].

2.1.2 Screen Printing

During the process of screen printing the ink is dispensed on a mask and spread over the substrate. The motive is created by spreading the ink quickly over the mask. This printing technique is interesting for printing big areas on a substrate. After printing the deposited material is usually cured thermally. Disadvantages are that individualized motives have to be formed by a mask and the mask has to be designed first. So fast prototyping is not possible. A completely flat surface is absolutely needed, therefore printing three dimensional structures such as microfluidic channels is not possible. There is also a high material waste compared with other printing methods.

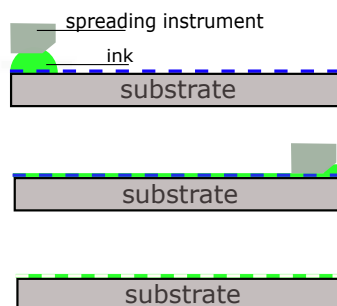


Figure 2.2: Scheme of Screen Printer

Mayr et al. showed that screen printing of opto-electronic sensors is possible for oxygen, carbon dioxide, ammonium and temperature [4]. An amperometric glucose sensor using water-based carbon ink, containing carbon, binder and GOx, was spread on a PVC substrate and left to dry overnight at room temperature. This overcomes the problem of curing enzymes, which are denatured at high temperatures [5].

2.1.3 Spraying

Spray coating is done by using an airbrush system. In this technique the nozzle is closed by a needle. When the needle lifts, the nozzle is open and ink can leave the airbrush. To gain a dispersion of the ink the nozzle is surrounded by an air or inert gas flow. Spraying requires low viscosity ink. To obtain small features a mask is necessary. Similar to knife coating and screen printing, spraying is used for covering big areas. The use of masks leads to a loss of ink and the spray beam does not have a consistent spraying intensity. The spraying beam has more droplets in the middle than at the outer parts.

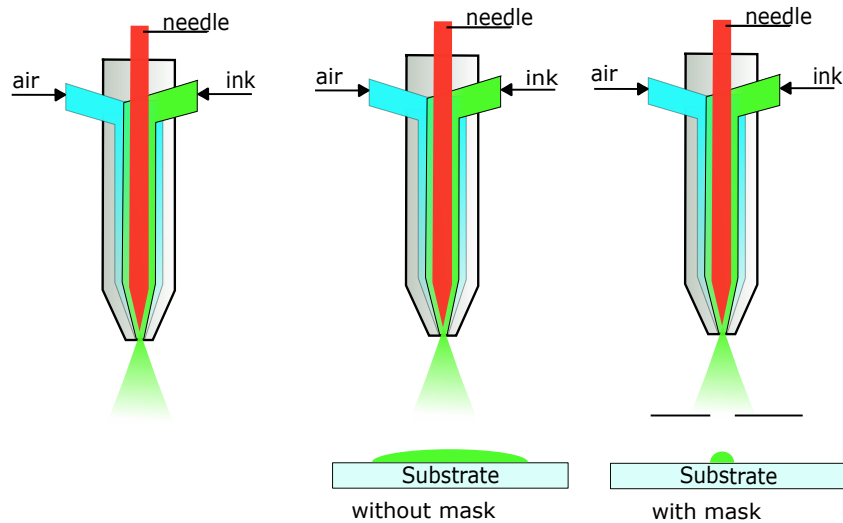


Figure 2.3: Spay Coating without and with a Mask

Hydrogen sensors consisting of carbon nanotubes functionalised with palladium were produced using airbrush technology. The ink was deposited on aluminium substrates and depending on the palladium, if functionalised or not, the sensors can detect H_2 at 200 °C or at room temperature [6]. Optical oxygen sensors consisting of porphyrines were printed in a microfluidic device. The sensors had a diameter of 100 μm and were printed using an automated airbrush spray. [7]

2.1.4 Spin Coating

In the process of spin coating the substrate is rapidly spinning and ink is dropped in the middle. Then the ink is distributed throughout the surface due to the centrifugal force. This produces a thin, flat surface. Spin Coating is a very reproducible and fast method but leads to a high loss of ink. It is suitable for flat surfaces without features.

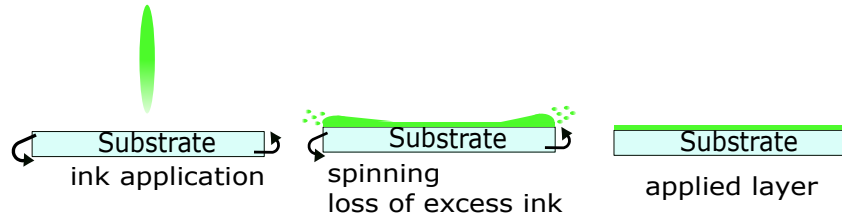


Figure 2.4: Scheme of the Spin Coating Procedure

$\text{In}(\text{OH})_3$, acetic acid and ammonium carboxymethyl cellulose are spincoated on alumina substrates. After tempering In_2O_3 was observed. These layers are used for the detection of CO and H_2 at 350°C [8].

2.1.5 Inkjet Printing

Nowadays inkjet printing is known as an everyday printing technology for everyday tasks. It is a non-contact printing technology where the pattern is fabricated by a dot matrix. The ejection of fluid drops is digitally controlled. The drops leave a nozzle and fall vertically under gravity to a pre-specified position. Furthermore, there is no mask required to achieve features on the substrate. It allows the deposition of very small volumes of ink and therefore cannot only be used to print nice photographs but also to print nanoscale sensors. Setti et al. reported a possible resolution up to 1200x1200 dpi, where the features were formed by droplets consisting of 10-12 pL ink [9]. Many inkjet printing techniques exist, but the four techniques, which are used most, are: thermal, piezoelectric, electrostatic and acoustic. The most common are thermal and piezoelectric.

I refer the interested reader to a comprehensive review on these techniques by Li et. al. [10].

Thermal Inkjet Printing

In this method a heat resistor heats the ink in an ink chamber up to $300\text{-}350^\circ\text{C}$. Due to evaporation a bubble is formed and so the pressure inside the chamber increases, up to the point when ink escapes through the nozzle, almost simultaneously with the collapse of the bubble. Then the pressure decreases and the ink chamber is refilled again.

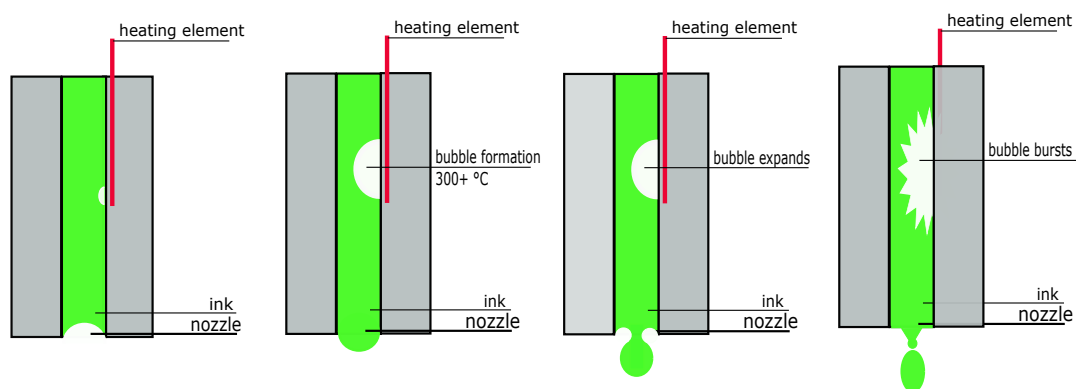


Figure 2.5: Scheme of a Thermal Inkjet Printer

As thermal inkjet printing is a versatile method, a lot of sensors have already been developed. Amperometric glucose sensors were designed using thermal inkjet printing [11]. It is also possible to produce blood type sensors on paper. The blood is immobilised using different antibodies. The blood type can be read out either by bare eye on the test paper [12] or by using a mobile app [13].

Piezoelectric Inkjet Printing

The piezoelectric inkjet printer uses a piezoceramic plate connected to a membrane. This membrane is a layer between the ink and the piezo actuator to prevent interactions. In the first step the piezoceramic plate deforms in response to an electric pulse. The membrane is lifted and more ink can flow into the ink chamber. As the piezo-actuator relaxes the ink is pushed out of the nozzle.

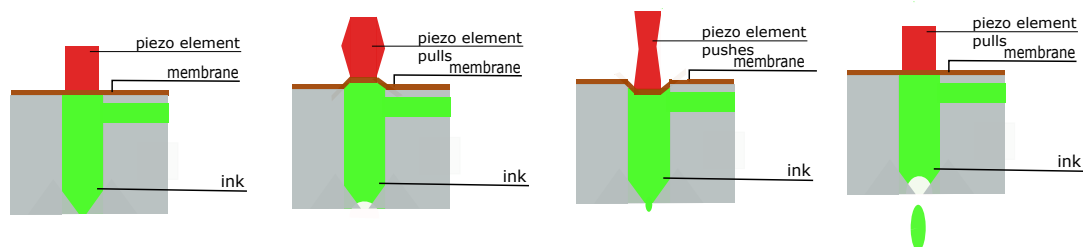


Figure 2.6: Scheme of a Piezoelectric Inkjet Printer

The piezoelectric inkjet printer can be classified according to the distortion of the piezoceramic plate into squeeze, bend, push and shear mode. In this context the voltage strength, the pulse duration and the nozzle size influence the size of the ink droplet on the substrate. It is possible to print H_2O_2 sensors using piezoelectric inkjet printing [14]. Printing silver nanoparticles onto hydrophobic paper using a piezoelectric inkjet printer forms microscale sensing arrays which are used for surface-enhanced Raman spectroscopy for lateral flow sensors [15].

Electrostatic Inkjet Printing

An electrostatic inkjet printer produces a stream of droplets. The droplets pass 2 sets of charged plates. The first set of charged plates selectively charges the droplets according to the printing signal. The charged droplets are deflected into a gutter for recirculation when passing through an electric field made by two other charged plates, while uncharged droplets escape the printer and form the feature on a substrate. The electrostatic inkjet printer is able to dispense small droplets but the ink has to be conductive, which limits the range of applications of the electrostatic inkjet printing.

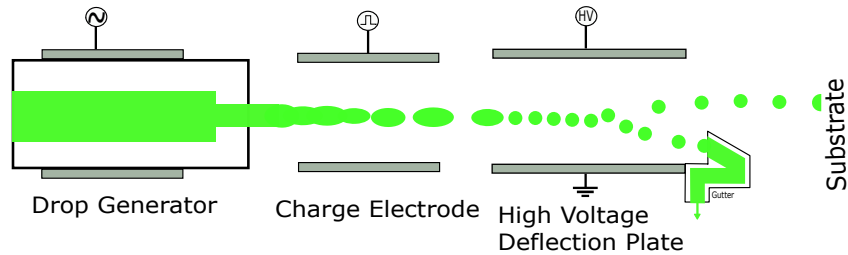


Figure 2.7: Scheme of an Electrostatic Inkjet Printer

An amperometric glucose sensor was developed by Newman et al. in 1992. Enzyme glucose oxidase and a mediator tetrathiafulvalene were deposited using electrostatic inkjet printing. The conductivity was increased adding tetrabutylammonium perchlorate to the mediator solution. Good reproducibility and wide operating range were achieved with these sensors compared to those developed with other techniques at that time [16].

Acoustic Inkjet Printing

The acoustic inkjet printer consists of a high-frequency transducer, which is fixed to the back of an acoustic lens. The transducer launches acoustic waves through the lens and the acoustic energy is focused so it induces a pressure wave to expell the ink from the surface to the substrate. The advantage of this printing technique is that there is no need for a nozzle and for this reason there is no nozzle clogging.

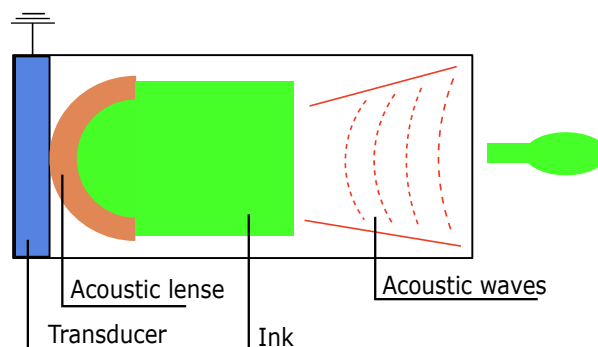


Figure 2.8: Scheme of an Acoustic Inkjet Printer

Soluble polymeric organic semiconductors were printed using acoustic inkjet printing to prepare organic thin-film transistors. The semiconductors had a resolution of $35\ \mu\text{m}$ [17].

2.1.6 Aerosol Jet Printing

In the aerosol jet printing process an ultrasonic transducer or an air-operated pump forms very small droplets. The volume of these droplets is about 0.001-0.005 pl.[18] Then excess gas is let out through an impactor and the aerosol is transported to the nozzle. The finely dispersed ink is sprayed on the substrate surface. It is possible to produce small features with aerosol jet printing, but a low viscosity is necessary and it is not possible to print large particles.

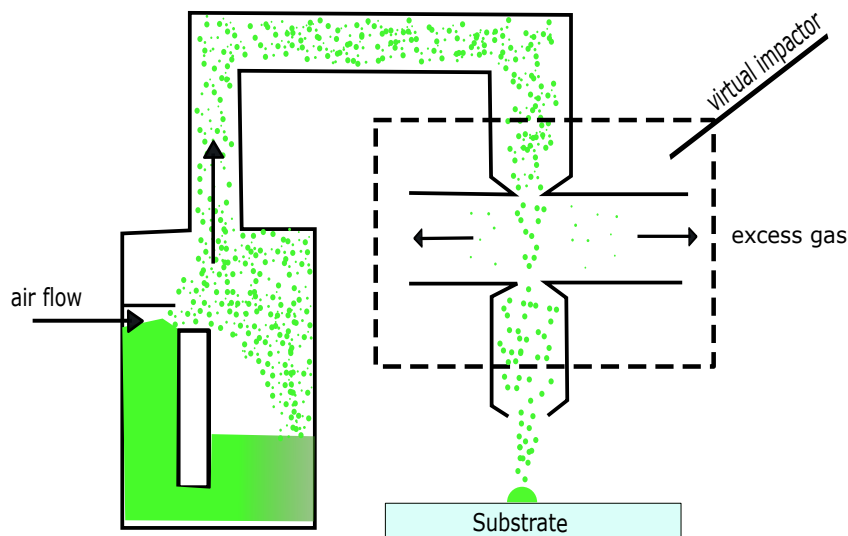


Figure 2.9: Scheme of Aerosol Jet Printer

Single walled carbon nanotubes with functionalized palladium can be printed using aerosol jet printing to prepare Hydrogen sensors [18].

2.1.7 Microdispenser

The microdispenser works with a piezoelectric device. The piezoelectric device controls a tappet that presses fluid droplets through a nozzle. This is called a dispensing. A dispensing can be divided in different steps.

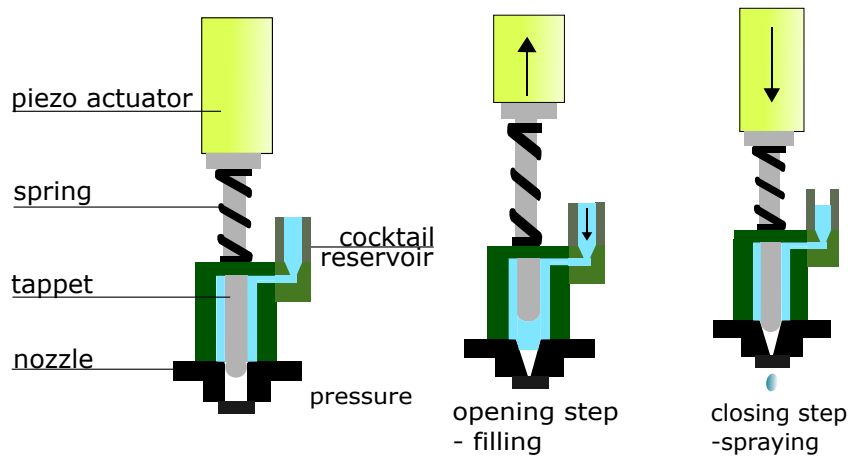


Figure 2.10: Steps of a Dispensing

In the first step or opening step the piezo actuator pulls the tappet up and liquid can flow into the space formed. To do so the cocktail reservoir is under pressure. Different parameters describing this step can be defined. The *tappet lift* describes how far the tappet is pulled up. The *rising time* defines how fast the tappet is pulled up. Then the tappet stays open for a defined time which is described as the *open time*.

To dispense the ink the piezo actuator pushes the tappet down, which presses the liquid through a nozzle out of the system. The nozzle can have different sizes. The *falling time* tells how fast the tappet is pushed down.

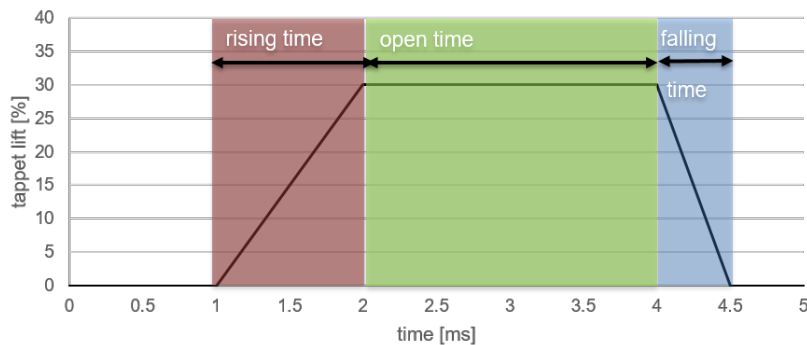


Figure 2.11: Tappet lift - Time Diagram of one Dispensing Step

In the diagram the piezo actuator opens the tappet 30% of the total possible lift, this happens in 1 ms. Then the tappet stays open for 2 ms and closes in 0.5 ms. The microdispenser can perform multiple successive dispensings.

pH sensors with two different dyes, to enable a higher pH range, were printed using the microdispenser. The pH sensors consisted of HydroMed D4, pH dye and Egyptian blue reference particles [19].

Spraying Add-On

The spraying add-on of the microdispenser was used instead of a nozzle, it worked after the following principle:

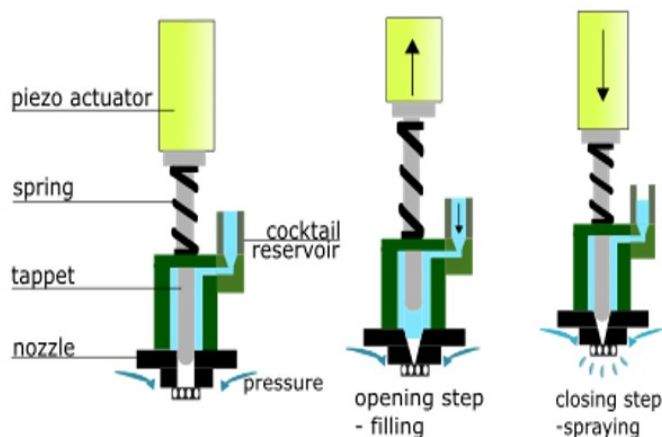


Figure 2.12: Scheme of the Microdispenser Spray Add-On

Here an air flow generates finely distributed droplets.

2.1.8 Microcontact Printing

In the process of microcontact printing the material of interest is selectively transferred to a substrate surface. First the template has to be prepared, this is usually done by photolithography, where a silicon wafer is covered with a photoresist. Then a mask is applied and the photoresist is exposed to UV light. The undeveloped photoresist is washed off and leaves the template behind. A stamp is fabricated by casting a polymeric elastomer (usually PDMS) against the template. Then the stamp is inked with a solution of the printing material and afterwards pushed on the surface of the substrate (often covered with gold). The printing material is transferred to the areas of the substrate, where the template has contact to, forming a pattern of monolayer.

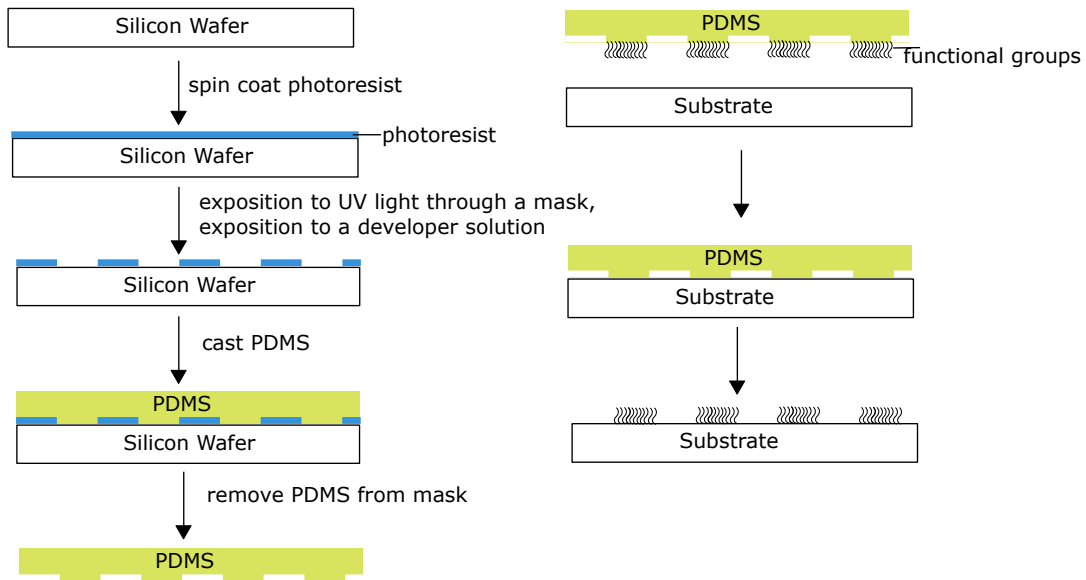


Figure 2.13: The Process of Microcontact Printing

A biosensor for drug, pathogen and toxin detection was prepared by disposing aldehyde-terminated groups on a substrate and then covalently attaching the protein on the aldehyde. The remaining areas were blocked by amino-poly-(ethylene glycole), which forms a cell-adhesion resistant area. Then cells were incubated on the surface, adhering to the proteins. The size and cell growth can be controlled and so drug, pathogen and toxin detection is possible [20].

2.1.9 Probe-Based Techniques

With the movement of miniaturisation of sensors and other analytical devices the change from microscale to nanoscale can be done by probe-based techniques. Dip-pen nanolithography and nanografting are some of the SPM-based techniques.

Dip-Pen Nanolithography

In the process of dip-pen nanolithography an atomic force microscopy tip is modified by dipping the cantilever into a solution of the chemical of interest or by evaporation. Then the tip is brought in contact with the surface of the substrate to be patterned and the chemical is transferred to the surface by capillary action. The resolution depends on the physical properties of the substrate, the scan speed and the features of the applied chemical [21].

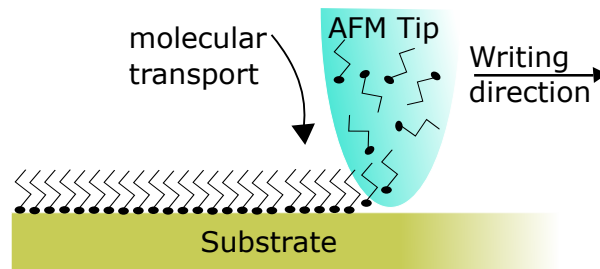


Figure 2.14: Scheme of Dip-Pen Nanolithography

A CO₂ sensor was developed by disposing doped polypyrrole on silicon-dioxide using dip-pen nanolithography. The resistance of the sensor changes in presence of CO₂ [22].

Nanografting

In the process of nanografting first the surface of the substrate is scanned by atomic force microscopy at low force. Then molecules are cleaved off by moving the tip over the surface with a force just higher than the displacement force. As the matrix molecules are removed, molecules from the contacting solution adsorb onto the areas created by the tip. Then the surface can be scanned and analysed with the same AFM tip.

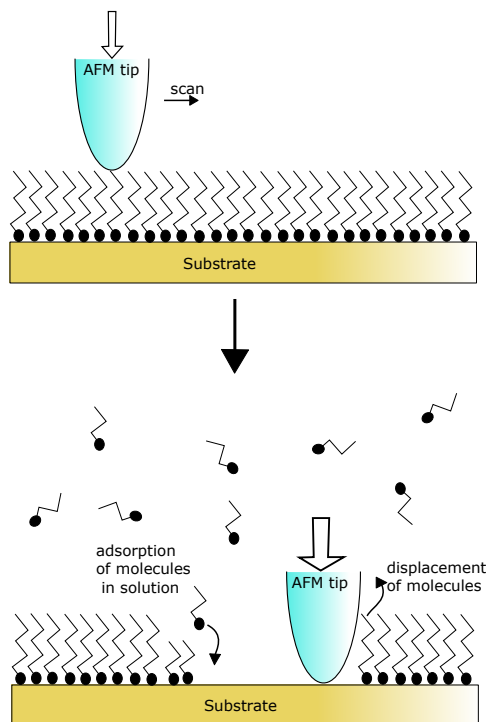


Figure 2.15: Scheme of the Nanografting Printing Process

With this method it is possible to graft proteins on different surfaces [23] and to study the stability of folded biopolymers as monolayers as well as at high density. It is also possible to

graft DNA on gold surface and to maintain the activity of the DNA at the same time [24].

2.2 Optical Sensors

This section is based on these references [25] , [26], all other references will be pointed out explicitly.

The IUPAC definition of a chemical sensor is [27]:

" A chemical sensor is a device that transforms chemical information from the concentration of a specific sample component to total composition analysis, into an analytically useful signal. The chemical information, mentioned above, may originate from a chemical reaction of the analyte or from a physical property of the system investigated. [...] Optical devices transform changes of optical phenomena, which are the result of an interaction of the analyte with the receptor part. This group may further be subdivided according to the type of optical properties which have been applied in chemical sensors: absorbance [...], reflectance [...], luminescence [...], fluorescence [...], refractive index [...], optothermal effect [...] and light scattering [...]. "

Chemical sensors measure the chemical information, which could be the concentration or the total composition of a sample, and turn it into an electric signal. The data may come from a chemical reaction or from a physical characteristic. Optical devices measure changes of optical properties, which exist because the analyte interacts with the receptor. Optical sensors may be classified according to the kind of measuring optical properties: absorbance, reflectance, luminescence, fluorescence, refractive index, optothermal effect and light scattering.

Optical sensors enable contact-less measurement, multi-analyte analysis and there is no need for a direct referencing system. There already exist a lot of sensors for different analytes. Oxygen sensors and glucose sensors are prepared in this thesis, for this reason the general principles are pointed out in this chapter.

2.2.1 Luminescence in General

Light can be described as electro-magnetic radiation, which consists of electromagnetic waves. Electro-magnetic waves are synchronised oscillations of electric and magnetic fields. Electro-magnetic radiation is characterised by the wavelength λ and the frequency ν .

$$\nu * \lambda = c \tag{2.1}$$

where c is the speed of light. A photon has the energy E , which is described as

$$E = h * \nu \tag{2.2}$$

where h is the Planck's constant.

When light hits matter basically two scenarios may happen. On the one hand light can pass through the sample without any interaction, this scenario is called transmission. On the other hand the matter can interact with the sample, which is called absorbance. These two effects can be described by the Lambert Beer Law.

$$A(\lambda) = \log \frac{I_{\lambda}^0}{I_{\lambda}} = -\log T(\lambda) \quad (2.3)$$

$$T(\lambda) = \frac{I_{\lambda}}{I_{\lambda}^0} \quad (2.4)$$

$A(\lambda)$... *Absorbance*

I_{λ}^0 ... *light intensity of the beams entering the medium*

I_{λ} ... *light intensity of the beams leaving the medium*

$T(\lambda)$... *Transmittance*

The matter absorbs the light and transforms it into energy, this leads to excitation. Then the molecule is in an electronically excited state. An electronic transition consists of the excitation of an electron from the ground state to an unoccupied orbital. The orbital of the ground state is called Highest Occupied Molecule Orbital (HOMO) and the orbital of the excited state is called Lowest Unoccupied Molecule Orbital (LUMO).

Luminescence is the relaxation from the excited state to the ground state and thereby ultraviolet, visible or infrared photons are emitted. The type of luminescence is given by the mode of excitation.

Table 2.1: Types of Luminescence

Type of Luminescence	Mode of excitation
Photoluminescence	Absorption of light
Electroluminescence	Electric field
Thermoluminescence	Heating
Chemiluminescence	Chemical process
Radioluminescence	Ionising radiation
Cathodoluminescence	Cathode rays
Bioluminescence	Biochemical process

In this thesis only Photoluminescence will be discussed. Photoluminescence can be the deexcitation via fluorescence, phosphorescence or delayed fluorescence.

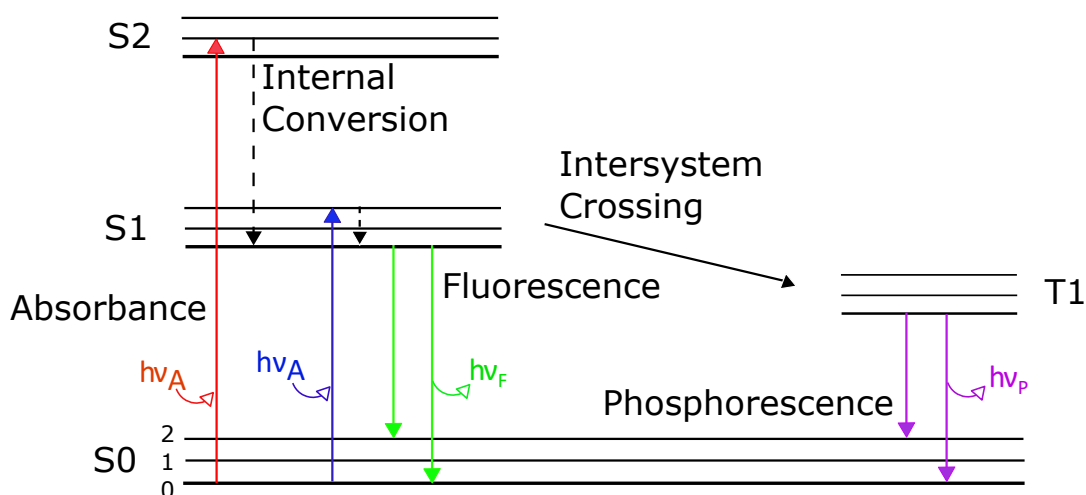


Figure 2.16: Jablonski Diagram

The Jablonski diagram shows the excitation of an electron from the ground state (S_0) to the excited singlet states S_1 or S_2 , according to the absorbed energy. Within 10^{-13} s to 10^{-11} s the electron relaxes from higher singlet states to S_1 . This relaxation is normally an internal conversion step because it is a radiation free transition. From S_1 fluorescing conversion to the ground state (S_0) or intersystem crossing, which is the transition from the singlet state to a triplet state, may happen. The singlet state S_1 has a lifetime of 10^{-9} s. Intersystem crossing is a spin forbidden conversion. Emission, which undergoes intersystem crossing, is much slower than fluorescence.

2.2.2 Luminescence Lifetime and Quenching

Two important parameters for fluorophores are the quantum yield and the luminescence lifetime. The quantum yield is described as the number of emitted photons in relation to the number of absorbed photons.

$$Q = \frac{\Gamma}{\Gamma + k_{nr}} \quad (2.5)$$

Q ... Quantum Yield

Γ ... emissive rate of fluorophore

k_{nr} ... rate of non – radiative decay to S_0

The lifetime of an excited state is defined by the average time the electron spends in the excited state. It is a combination of both emissive and non-radiative relaxation processes.

$$\tau = \frac{1}{\Gamma + k_{nr}} \quad (2.6)$$

τ ... lifetime

The quantum yield is an important parameter for the luminescence intensity. Fluorophores with high quantum yields are often used for optical sensors. The fluorescence lifetime is dependent on different physical and chemical parameters. Decreasing the lifetime and the fluorescence lifetime is called quenching.

Quenching can happen due to different interactions, for example the interaction with a heavy atom, an electron, it can happen because of excimer formation, exciplex formation, proton transfer or energy transfer. All of these transitions have a fast transfer process to an acceptor in common. There are different types of luminescence quenching.

Static Luminescence Quenching

Static luminescence quenching describes the formation of a non-fluorescent ground-state complex between the fluorophore and a quencher. When this complex is excited it immediately relaxes to the ground state without emission of light. This quenching can be easily described by the association constant of the complex. Static quenching has no influence on the luminescence lifetime.

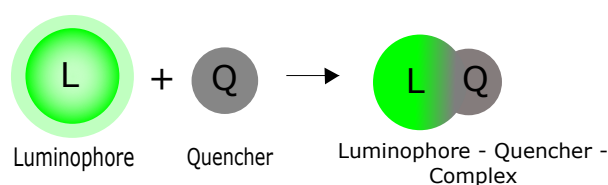


Figure 2.17: Luminescence Quenching through Complex Formation

For optical sensors this kind of quenching can be used to determine analyte concentration. The analyte forms a complex with the luminophore and therefore the luminescence intensity decreases.

Dynamic Luminescence Quenching

At dynamic luminescence quenching the luminophore and the quencher collide which results in an energy transfer from the luminophore to the quencher. This quenching does not only decrease the luminescence intensity but at higher quencher concentrations the luminescence lifetime is quenched.

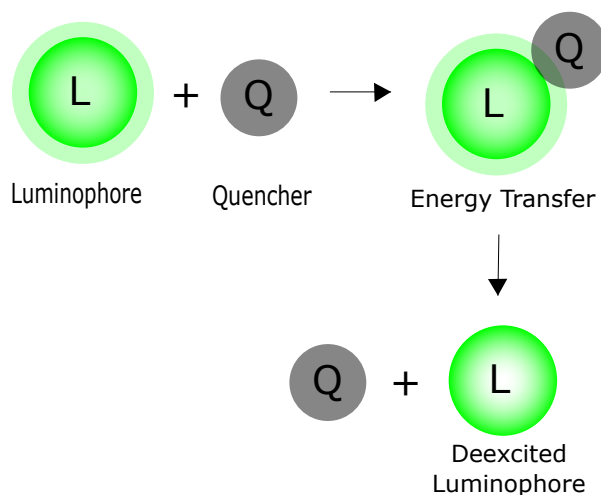


Figure 2.18: Dynamic Quenching Mechanism

The lifetime and intensity decrease are given by the Stern-Volmer equation:

$$\frac{I_0}{I} = \frac{\tau_0}{\tau} = 1 + k_Q\tau_0[Q] = 1 + K_{SV}[Q] \quad (2.7)$$

I_0	...	<i>luminescence intensity in absence of quencher</i>
I	...	<i>luminescence intensity at given quencher concentration</i>
τ_0	...	<i>luminescence lifetime in absence of quencher</i>
τ	...	<i>luminescence lifetime at given quencher concentration</i>
k_Q	...	<i>bimolecular quenching constant</i>
$[Q]$...	<i>quencher concentration</i>
K_{SV}	...	<i>Stern – Volmer constant</i>

2.2.3 Luminescence Measurement Techniques

Several techniques to measure the luminescence lifetime are available.

Time-Correlated Single-Photon Counting

At time-correlated single-photon counting the sample is excited with a short laser pulse and single photons are detected by a photodetector. Plotting the measured time between the excitation pulse and the detected photon against the luminescence intensity gives the decay curve.

Gate Detection

At the gate detection the intensity of the emission phase is measured after an excitation pulse in successive time gates. This method is especially useful for specimen with long decay times.

Phase Modulation

The sensor is illuminated by a sinusoidally modulated excitation signal. Since the luminophore stays excited for some time, the emission signal is delayed, but follows the modulation. The delay depends on the lifetime of the fluorophore, it is measured as a phase shift.

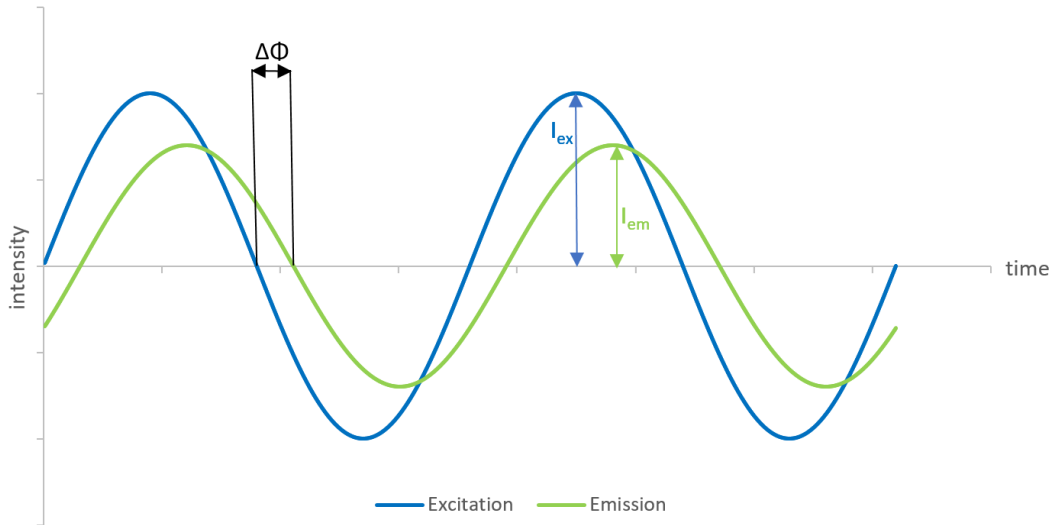


Figure 2.19: Emission and Shifted Excitation Signal

In phase fluorimetry the lifetime is connected to $\Delta\Phi$, which can be described as:

$$\Delta\Phi = \arctan \omega\tau = \arctan 2\pi f\tau \quad (2.8)$$

$$\tau = \frac{\tan\phi}{2\pi f} \quad (2.9)$$

- $\Delta\Phi$... *phase shift*
 ω ... *circular modulation frequency*
 f ... *modulation frequency*

2.3 Glucose Sensors

The quantification of glucose is amongst the most important analytical tasks. Glucose has to be determined in various situations, including blood measurements, food analyses or bioprocess

monitoring. There are various types of existing glucose sensors and different sensing techniques.

- Electrochemical Glucose Sensors
 - Enzymatic Electrochemical Glucose Sensors
 - Non-Enzymatic Electrochemical Glucose Sensors
- Optical Glucose Sensors
 - Glucose Sensors via the Optical Properties of Enzymes
 - Glucose Sensors Measuring Reaction Products
 - Glucose Sensors Using Synthetic Boronic Acids
 - Glucose Sensors Using Glucose-Binding Proteins

The next chapter will review some of the existing glucose sensors.

2.3.1 Electrochemical Glucose Sensors

Electrochemical Glucose Sensors are usually amperometric sensors. They can be divided according to their use of enzymes. Enzymatic glucose sensors are not as long lasting as non-enzymatic glucose sensors.

Enzymatic Electrochemical Glucose Sensors

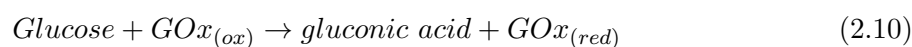
The first amperometric glucose sensor was developed by Clarke and Lyone in 1962 [28]. The sensor consisted of an oxygen electrode covered with a thin layer of entrapped glucose oxidase via a semipermeable dialysis membrane. The decrease of oxygen due to the enzymatic reaction was recorded by the electrode. For general working principles of the different sensors a review of Wang et. al. [29] is recommended.

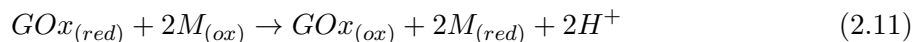
First Generation

The first generation of electrochemical glucose sensors consists of electrodes covered with a thin layer of enzymes. Malitesta et al. [30] developed a glucose sensor, consisting of a platinum electrode covered with glucose oxidase. The concentration of hydrogen peroxide was measured during enzymatic reactions. The problems of this kind of sensors were interferences, they were minimized by permselective coating. The sensors are dependent on the oxygen concentration.

Second Generation

The problem of the dependency on the oxygen consumption had to be diminished and so new sensors were developed. A different electron acceptor which transported the electrons from the redox centre of the enzyme to the electrode had to be established. This carrier is called mediator and reacts according to following equations:





Cass et al. incorporated 1,1-di-methylferrocene into a graphite electrode covered with glucose oxidase [31]. Here the ferricinium ion resembles the mediator which is responsible for the electron transfer.

Third Generation

The ultimate goal in the development of amperometric glucose sensors which work with enzymes is the elimination of a mediator. This can lead to very high selectivity. The mechanism of these sensors is not clearly understood yet and there are suggestions that there is still a mediator. A third generation of amperometric glucose sensors was developed, covalently binding glucose oxidase on an oxidised boron-doped diamond electrode. Oxygen has no influence on this electrode [32].

Non-Enzymatic Electrochemical Glucose Sensors

This section is based on reference of Toghil et. al. [33], all other references will be pointed out explicitly.

At non-enzymatic electrochemical glucose sensors the glucose is supposed to react with atoms at the surface of the electrode. Two mechanisms could work to which principles the glucose can react with atoms.

The first one suggested by Pletcher [34] is called the activated chemisorption model. Glucose adsorbs on the electrode surface. Due to the developed bond, hydrogen is cleaved off the hemiacetal carbon. Then the hydrogen reacts with the electrode, adjacent to the bound glucose. This causes a change in the oxidation state of the glucose and consequently a change of the glucose-metal interaction and so this leads to a desorption of glucose. Both the adsorption and desorption processes are conductive.

The second mechanism was suggested by Burke [35]. It is called Incipient Hydrous Oxide Adatom Mediator and in this case active metal atoms, which are on the surface and have low lattice stabilisation and enhanced reactivity, undergo a premonolayer oxidation step where a monolayer of incipient oxygen hydrogen is formed. Then the oxygen hydrogen mediates the glucose oxidation.

There are different types of non-enzymatic electrochemical glucose sensors, including metal based glucose sensors, for example platinum [36], gold [37], nickel [38] and copper [39]. There are also electrochemical non-enzymatic glucose sensors using carbon nanotubes [40] or graphene [41].

2.3.2 Optical Glucose Sensors

The basic working principles of different sensors are summarised by a review of Steiner et. al. [42].

One of the first devices to measure blood glucose was the Ames Reflectance Meter which automatically determines the change of colour of enzyme-based reagent strips. [43]

Optical sensing methods are based on the measurement of photons and therefore they have some advantages in comparison to electrochemical glucose sensors. The main advantage is that they do not require a reference electrode. They can be subdivided into different types according to the recognition of glucose.

Glucose Sensors via the Optical Properties of Enzymes

These sensors are making use of the fact that enzymes, including glucose oxidase, change their optical characteristics in the presence of glucose. The enzymes can be either labelled or non-labelled.

Non-labelled Enzymes

With non-labelled enzymes the intrinsic fluorescence of glucose-converting enzymes is observed. Various sensors were developed using this system. Sierra et al. entrapped glucose oxidase in a sol-gel and measured the change in fluorescence in presence of glucose. If glucose is present the glucose oxidase changes its conformation [44].

Labelled Enzymes

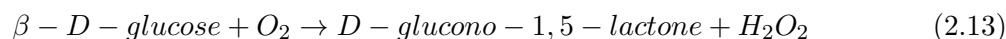
Instead of measuring the optical qualities of enzymes, the optical properties of luminophores labelled on the enzymes can be quantified. It is possible to label glucose oxidase with fluorescein. The fluorescence increases in the presence of glucose. The glucose oxidase can be immobilised using polyacrylamide. [45]

Glucose Sensors Measuring Reaction Products

Enzymatic reactions, which digest glucose, have different side compounds, including oxygen or hydrogen peroxide. The concentrations of those compounds are directly related to the glucose concentration.

Sensing the consumption of oxygen

The consumption of glucose happens according to the following equation:



The consumption of oxygen can be measured by using fluorophores, which are quenched in the presence of oxygen. The sensors can be designed using different technical layouts. There are:

- Planar optical sensors

- Glucose oxidase can be incorporated in a nylon membrane. The sensing layer consists of decacyclene in a silicone membrane. The change in fluorescence intensity is measured. [46]
- Enzyme based biosensors on optoelectrodes were prepared using phosphorescent metallo-porphyrins. In presence of oxygen the luminescence lifetime is quenched. [47]
- Fibre optical sensors
 - Pasic et al.[48] produced a sensor consisting of two fibres. The first is a referencing optical fibre, which is coated with an oxygen sensing layer to measure the oxygen concentration in the liquid. The second is coated with an oxygen sensitive layer, an enzyme layer and a diffusion layer, through which oxygen can pass unhinderedly and glucose is kinetically hindered.
- Sensors based on microparticles and nanoparticles
 - Magnetite-based nanoparticles, which glucose oxidase was covalently bound on, can monitor the oxygen consumption using a probe Ru(phen). The immobilisation of glucose oxidase increased the stability of the enzyme but decreased the activity. [49]

Sensing the formation of hydrogen peroxide

During the enzymatic reaction hydrogen peroxide is formed. The hydrogen peroxide concentration can be measured and the advantage of this measurement is that there is almost zero background. Endo et al. [50] developed a surface plasmon resonance glucose biosensor by embedding silver nanoparticles and glucose oxidase in a hydrogel. The hydrogen peroxide degrades the clustered silver nanoparticles. Due to this, the distance between the nanoparticles and the hydrogel increases and this leads to a decreased localised surface plasmon resonance.

Sensing via the changes in pH

Protons are produced during the reaction of gluconolactone with water, which changes the pH. However, it is not suitable for a lot of samples because the initial pH is often unknown. A working sensor consists of pH sensitive azlactone and glucose oxidase embedded in hydrogel. Single layer sensors showed high leaching and therefore dual layer sensors were developed. [51]

2.3.3 Glucose Sensors Using Synthetic Boronic Acids

Boronic acids can reversibly form 5- or 6- membered cyclic esters by reaction with diols. These diols can often be found in saccharides including glucose. During the binding of saccharides the trigonal form of boronic acids transforms into a tetrahedral form, upon which a proton is released. This changes the pH value. Additionally the boronic acids can be attached to a fluorophore and the geometric changes alter the fluorophore's characteristic emission. Disposable plastic contact lenses were doped with quinoline-based probes for the glucose determination in tear fluid. [52]

2.3.4 Glucose Sensors Using Glucose-Binding Proteins

A glucose binding protein is for example the plant lectin protein Concanavalin A, which has four binding sites for glucose, but also for other carbohydrates. The protein and the competitor can be labelled with fluorescent dyes and therefore the glucose concentration can be determined. Surface plasmon resonance sensors consist of gold colloids on which dextran covalently bound to Concanavalin A was coated. In presence of glucose the dextran and Concanavalin A would dissociate and that leads to a reduction of plasmon absorbance. [53] Other proteins, e.g. glucose oxidase, can be used by removing the metabolising co-enzyme. Enzymes with a removed co-enzyme are called apo-enzymes. Apo-glucose oxidase can be labelled with 8-Anilino-1-naphthalenesulfonic acid. After binding glucose the fluorescence lifetime of the 8-Anilino-1-naphthalenesulfonic acid decreases. [54]

2.4 Glucose

The theoretical background of Glucose and Enzymes was taken out of Harper's Illustrated Biochemistry [55].

Carbohydrates are a product of photosynthesis. Glucose is a carbohydrate belonging to the monosaccharides. A monosaccharide cannot be hydrolysed to simpler carbohydrates. Glucose can adapt in different ways.

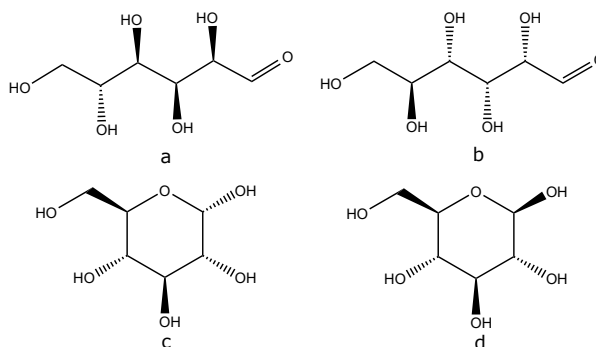


Figure 2.20: Conformations of Glucose: a: D-Glucose, b: L-Glucose, c: α -D-Glucose, d: β -D-Glucose

The ring structure is the thermodynamically favoured ground state. Glucose is known as the sugar of the body. It is carried by the blood to the different tissues of the body and degradation of glucose releases energy. Glucose forms cyclic structures by a reaction between the first and the second carbon atom. The formation of cyclic glucose creates an asymmetric carbon at the first carbon atom and therefore, α and β -D-Glucose are in an equilibrium.

2.5 Enzymes

Enzymes are biological polymers that catalyse chemical reactions. Most of the enzymes are proteins. Like all catalysts enzymes are not consumed during the reaction but alter the reaction velocity. They are extremely selective towards the reaction and the substrate and can be regioselective. Enzymes are categorised according to their type of reaction. There are following types of possible enzymes.

Table 2.2: Classes of Enzymes

Enzyme class	Type of Reaction
Oxidoreductases	catalyse oxidations and reductions
Transferases	catalyse transfer of groups from a donor to an acceptor
Hydrolases	catalyse hydrolysis
Lyases	catalyse the addition to a double bond or cleaves off groups to form a double bond
Isomerases	catalyse geometric or structural changes
Ligases	catalyse the joining together of two molecules

The selectivity of enzymes can be explained by the lock and key principles. Enzymes have a reactive site which only specific substrates can reach or bind to. Some enzymes only unwind in presence of specific substrates. In a lot of enzymatic reactions electrons or other substances are transferred from one substrate to another, this is done with the help of coenzymes.

Glucose oxidase is a very stable enzyme. At 0°C it is stable for 2 years, at -15°C even for 8 years. The stability depends on the pH. The enzyme is most stable around pH 5 but can be used between pH 2 and 8. Glucose oxidase can be inhibited easily by heavy metals. β -D-Glucose is the most effective substrate for glucose oxidase and has a high turnover.

Glucose oxidase is an oxidoreductase with a FAD coenzyme. FAD stands for Flavin Adenine Dinucleotide. For a general review about glucose oxidase a review by Wilson and Turner [56] is recommended.

3 Materials and Methods

3.1 Devices

Table 3.1: Printer Parts

Manufacturer	Device	Description
VERMES	MDC 3200+	microdispensing control unit
VERMES	MDV 3200A-HS-UF	microdispenser
Benezan Electronics	Triple Beast	CNC microstep driver
Isert-Electronic	axis motor	step motor for single axis movement

Table 3.2: Devices for measurement

Manufacturer	Device	Description
Pyrosience	FireStingO2	phase fluorimeter with fibre
Bruker	Dektak XT	stylus surface profiler
Tecan	Cavro-XLP-Pump	12 way pump
Carl Zeiss	Axiovert 25	microscope
Vögtlin Instruments	Red-y smart series for gasflow	gas mass flow controller



Figure 3.1: Picture of a FireStingO2, Phase Fluorimeter

Table 3.3: Sonifier parts

Manufacturer	Device	Description
Branson	W-450 D	20kHz sonification control unit
Branson	102-C Converter	ultrasound controller module
Branson	1/8" Tapered Microtip	metal tip for energy transmission

3.2 Chemicals

Solvents

Ethanol (C_2H_5OH), **Isopropanol** (C_3H_7OH) and **Tetrahydrofuran** (C_4H_8O) were bought from VWR Chemicals and used as received

Table 3.4: Polymers used

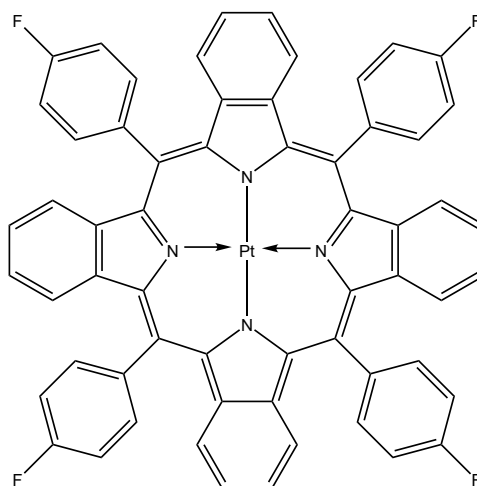
Name	Formula	Distributor
Polystyrene	$(C_8H_8)_n$	Carl Roth
D4 hydrogel	ether based hydrophilic urethans	AdvanSource
Polyhydroxyethylmethacrylate	$(C_6H_{10}O_3)_n$	PolyScience
Ethylcellulose	ethylated cellulose	ScientificPolymer Inc.

Table 3.5: Dyes and Enzymes

Name	Formula	Distributor
Sensor Particles	PtTPTBPF in 1% PS	synthesised in house
Glucose Oxidase	GOx-Cleas	prepared in house

Table 3.7: Phosphate Buffer

Name	Formula	Distributor
Sodiumdihydrogenphosphate waterfree	NaH_2PO_4	Carl Roth GmbH
Disodiumhydrogenphosphate waterfree	Na_2HPO_4	Carl Roth GmbH
Sodiumchloride	NaCl	VWR chemicals
Sodium Azide	NaN_3	Carl Roth GmbH
α -D(+)-Glucose Monohydrate	$\text{C}_6\text{H}_{12}\text{O}_6$	Carl Roth GmbH

**Figure 3.2:** Structure of the Oxygen Sensor Particles

3.3 Polymer Slides

Table 3.6: Polymer Slides

Name	From	Distributor
Glass Microscope Slides	1mm thick slides	Carl Roth
Polymethylmethacrylate Slides	1mm thick slides	Microfluidic Chip Shop
Polystyrene Slides	1mm thick slides	Microfluidic Chip Shop
Topas Slides	1mm thick slides	Microfluidic Chip Shop
Polycarbonate Slides	1mm thick slides	Microfluidic Chip Shop
Polymethylmethacrylate 250 μ l		
Rhombic Chamber Chip	see picture below	Microfluidic Chip Shop
Polymethylmethacrylate 120 μ l		
Rhombic Chamber Chip	see picture below	Microfluidic Chip Shop

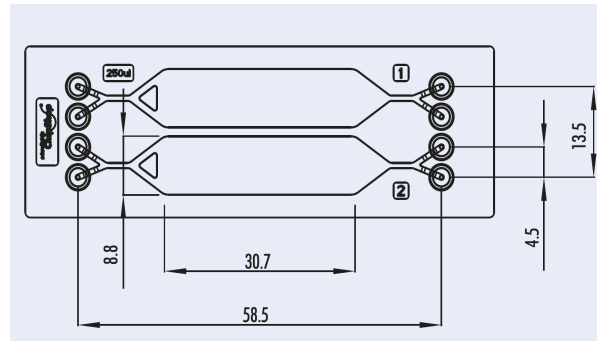


Figure 3.3: Layout of a 250 μl Rhombic Chamber Chip, the Chip is 800 μm Deep

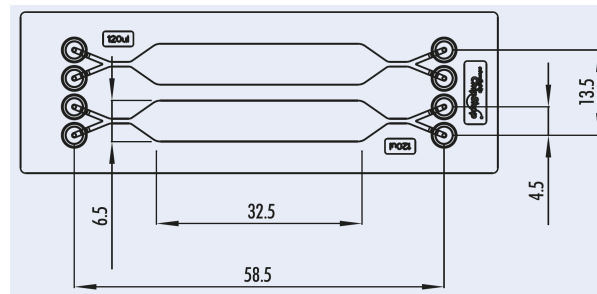


Figure 3.4: Layout of a 120 μl Rhombic Chamber Chip, the Chip is 500 μm Deep

Both figures were taken out of the microfluidic Chip Shop Lab-on-a-Chip Catalogue

4 Experimental

4.1 Preparation of the Sensor Cocktails

The cocktails used were always prepared in the same way, as written below.

4.1.1 Oxygen Sensor Cocktail

The composition of the oxygen sensor layer was: 6 w% of the sensor particles (1 w% particles in polystyrene), 6 w% Hydrogel D4 and 88 w% isopropanol and water at a ratio of 3:1. The composition of the cocktail could be changed but the ratio of sensor particles to D4 should always stay 1:1.

After dissolving the components, the cocktail was suspended. To homogenise the cocktail it was sonified by a Branson Ultra Sonifier and in the meantime cooled in an ice bath. The settings of the sonifier were:

Table 4.1: Settings of the Sonifier to homogenise the oxygen sensor cocktail

Parameter	Description	Value
Energy	ultrasonic energy in percent	25 %
Duration	overall sonification time	60 s
Pulse Duration	sonification time per cycle	1 s
Pause Duration	pause time between cycles	10 s

The cocktails were always prepared freshly but could also have been stored at room temperature. To re-use the cocktail after storage it had to be re-suspended.

4.1.2 Glucose Oxidase Enzyme Layer Cocktail

The composition of the glucose oxidase enzyme layer cocktail was: 6 w% Hydrogel D4 and 2 w% GOx-CLEAs dissolved in 92 w% ethanol and water at a ratio of 9:1. The composition of the cocktail could be changed but the ratio of glucose oxidase and D4 should always stay the same. After dissolving the components the cocktail was sonified whilst being cooled in an ice bath.

Table 4.2: Settings of the Sonifier to Homogenise the Enzyme Layer Cocktaill

Parameter	Description	Value
Energy	ultrasonic energy in percent	25 %
Duration	overall sonification time	60 s
Pulse Duration	sonification time per cycle	1 s
Pause Duration	pause time between cycles	10 s

4.1.3 Diffusion Barrier Cocktails

In this master thesis two different diffusion barriers were used.

One diffusion barrier consisted of polyhydroxyethylmethacrylate dissolved in ethanol and water at a ratio of 19:1. The concentration of the polyHEMA was adapted during the different experiments and will be pointed out explicitly.

The second diffusion barrier cocktail consisted of 6 w% D4 and ethylcellulose at different ratios, in ethanol and water at a ratio of 9:1. Cocktails were prepared consisting of 20, 40, 50, 60, 70, 80 w% ethylcellulose in 6 w% D4 and ethylcellulose.

4.2 Profilometer Measurements

A Profilometer is an instrument to measure the vertical depth of a sample. A cantilever, or stylus, runs with an applied force across the sample and measures the depth or height of different features. The position of the cantilever, the measuring length, the duration and the force of the cantilever can be set manually. Sensors were measured by moving the cantilever over the centre of the sensor spot. Profilometer measurements were performed after inking each individual layer.

Table 4.3: Used Parameters of the Profilometer

Parameter	Description	Value
Scan Type	Sets when the stylus is reset and enables 3D scanning	Standard Scan
Range	Indicates the vertical resolution of the scan	65.5 μ m for Oxygen Spots 524 μ m for Enzyme and Diffusion Layers
Profile	Provides the measurement below or above the zero horizontal guideline	Hills & Valleys
Stylus Type	The currently used stylus type	Radius: 12.5 μ m
Stylus Force	Force of the scanning stylus	3 mg
Length	Determines the scan length	30000 μ m
Duration	Amount of time it takes to finish the scan	70 s
Resolution	Horizontal resolution with the given scan rate	1478 μ m/pt

The whole length of a slide, on which the sensors were printed, was measured and the

established data were cut in separated data that resembled each sensor on its own afterwards.

4.3 Assembling the Sensor Chips

The sensors were printed on polymer slides and then glued with adhesive tape on a rhombic chamber chip.

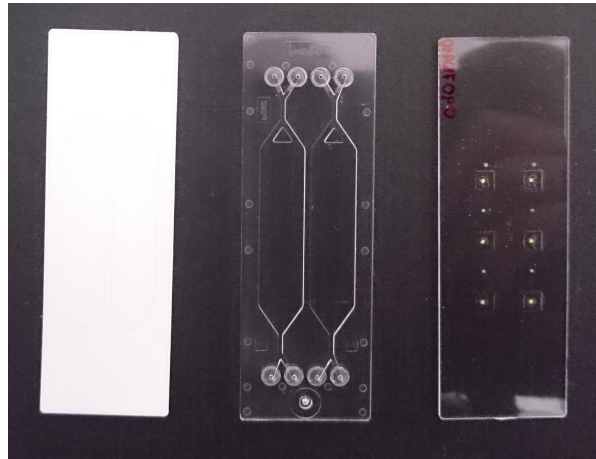


Figure 4.1: Picture of the Adhesive Tape, the Rhombic Chamber Chip and the Polymerslide with the Sensors

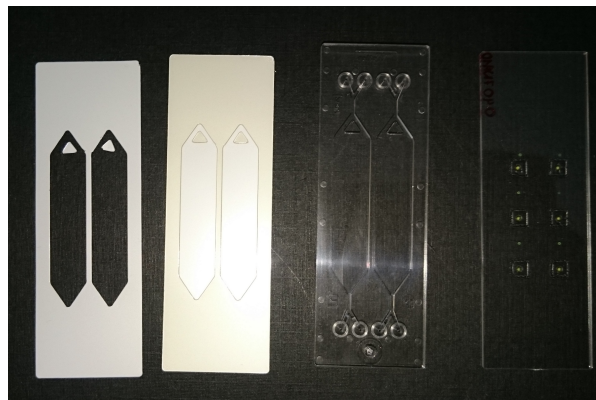


Figure 4.2: Picture of how one Side of the Adhesive Tape is Peeled off

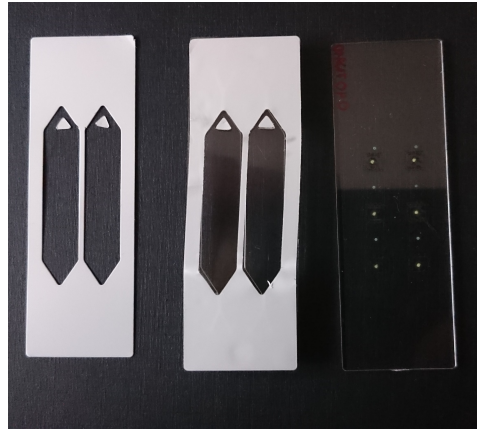


Figure 4.3: Picture of the Adhesive Tape Fixed on the Rhombic Chamber Chip

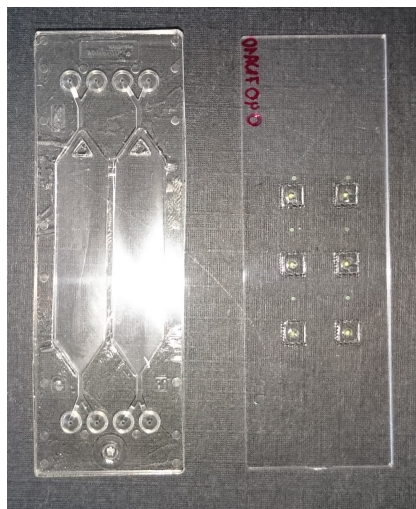


Figure 4.4: Picture of how the Cover of the Adhesive Tape is Peeled off the Rhombic Chamber Chip

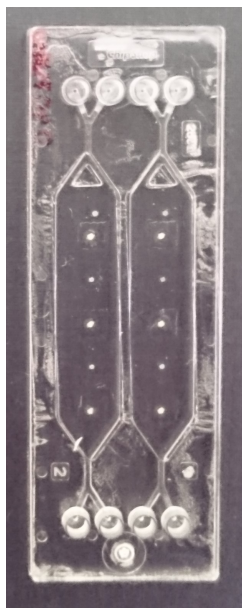


Figure 4.5: Picture of the Final Sensor Chip; the Chips consist of Oxygen and Glucose Sensors in Alternative Order, Beginning with an Oxygen Sensor

4.4 Glucose Buffer

Five litres of a pH 7.2 phosphate buffer (ionic strength 150 mmol) were prepared. The buffer contained 0.074 mmol sodiumdihydrogenphosphate, 0.1759 mmol disodiumhydrogenphosphate, 148.27 mmol sodiumchloride and 0.1 w% sodium azide. These compounds were dissolved in distilled water, the pH value was corrected to pH 7.2 using a 1 molar sodium hydroxide solution. The buffer was diluted up to 5 litres and to achieve full aeration it was bubbled using a porous stone with pressurised air for one hour.

A glucose stock solution was prepared with a concentration of 100 g/L glucose. For this purpose, the glucose was solved in the phosphate buffer and stored in the fridge for at least 24 hours to guarantee an equilibrium between α - and β -D(+)-Glucose.

Glucose buffer solutions with the following concentrations were prepared: 0, 0.5, 1, 2.5, 5, 7.5, 10, 12.5, 15 and 20 mM glucose.

4.5 Primary Sensors

The computerised numerical control and the microdispenser were already installed and ready to go. The different parameters used will be discussed individually but the meaning of the parameter are pointed out in 2.10.



Figure 4.6: The Setup of the Computerised Numerical Control and the Microdispenser

The different layers were printed on an PMMA slide. 5 sensors were printed next to each other. The first of them was an oxygen sensor spot. The distance between the sensors was 6 mm.

The different layers were printed using following microdispenser parameters:

Table 4.4: Microdispenser Settings

Oxygen Spot		Enzyme Layers		Diffusion Layers	
Parameter	Value	Parameter	Value	Parameter	Value
Pressure	0.4 bar	Pressure	0.4 bar	Pressure	0.4 bar
Nozzle	70 μm	Nozzle	200 μm	Nozzle	70 μm
Tappet	TTF-7	Tappet	TTF-7	Tappet	TTF-7
Tappet Lift	65 %	Tappet Lift	80 %	Tappet Lift	65 %
Rising Time	0.3 ms	Rising Time	0.3 ms	Rising Time	0.3 ms
Open Time	0.1 ms	Open Time	0.1 ms	Open Time	0.1 ms
Falling Time	0.1 ms	Falling Time	0.3 ms	Falling Time	0.2 ms
Delay	0.1 ms	Delay	0.2 ms	Delay	0.2 ms
Pulses	3	Pulses	15	Pulses	4

Three enzyme spot layers were printed as single droplets on top of the oxygen sensor spot. The Diffusion Barrier Layer was also dispensed as single droplets. Four diffusion barrier layer droplets were printed on top of each other. The profiles of the prepared layers were measured by profilometer.

4.5.1 The Microdispenser Spraying Add-On

To achieve a more homogeneously distributed diffusion barrier layer a microdispenser spraying add-on was tested. 2.5 w% polyHEMA dissolved in ethanol water were used because solutions with higher polyHEMA concentrations were too viscous. To test the reproducibility of the spraying add-on, layers were sprayed with the same parameters at different days. The spray add-on was moved over the polymer slide as tracks or as circles. The parameters of the microdispenser can be found in section 5.2.1.

4.5.2 Influence of the Substrate Materials and Properties of the Morphology of the Enzyme Layers

The diffusion layer was dispensed as a 4x4 matrix. The enzyme layer was printed by depositing one big droplet and 2 smaller ones on top of each other. The following parameters were used to print the oxygen layer, the enzyme and the diffusion layers.

Table 4.5: Microdispenser Parameters

Oxygen Spot		Enzyme Layers		Diffusion Layers	
Parameter	Value	Parameter	Value	Parameter	Value
Pressure	0.4 bar	Pressure	0.4 bar	Pressure	0.4 bar
Nozzle	70 μm	Nozzle	200 μm	Nozzle	70 μm
Tappet	TTF-7	Tappet	TTF-7	Tappet	TTF-7
Tappet Lift	65 %	Tappet Lift	53 %	Tappet Lift	37 %
Rising Time	0.3 ms	Rising Time	0.2 ms	Rising Time	0.2 ms
Open Time	0.1 ms	Open Time	0.5 ms	Open Time	0.1 ms
Falling Time	0.1 ms	Falling Time	0.1 ms	Falling Time	0.2 ms
Delay	0.1 ms	Delay	0.1 ms	Delay	0.2 ms
Pulses	3	Pulses	5x, 3x, 1x	Pulses	3

The diffusion barrier layer was dropped as a 4x4 matrix and 10 w% polyHEMA in ethanol and water were used. Further on the behaviour of the enzyme layer was examined on different support materials (slides), including glass, silanised glass, PMMA, plasma etched PMMA, PS, plasma etched PS, PC, plasma etched PC, Topas and plasma etched Topas.

To investigate the behaviour of sensors on different support materials the slides were glued on a 250 μl rhombic chamber chip. Then changes in phaseangles of the sensors were measured while they were being flushed with different glucose buffers of concentrations 0, 0.5, 1, 2.5, 5, 7.5, 10, 12.5, 15 and 20 mM glucose at a flow velocity of 5 mm/s. The flushing lasted 120 s.

4.6 Final Sensors

The enzyme layer was printed by depositing one big droplet and 2 smaller ones on top of each other. The number of layers of the diffusion barrier layer, which consisted of polyHEMA, was variated. The amount of ethylcellulose was varied by changing the ratio between ethylcellulose and Hydrogel D4 in solution.

The parameters which were used to microdispense the sensors can be seen in the following table. The polyHEMA diffusion layer was printed as a 4x4 matrix, the ethylcellulose diffusion barrier was dispensed as a 6x6 matrix.

Table 4.6: Printing Parameters of the Microdispenser

Oxygen Spot		Enzyme Layers		Diffusion Layers	
Parameter	Value	Parameter	Value	Parameter	Value
Pressure	0.4 bar	Pressure	0.4 bar	Pressure	0.4 bar
Nozzle	70 μm	Nozzle	200 μm	Nozzle	70 μm
Tappet	TTF-7	Tappet	TTF-7	Tappet	TTF-7
Tappet Lift	65 %	Tappet Lift	50 %	Tappet Lift	37 %
Rising Time	0.3 ms	Rising Time	0.2 ms	Rising Time	0.2 ms
Open Time	0.1 ms	Open Time	0.5 ms	Open Time	0.1 ms
Falling Time	0.1 ms	Falling Time	0.1 ms	Falling Time	0.2 ms
Delay	0.1 ms	Delay	0.1 ms	Delay	0.2 ms
Pulses	3	Pulses	5x, 5x, 3x, 1x	Pulses	3 ms

Sensors prepared in the following chapters were microdispensed using the parameters from above. The slides, which the sensors were printed on, were glued on an 250 μl rhombic chamber chip. Then changes in phase angle of the sensors were measured while the chambers were being flushed with different glucose buffers of concentrations 0, 0.5, 1, 2.5, 5, 7.5, 10, 12.5, 15 and 20 mM glucose at a flow velocity of 5 mm/s. The flushing lasted 120 s.

4.7 Sensor Reproducibility

To measure if the production of the sensors is reproducible the same sensors (using the same microdispenser parameters and the same number of layers) were printed next to each other on a PMMA slide. The slides, on which the sensors were printed, were glued on a 250 μl rhombic chamber chip. Then changes in phase angle of the sensors were measured while the chambers were being flushed with different glucose buffers of concentrations 0, 0.5, 1, 2.5, 5, 7.5, 10, 12.5, 15 and 20 mM glucose at a flow velocity of 5 mm/s. The flushing lasted 120 s.

The same sensors were measured after 10 days with the same measurement parameters. Sensors with polyHEMA as diffusion barrier layer consisted of 14 diffusion layers, ethylcellulose as diffusion layer consisted of 60% ethylcellulose and 40% D4.

4.8 Flow Velocity Dependency

To investigate the flow rate dependency of the sensors, slides with sensors were glued to 250 μl and 120 μl rhombic chamber chips. The sensors were printed on a PMMA slide. Then the shifts in the phase angles were measured while the sensors were being flushed with different glucose buffers of concentrations 0, 0.5, 1, 2.5, 5, 7.5, 10, 12.5, 15 and 20 mM glucose at different flow velocities of 11, 8, 5, 3.5, 3, 2, 1.5 mm/s for 120 s. Sensors with polyHEMA as diffusion barrier layer consisted of 22 diffusion layers.

The sensors were measured again at slower flow velocities of 5, 1, 0.1, 0.01, 0.01, 0.001 mm/s and at steady state.

4.9 Bulk Measurements

To measure the behaviour of glucose sensors, printed on PMMA slides, in higher volumes an oxygen sensor and a glucose sensor, consisting of 20 layers of polyHEMA as diffusion barrier layer, were fixed on a fibre and put into a beaker. The beaker was filled with different glucose buffer solutions and alternatively stirred or not stirred. The change of the phaseangle was measured.

4.10 Oxygen Calibration

One glucose sensor, printed on a PMMA slide, was fixed on a fibre and dipped into 0 mM glucose buffer. Then the solution was bubbled with ratios of air and nitrogen using a gas mass flow controller. 100, 80, 60, 40, 20, 0 % air were bubbled through the solution for 5 hours.

5 Results and Discussion

5.1 The Glucose Sensors Prepared in this Thesis

The glucose sensors prepared in this thesis consist of three different layers.

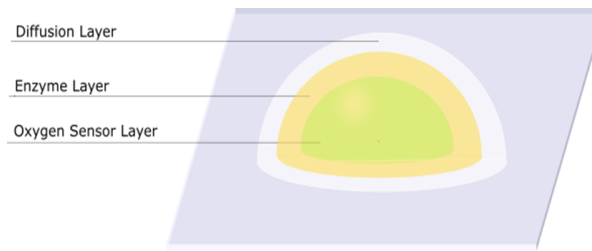


Figure 5.1: Composition of the Glucose Sensor

The uppermost layer is a diffusion layer. Through this layer oxygen can pass unhinderedly but the diffusion of glucose is controlled. So only a fraction of the glucose in solution reaches the next layer. With the diffusion layer it is possible to make the reaction velocity dependent on diffusion and not dependent on the enzyme activity.

The next layer is an enzyme layer. Glucose is metabolised according to following equation.



In the last layer the luminescence lifetime of a fluorophore is quenched in presence of oxygen. Therefore, a high glucose concentration in the solution leads to a lot of metabolised glucose and used-up oxygen. Following this the quenching of the lifetime is low if there is only little glucose present which is the case if there is a lot of glucose in the solution.

5.2 Optimisation of the Printing Parameters

The sensors were printed according to chapter 4.5. Profilometer measurements of the single layers were performed and evaluated. The resulting height profiles of the sensors and the height evolution after printing each layer individually can be seen in the following diagram.

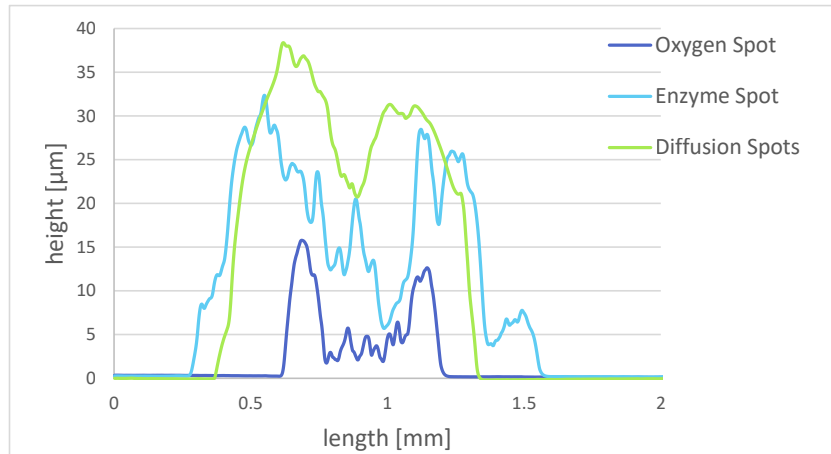


Figure 5.2: Profilometer Measurements of a Sensor

The oxygen sensor spot is about $600\ \mu\text{m}$ wide and at the highest point $15\ \mu$ high. A strong coffee ring effect can be seen with the height in the centre being much lower than at the edge. The coffee ring effect happens when a drop of liquid dries on a surface, its particulate matter is deposited in a ring like way. The capillary flow outward of the centre brings particles to the edge of the drop as evaporation proceeds. The height in the centre of the droplet is about 3 to $5\ \mu\text{m}$. The coffee ring effect inhibits the homogenous deposition of single layers. As the oxygen spot has a diameter of $600\ \mu\text{m}$ and the optical fibre, which the sensor is measured with, has a diameter of $1\ \text{mm}$, the whole sensor can be measured. Therefore, the influence of the coffee ring effect for the oxygen sensor layer is negligible.

The three on top of each other deposited enzyme droplets have a length of $1.4\ \text{mm}$ and the height at the highest point is about $32\ \mu\text{m}$. The enzyme layer also shows a coffee ring effect with the lowest point being $7\ \mu\text{m}$.

Four droplets of diffusion barrier layer are printed on top of each other. The total diffusion barrier has a maximum height of $38\ \mu\text{m}$, but also forms a coffee ring. The lowest measured point has a height of $22\ \mu\text{m}$. The diffusion barrier layer does not cover the enzyme layer completely. As a next step the microdispenser spraying add-on is evaluated.

5.2.1 Evaluation of the Microdispenser Spraying Add-On for the Application of Diffusion Barrier Layer

The nozzle of the microdispenser is replaced by the microdispenser spraying add-on. The spraying add-on enables a fine distribution of droplets due to an air stream. $2.5\ \text{w\%}$ polyHEMA dissolved in ethanol and water are dispensed on a PMMA slide as tracks and as circles. Printing as tracks means that the microdispenser is moved across the polymer slide in one direction and that the tappet is lifted at places where the final diffusion barrier layer should be situated. Spraying as circles means that the tappet opens and the microdispenser moves in a circle around the spot where the final diffusion barrier layer should be situated. The parameters

of the microdispenser, which were used to print the diffusion barrier layers as tracks, are the following:

Table 5.1: Parameters of the Microdispenser

Parameter 1	Value	Parameter 2	Value
Pressure	0 bar	Pressure	0 bar
Tappet	TTF-7	Tappet	TTF-7
Tappet Lift	22 %	Tappet Lift	25 %
Rising Time	0.1 ms	Rising Time	0.1 ms
Open Time	0.5 ms	Open Time	0.5 ms
Falling Time	1 ms	Falling Time	0.5 ms
Delay	0.1 ms	Delay	0.1 ms
Pulses	100	Pulses	10

50 layers of 2.5 w% polyHEMA in ethanol and water at a ratio of 19:1 were printed on top of each other. There was a waiting time of 10 minutes between every sprayed layer. Layers were printed on three different days. The height profiles of the different diffusion layers with different parameters were measured.

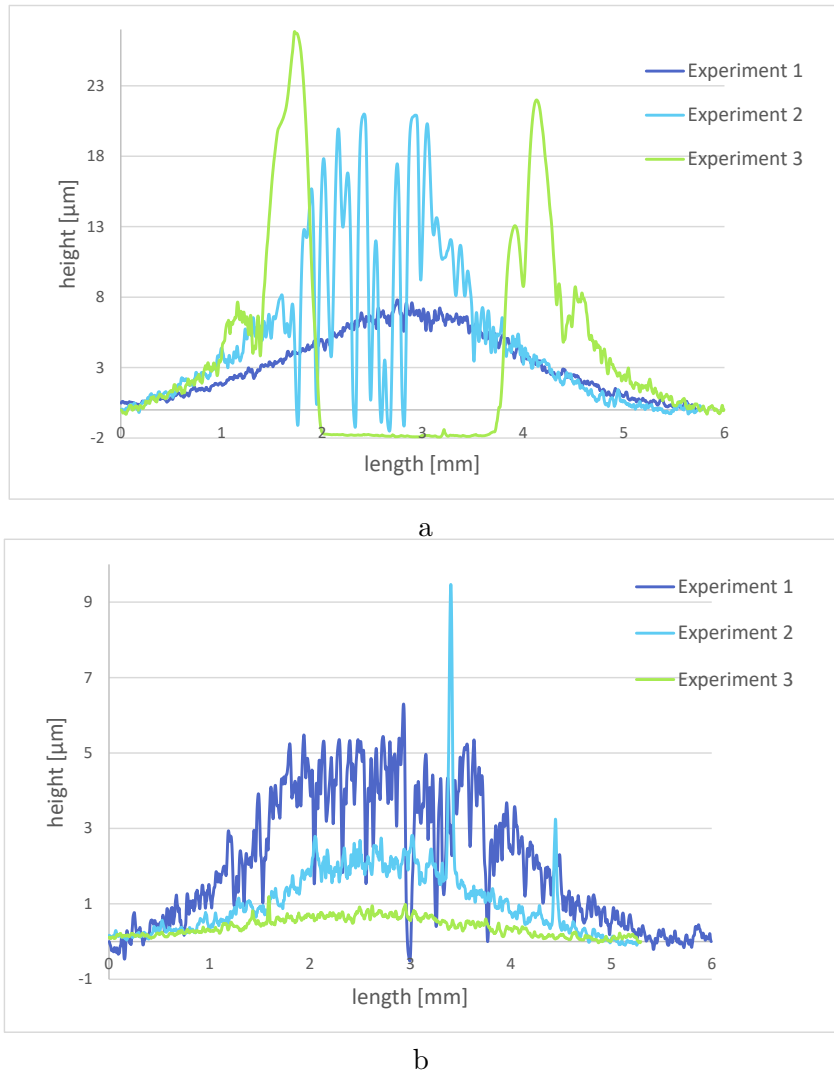


Figure 5.3: Profilometer Measurements of the Diffusion Barrier Layers Sprayed as Tracks with Different Properties,
a: Parameters 1
b: Parameters 2

The spraying of tracks via the microdispenser spraying add-on is not reproducible. The diffusion barrier layers sprayed with parameters 1 show different height profiles. While the diffusion barrier layers printed in experiment 1 shows a homogenous distribution of the poly-HEMA particles around a central point, layers printed in experiment 2 formed a small coffee ring and the outer parts of the layers are higher than in experiment 1. In experiment 3 the air flow of the spray add-on was too strong in the centre of the track, so that no polyHEMA was dispensed there.

In the second diagram height profiles of diffusion layers sprayed as tracks with parameters 2 can be seen. In experiment 1 polyHEMA was sprayed evenly with a centre point and a good height development. In experiment 2 and 3 the height decreases drastically and in experiment

3 hardly any deposition of polyHEMA was observed.

Spraying the diffusion layer as tracks is not reproducible and as a consequence polyHEMA was sprayed as circles. The circles were sprayed with following parameters:

Table 5.2: Parameters of the Microdispenser

Parameter	Value
Pressure	0 bar
Tappet	TTF-7
Tappet Lift	22 %
Rising Time	0.1 ms
Open Time	0.5 ms
Falling Time	1 ms
Delay	0.1 ms
Pulses	100

50 layers of 2.5 w% polyHEMA in ethanol and water at a ratio of 19:1 were printed on top of each other. There was a waiting time of 10 minutes between every layer sprayed. Layers were printed on three different days. The height profiles of the different diffusion layers with different parameters were measured.

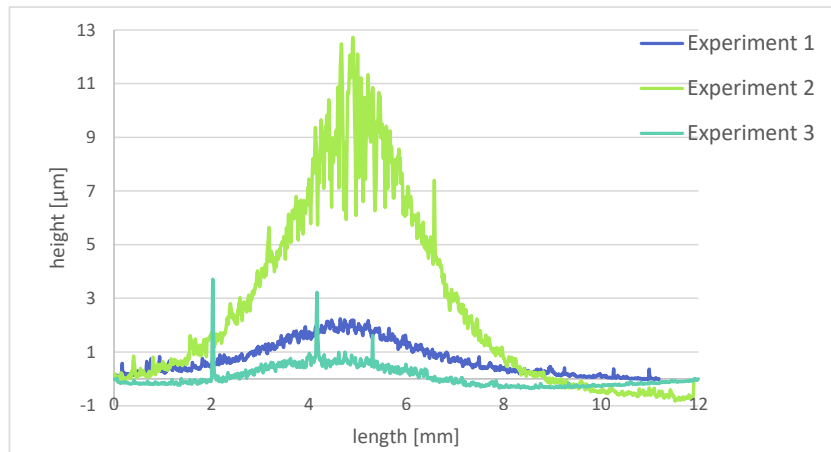


Figure 5.4: Profilometer Measurements of the Diffusion Barrier Layer Sprayed as Circles

The diffusion barrier layers sprayed in experiment 1 had medium height evolution, in experiment 2, however, the height of the layers increased by about $11 \mu\text{m}$. In experiment 3 the height of the layers decreased to less than $1 \mu\text{m}$.

The microdispenser spray add-on is not reproducible for 2.5 w% polyHEMA solutions. A possible reason is that the spray itself is not reproducible or the polyHEMA cocktail clogs the system. The system cannot be cleaned properly between the dispensings but was cleaned at the end of each experiment. Diluting the polyHEMA diffusion barrier cocktail to lower

concentrations is possible, but this would lead to higher concentrations of solvents in the cocktail and consequently also more solvent molecules dispensed. This results in longer drying periods to evaporate the whole solvent. Furthermore, more layers have to be dispensed to achieve the same diffusion barrier layer thickness. This is a very time-consuming factor and was therefore not tried in this thesis.

5.2.2 Influence of the Substrate Materials and Properties on the Morphology of the Enzyme Layers

Two methods were tried to reduce the coffee ring effect in the glucose oxidase enzyme layer. The microdispenser parameters were adjusted so that the lowermost droplet was the biggest one and smaller droplets were dispensed in the middle of the first big enzyme droplet. The parameters used are pointed out in section 4.5.2.

The second method implied trying and printing on different support materials and evaluating if the surface tension of different slides had any influence on the coffee ring formation. Glass, silanised glass, PMMA, plasma etched PMMA, PS, plasma etched PS, Topas, plasma etched Topas, PC and plasma etched PC were used as different support material slides. Silanising means that silane compounds are bound to a surface, in this case glass. Silanised glass is used to prevent the adhering of polar components. Plasma etching removes the uppermost atom layer of a substrate and other atoms can adsorb on the surface. Oxygen plasma etching produces a more hydrophilic surface.

To find out if different surface tensions change the coffee ring effect, the sensors were measured using the profilometer. To provide better visualisation of the sensors only the oxygen layer and the enzyme layers are shown in the following graphs.

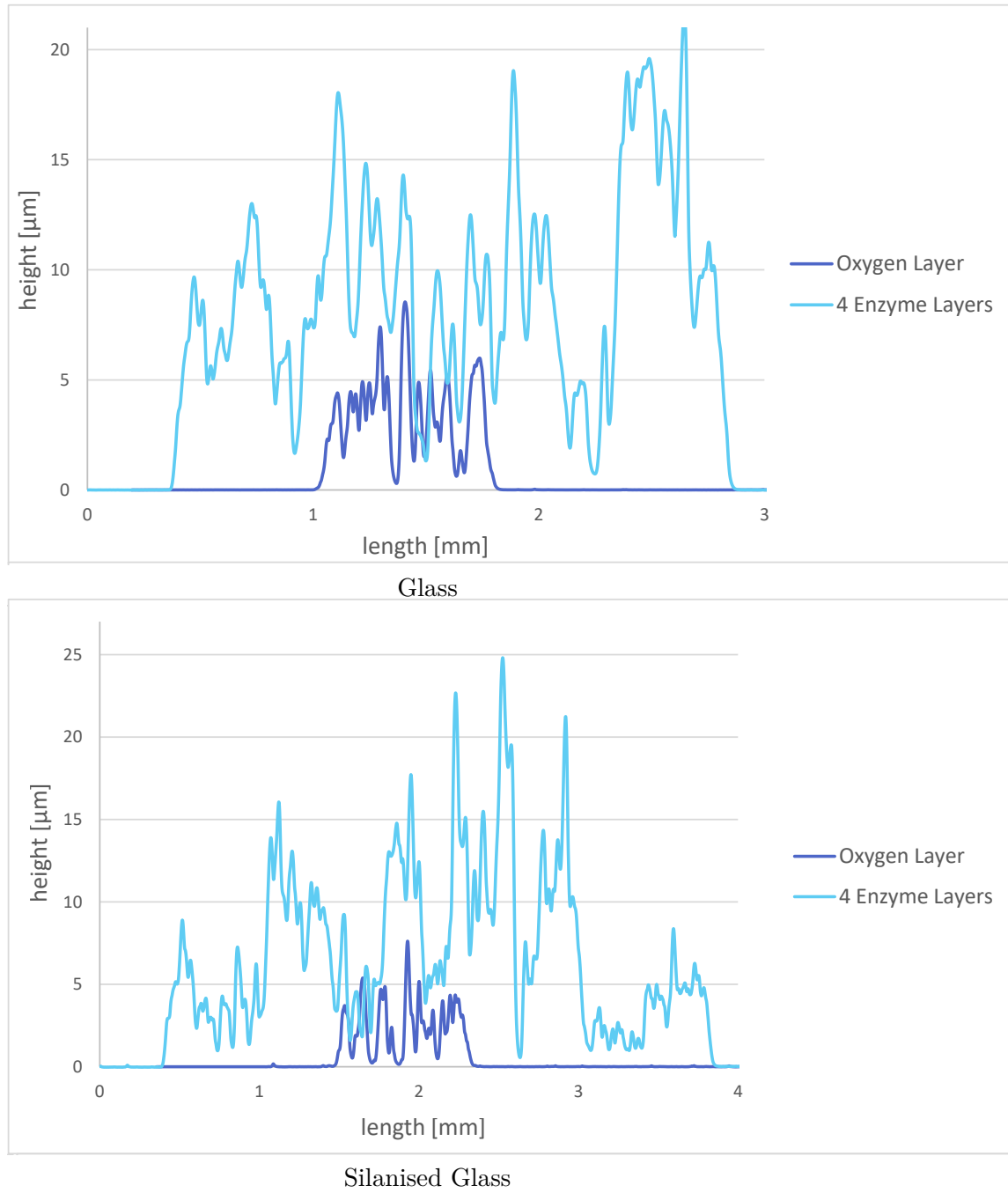
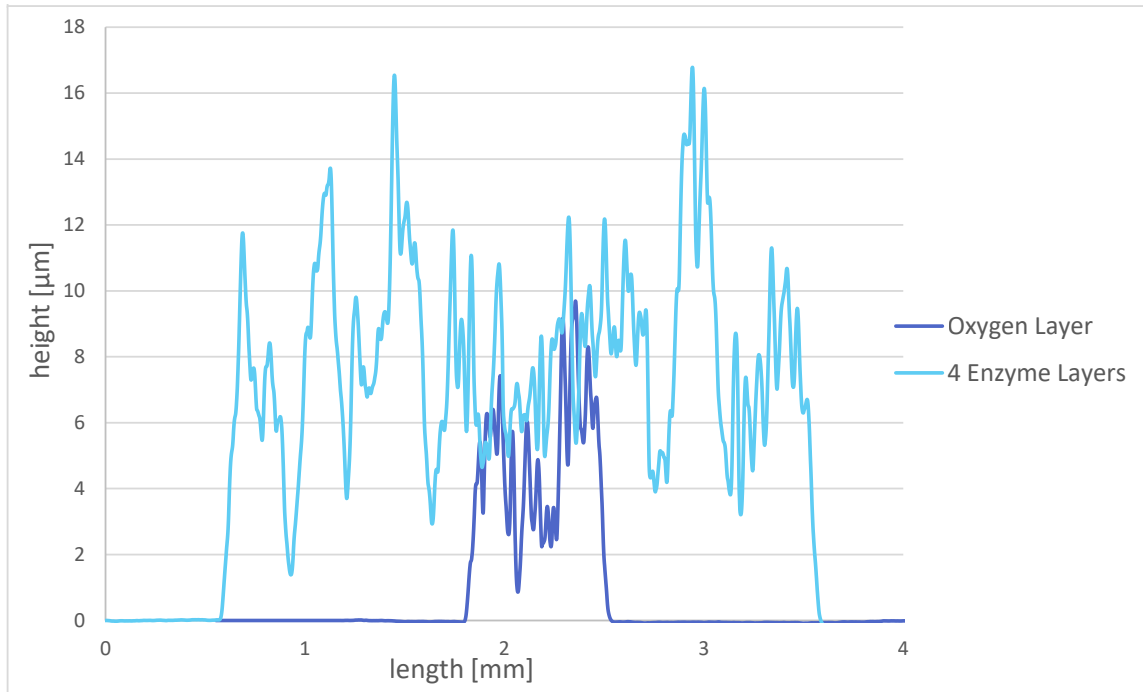
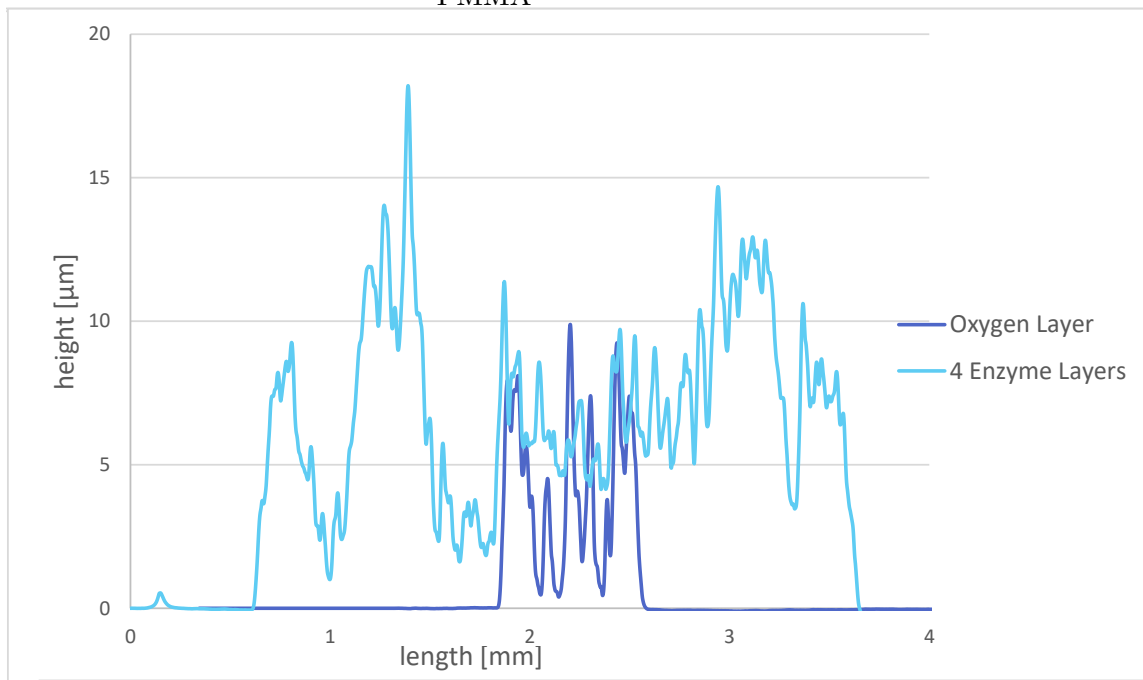


Figure 5.5: Profilometer Measurements of the Oxygen Layer and the Enzyme Layer on Glass and Silanised Glass

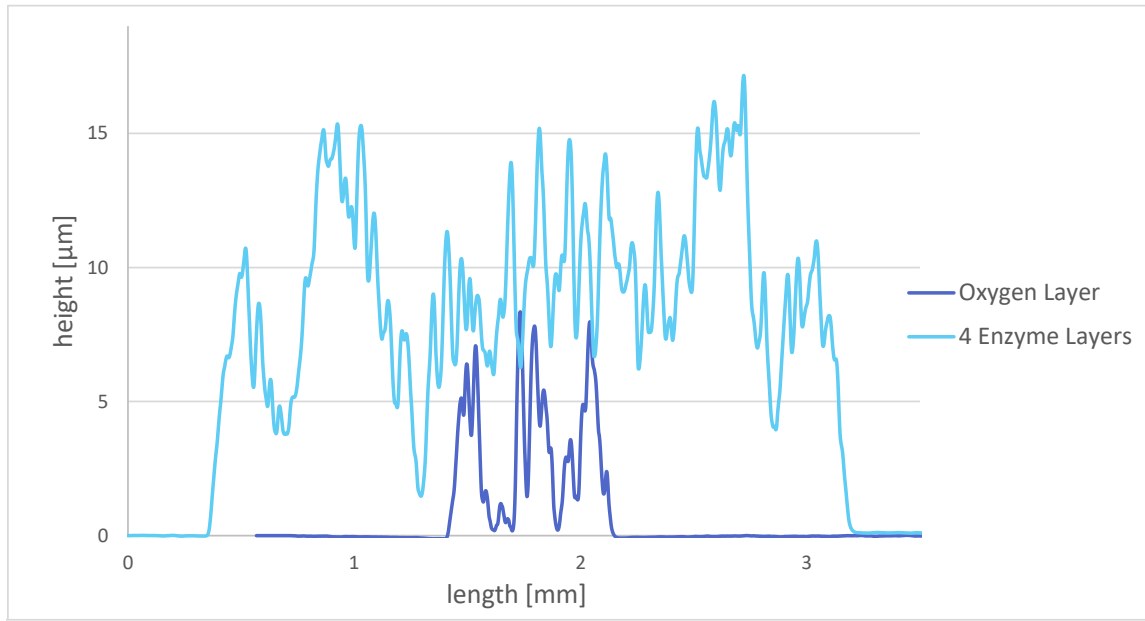


PMMA

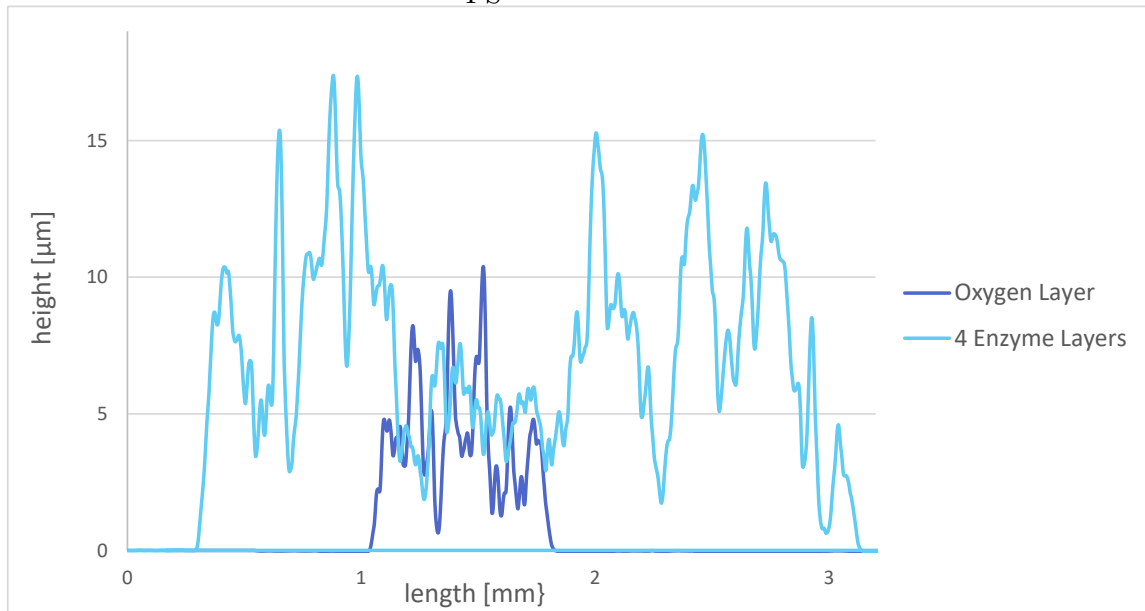


Plasma Etched PMMA

Figure 5.6: Profilometer Measurements of the Oxygen Layer and the Enzyme Layer on PMMA and Plasma Etched PMMA



PS



Plasma Etched PS

Figure 5.7: Profilometer Measurements of the Oxygen Layer and the Enzyme Layer on PS and Plasma Etched PS

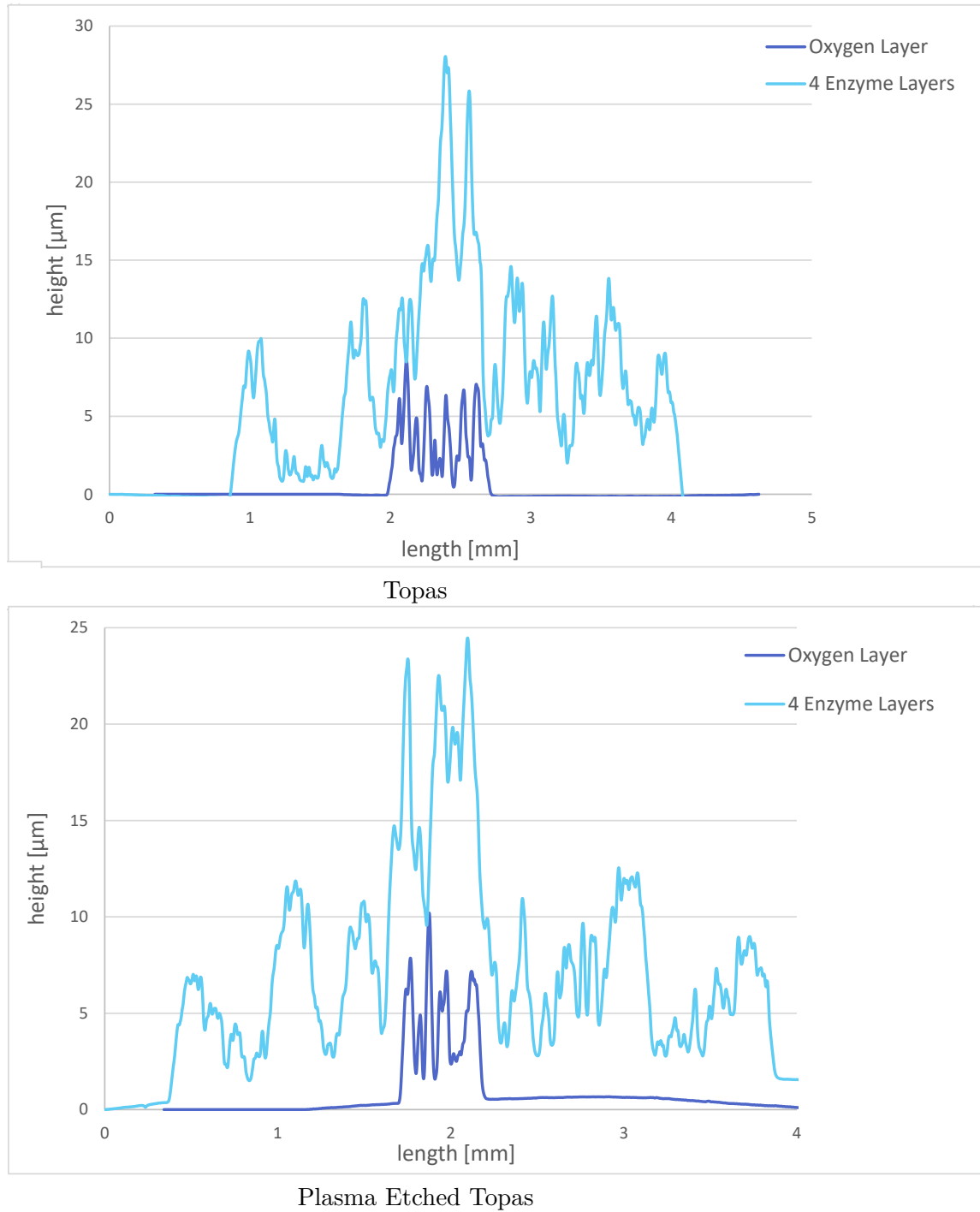
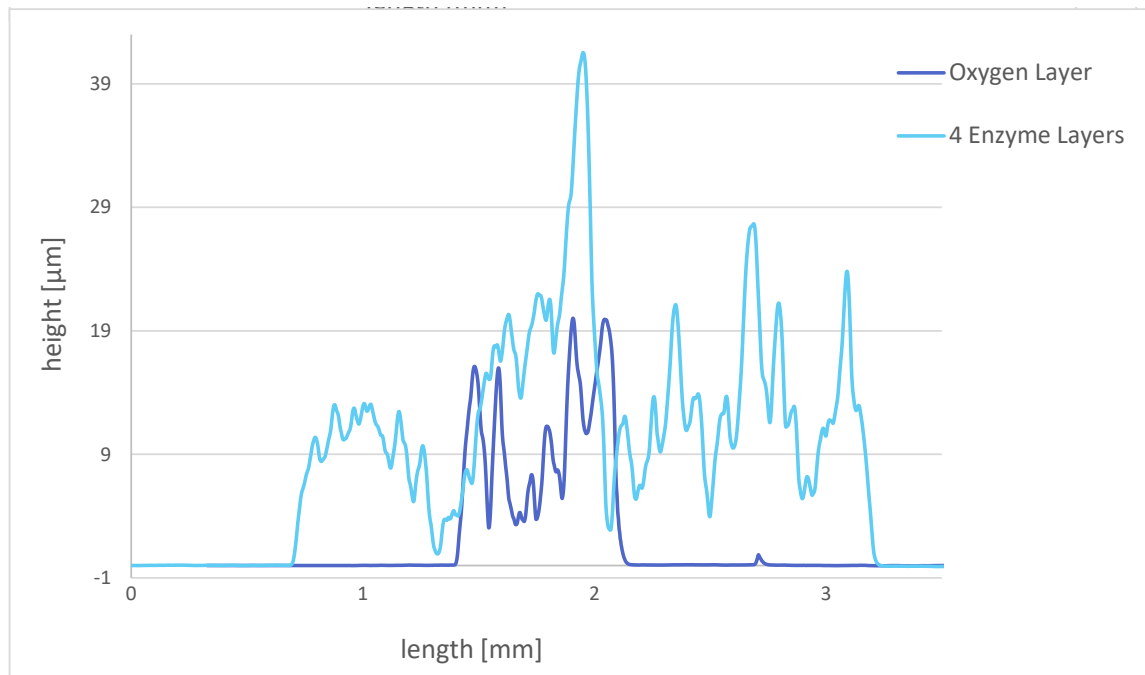
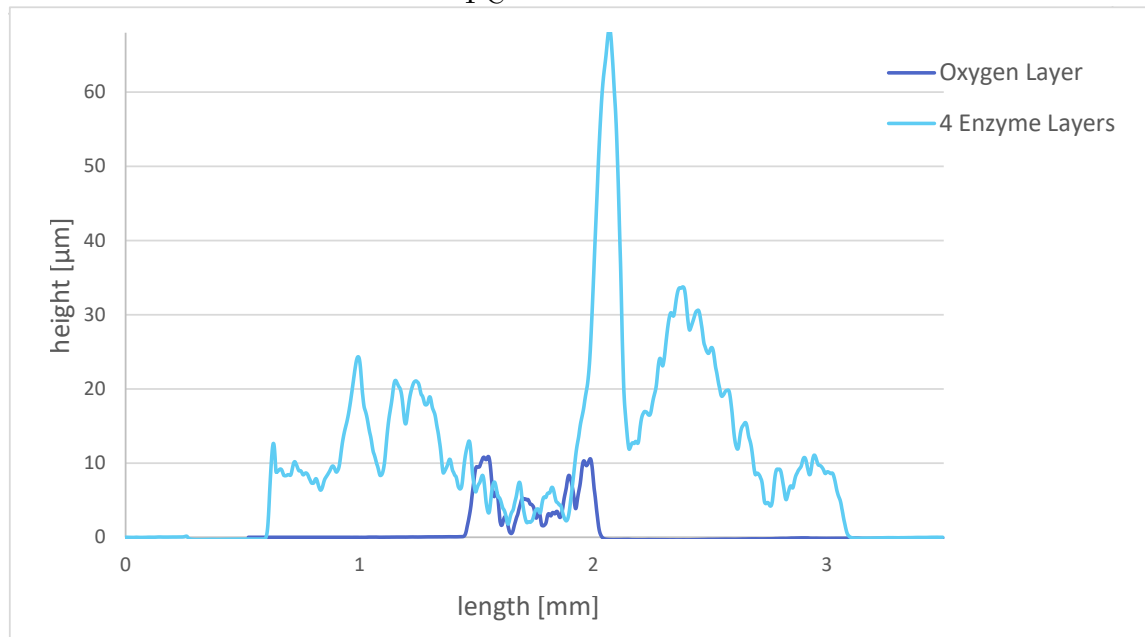


Figure 5.8: Profilometer Measurements of the Oxygen Layer and the Enzyme Layer on Topas and Plasma Etched Topas



PC



Plasma Etched PC

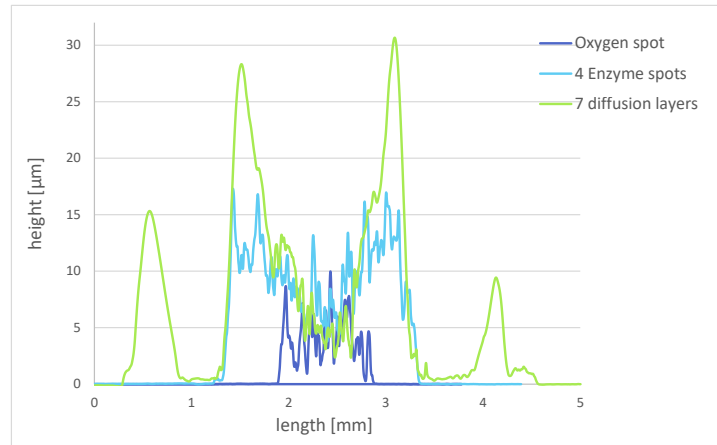
Figure 5.9: Profilometer Measurements of the Oxygen Layer and the Enzyme Layer on PC and Plasma Etched PC

The coffee ring effect is minimized for glass, silanised glass, PMMA, PS, Topas and PC. Dispensing one big droplet and smaller ones on top of this droplet reduce the coffee ring effect, but form a rather rough surface. For the plasma etched polymer slides the coffee ring effect is still visible. Topas behaves differently in comparison with the other support slides, where a big

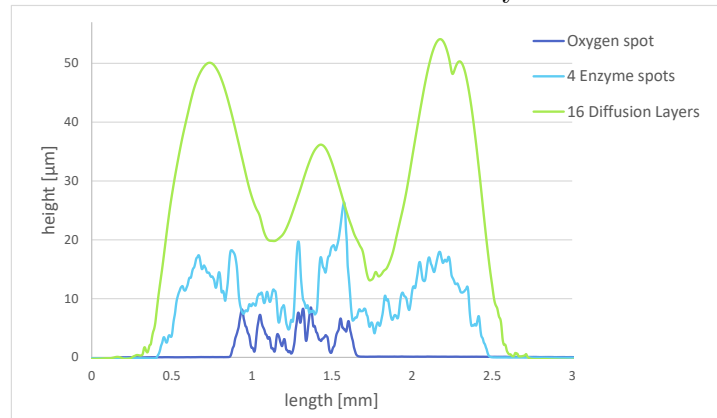
hill is formed in the middle, this is sign that there are air bubbles as inclusions in the glucose oxidase enzyme layer. The different layers show good adhesion to every material and can also be characterised by different glucose buffer solutions as can be seen in section 5.4.

5.2.3 Diffusion Barrier Height Variation

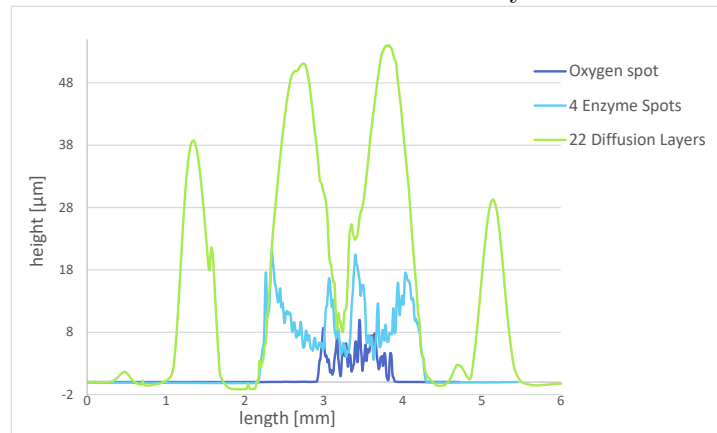
To tune the dynamic range of the glucose sensors, different numbers of polyHEMA diffusion barrier layers were printed on top of each other on PMMA slides. In order to see how these layers influence the height of the diffusion barrier layer, profilometer measurements were performed with sensors of different heights. Diagrams of profiles with 7, 16 and 22 polyHEMA diffusion barrier layers are shown below.



Sensor with 7 Diffusion Barrier Layers



Sensor with 16 Diffusion Barrier Layers



Sensor with 22 Diffusion Barrier Layers

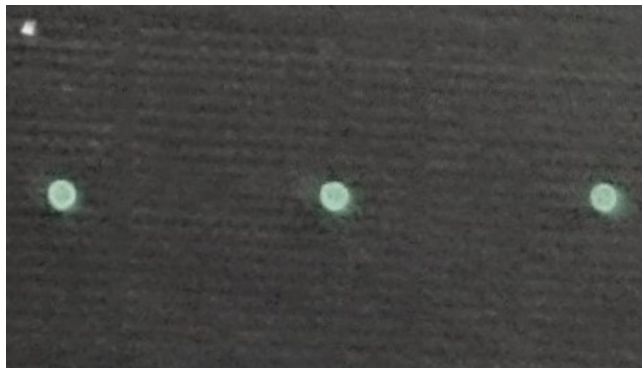
Figure 5.10: Profilometer Measurements of Sensors with Different Numbers of Diffusion Barrier Layers

The oxygen sensor spots are about 1 mm long and $8 \mu\text{m}$ high. The glucose oxidase diffusion layer is 2 mm long and $17 \mu\text{m}$ high. The length of the diffusion barrier layer varies from chip to chip. The height of the diffusion layer increases (from maximum to maximum) from $30 \mu\text{m}$

for 7 diffusion layers to 53 μm for 16 diffusion layers. Also at the minimum the diffusion layer becomes higher. From 16 diffusion barrier layers to 22 diffusion barrier layers the height does not change anymore, but the coffee ring effect increases drastically. So depositing more layers on top of each other increases the height of the sensors for up to 16 diffusion barrier layers, but at even more layers only the coffee ring effect gets bigger.

5.3 Final Printed Sensors

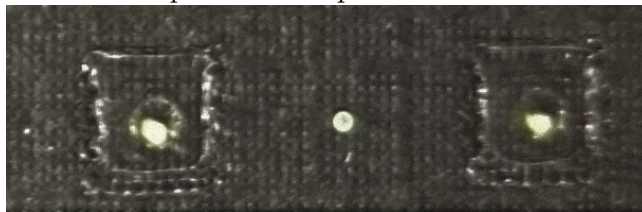
After reducing the coffee ring effect, all the sensors were printed the same way, as described in section 4.6.



Oxygen Sensor Spots



Oxygen Sensor Layer with Enzyme Layers
Deposited on top of it



On the Left and on the Right are 2
Finished Glucose Sensors, in the Middle is
an Oxygen Sensor



The Finished Sensors in a 250 μ L Rhombic Chamber Chip. Beginning from the Left there is Alternatively a Glucose Sensor and an Oxygen Sensor Next to Each Other.

Figure 5.11: Pictures of the Different Layers and a Finished Chip

5.3.1 Performance of the Oxygen Sensor Spot

The oxygen calibration was performed as explained in section 4.10 and a calibration curve was recorded.

The resulting ϕ values were converted to lifetime values with the following formula:

$$\tau = \frac{\tan\phi}{2\pi f} \quad (5.2)$$

- $\Delta\Phi$... *phase shift in radian*
 τ ... *luminescence lifetime*
 ω ... *circular modulation frequency*
 f ... *modulation frequency*

Then the resulting value of τ was divided by the τ at anaerobic conditions, also called τ_0 . The calculated values were plotted against the partial pressure of oxygen which was bubbled into the buffer solution.

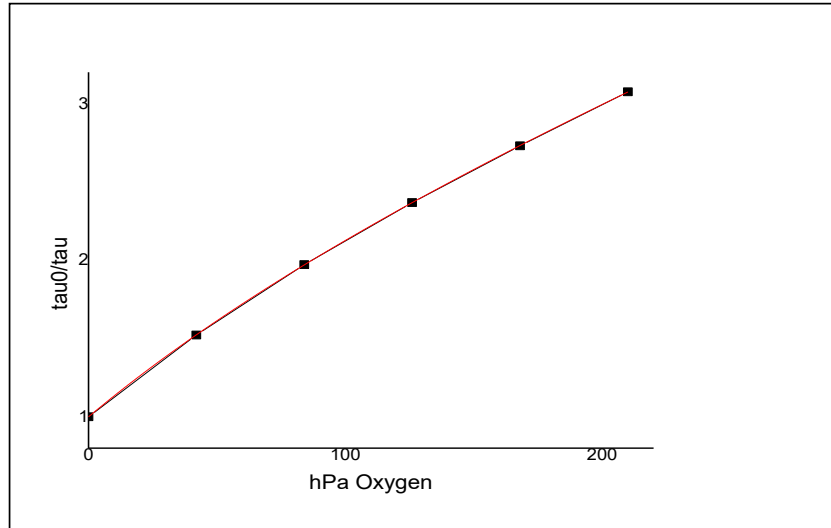


Figure 5.12: Oxygen Calibration and Stern-Volmer Two-Site Model

Using a modified Stern-Volmer equation, adapted from a two-site model [57], the calibration fits the non-linear Stern-Volmer plots. The two-site model assumes the localisation of the indicator in two regions of different microenvironments.

The resolution equation was:

$$\frac{\tau}{\tau_0} = \frac{f_1}{1 + K_{SV1} * pO_2} + \frac{f_2}{1 + K_{SV2} * pO_2} \quad (5.3)$$

τ ... lifetime at given oxygen concentration

τ_0 ... lifetime under anaerobic conditions

K_{SV} ... Stern – Volmer constants

f ... fractions of the total emission

$$\frac{\tau}{\tau_0} = \frac{1}{\frac{0.80079}{1+0.01676*pO_2} + \frac{1-0.80079}{1+0.00164*pO_2}} \quad (5.4)$$

Using the values from the Stern-Volmer equation of the calibration curve, the oxygen partial pressures can be calculated from the measured dphi values.

5.3.2 Response of Printed Sensors to Glucose

A sensor response curve was recorded with a sensor with 20 layers of polyHEMA in the diffusion barrier layer, in a 250 μ L rhombic chamber chip, which was flushed with different glucose buffers at a flow velocity of 1.5 mm/s. The diagram below shows how the difference in the partial pressure changes with time and with different glucose concentrations.

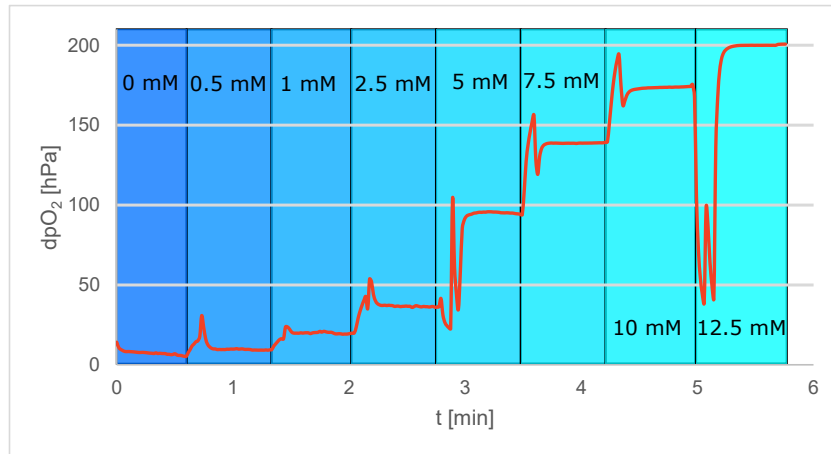


Figure 5.13: Response Curve of a Sensor

The figure shows that after beginning to flush with different glucose buffer solutions at a flow velocity of 2 mm/s the signal reaches a constant value in about 20 seconds. The spikes in the graph result from the stopped flow, where the pump refills with buffer.

5.4 Glucose Sensors Printed on Different Support Materials

Sensors printed on different support materials were tested by flushing them with glucose buffer solutions.

Table 5.3: Phase Angle Values of Sensors exposed to Air Saturated pH 7.2 Phosphate Buffer

Substrate	dphi of Oxygen Spot	dphi of Glucose Sensor at 0 mM Glucose	Standard Deviation of the dphi of the Glucose Spot
Glass	18.62	19.276	0.813
silanised Glass	18.3	18.776	1.243
PMMA	18.48	19.001	0.560
plasma etched PMMA	19.497	18.761	0.473
PS	17.65	19.485	0.787
plasma etched PS	19.717	16.834	3.526
Topas	19.227	19.142	1.600
plasma etched Topas	18.489	20.655	0.361
PC	19.742	19.981	0.988
plasma etched PC	18.793	19.846	0.399

The phase angle values in an air saturated solution for oxygen spots and glucose sensors spots were different and therefore, the difference in the partial pressure of oxygen was not calculated. The following diagrams show the change in phase angle of glucose and oxygen sensors on different substrates.

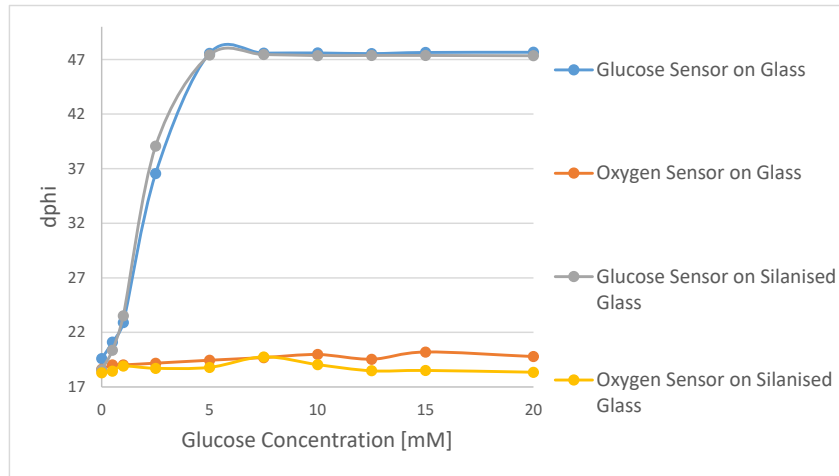


Figure 5.14: Sensors on Glass and Silanised Glass Exposed to Various Glucose Concentrations in Phosphate Buffer pH 7.2

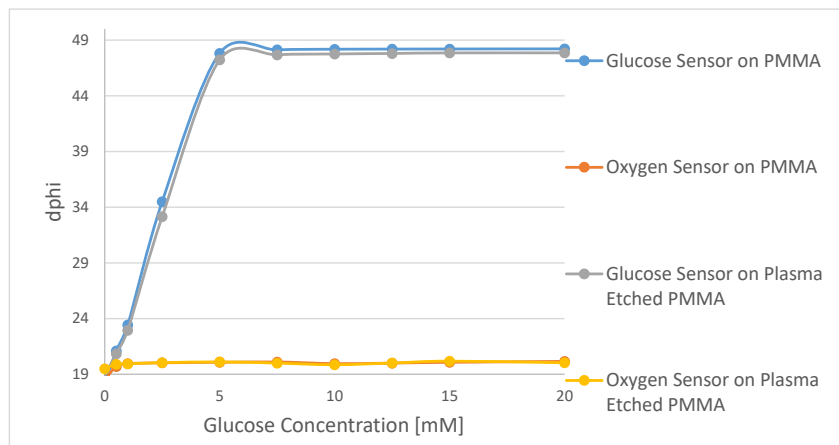


Figure 5.15: Sensors on PMMA and Plasma Etched PMMA Exposed to Various Glucose Concentrations in Phosphate Buffer pH 7.2

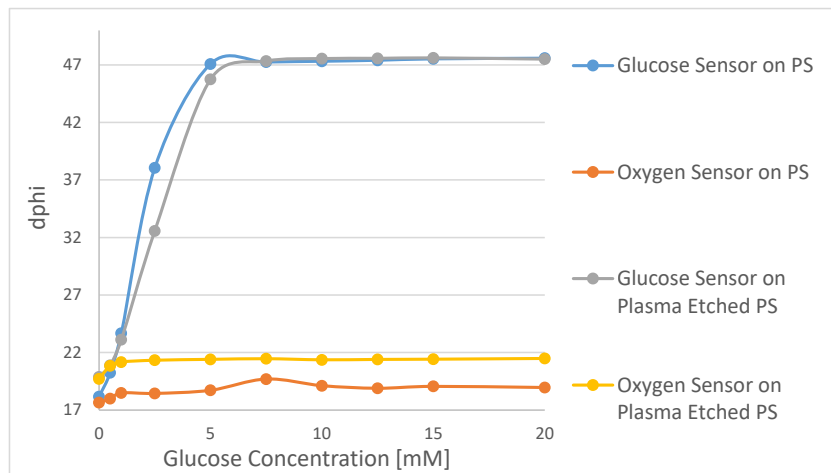


Figure 5.16: Sensors on PS and Plasma Etched PS Exposed to Various Glucose Concentrations in Phosphate Buffer pH 7.2

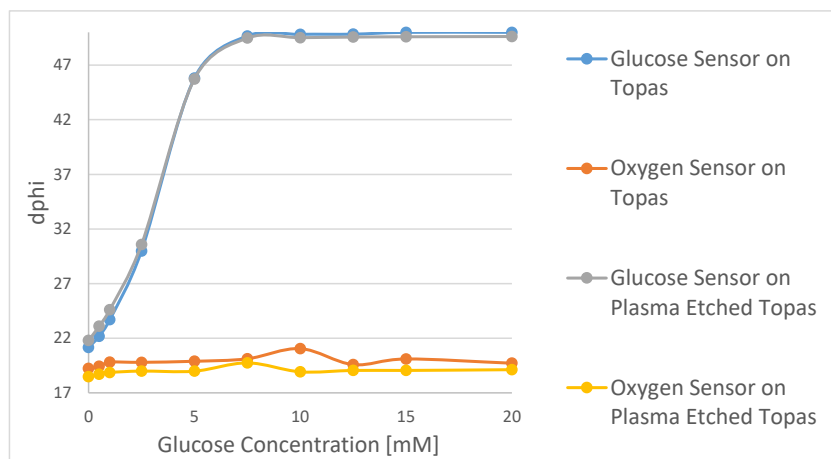


Figure 5.17: Sensors on Topas and Plasma Etched Topas Exposed to Various Glucose Concentrations in Phosphate Buffer pH 7.2

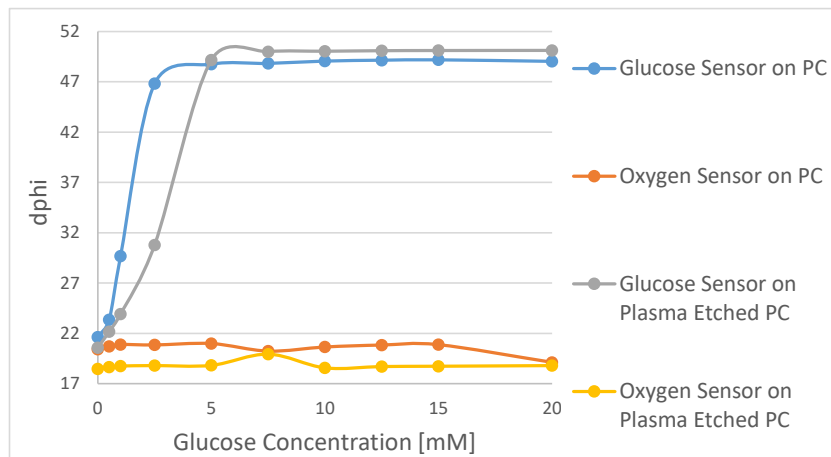


Figure 5.18: Sensors on PC and Plasma Etched PS Exposed to Various Glucose Concentrations in Phosphate Buffer pH 7.2

The oxygen sensor on plasma etched polymers differed more from the glucose values on the same plasma etched polymer slide in air saturated solutions than on non-plasma etched polymer slides. In general the dynamic range of the sensors stayed the same for every support material except for Polycarbonate. The difference in the phase angles of the oxygen sensor and the glucose sensor are possibly a sign that the solvents swell the polymer slides.

5.5 Influence of Diffusion Layer Height on Dynamic Range

The dynamic range of the glucose sensors can be changed by varying the height of the diffusion barrier layer or the diffusion barrier layer itself. Diffusion barrier layers with higher thickness indicate that glucose reaches the enzyme layer more slowly due to diffusion speed. Therefore, at higher glucose concentrations oxygen is still present and measuring higher glucose concentrations is possible.

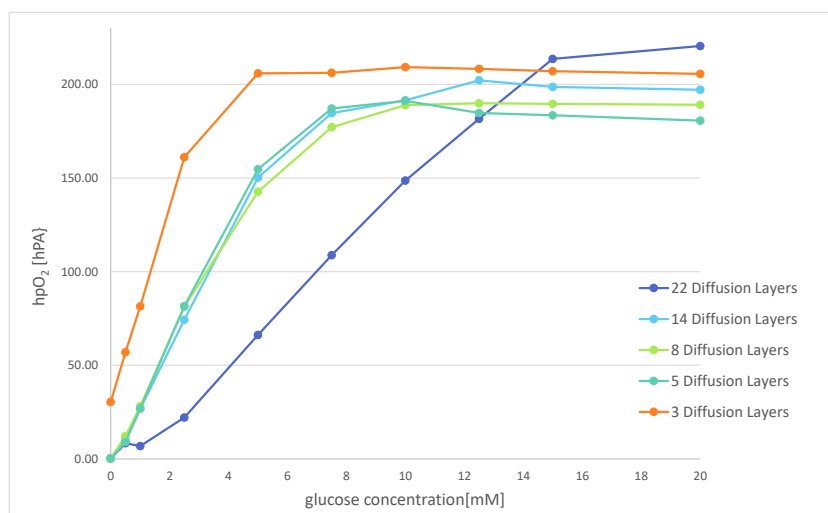


Figure 5.19: Dynamic Range of Different Sensors with Different Numbers of polyHEMA Diffusion Barrier Layers on PMMA Slides

The diagram showing the phase angles and the standard deviation of the phase angles of the different sensors can be found in the appendix in diagram 11.1.

Sensors with 3 polyHEMA diffusion barrier layers are very sensitive to low glucose concentrations. The signal changes quite drastically. At higher concentrations, above 5 mM glucose, the oxygen in the solution is used up by the enzyme layer and so no glucose can be consumed any longer. Therefore the signal stays constant.

Sensors with 5 diffusion barrier layers are already less sensitive in lower concentrations but the signal changes up to 7.5 mM glucose. Sensors with 8 diffusion barrier layers can measure up to 10 mM glucose, with 15 diffusion layers on top of each other up to 12.5 mM glucose. Sensors with 22 diffusion layers have a dynamic range of up to 15 mM glucose, tuning the dynamic range, so even higher glucose concentrations could be measured, which is not possible with polyHEMA because of the coffee ring effect of the diffusion barrier layers.

Measuring higher glucose concentrations is possible with stronger diffusion layer barriers. A stronger diffusion barrier for glucose is for example ethylcellulose. Sensors using ethylcellulose as diffusion barrier layer were prepared using 6 w% ethylcellulose and water with 20 w%, 40 w%, 50 w%, 60 w%, 70 w% and 80 w% ethylcellulose and the rest Hydrogel D4 in an ethanol-water mixture at the ratio of 9:1. The dynamic ranges of the glucose sensors can be seen below.

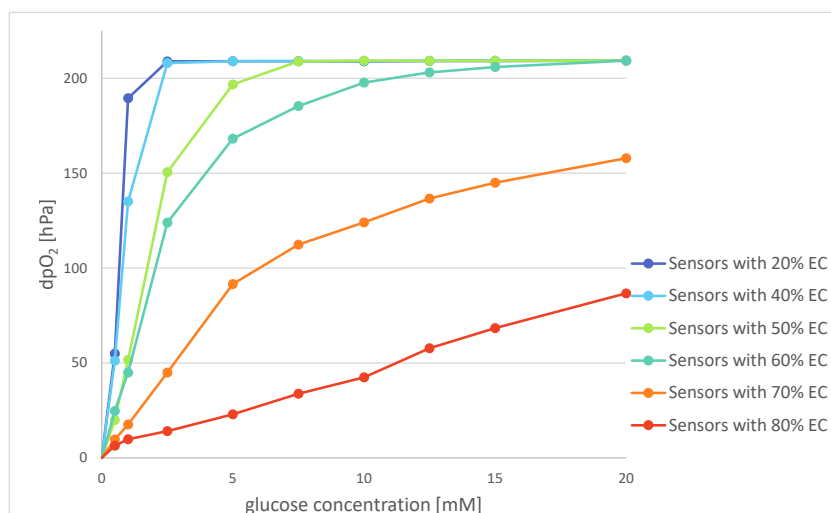


Figure 5.20: Dynamic Range of Different Sensors with Different Concentrations of Ethylcellulose in the Diffusion Barrier Layers on PMMA Slides

The diagram showing the phase angles and the standard deviation of the phase angles of the different sensors can be found in the appendix in diagram 11.2.

In the diagram sensors with 20 w% ethylcellulose in the diffusion barrier layer have a quite good response for lower concentrations but measuring higher concentrations than 1 mM glucose is not possible with this sensor. As the amount of ethylcellulose in the sensor increases the dynamic range shifts to higher concentrations, with 40 % ethylcellulose in the diffusion barrier it is possible to measure up to 2.5 mM glucose, with 50 % up to 7.5 mM, with 60 already up to 15 mM glucose. The sensors with 70 % and 80 % ethylcellulose in the diffusion barrier layer are rather insensitive to lower glucose concentrations but the oxygen has not been used at 20 mM glucose. Consequently these sensors can measure even higher glucose concentrations.

Varying the number of diffusion layers or the amount of diffusion barrier molecules in the diffusion barrier layer the dynamic range can be changed. With hardly any glucose diffusion barrier the sensors are sensitive to lower concentrations, but the oxygen in solution is consumed fast and so higher glucose concentrations cannot be measured. With thicker glucose diffusion barrier layers or concentrations the sensors are less sensitive to lower glucose concentrations but as the glucose diffuses through the diffusion barrier layer more slowly, less glucose reaches the enzyme layer and less oxygen is consumed. As a consequence higher concentrations can be measured.

5.6 Reproducibility of the Sensors

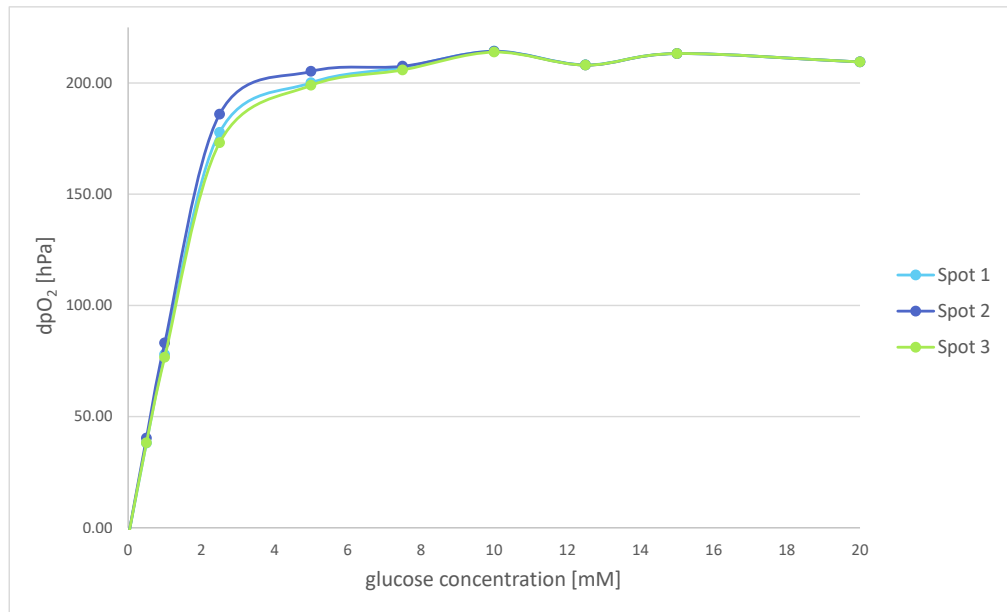
Reproducibility of sensors is an important feature of sensors and simplifies the application, which is especially important if the sensors are used by unskilled persons.

Reproducible sensors do not need to be calibrated sensor by sensor but calibration of one sensor

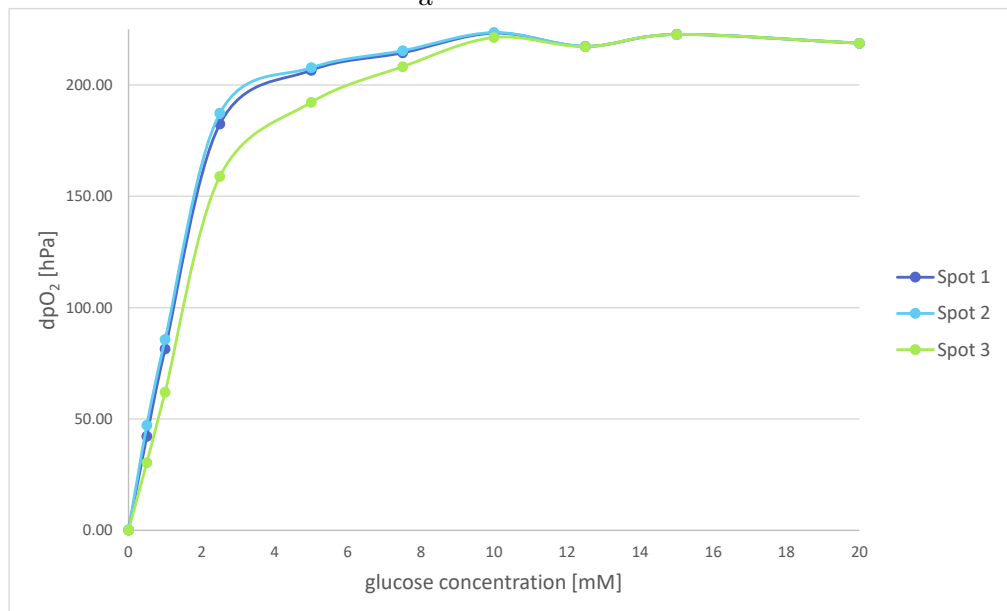
alone is sufficient. This facilitates the application of sensors.

Another important feature of sensors is the storage stability. If the measured phase angle of the sensor does not change over time, time reproducibility is given. The sensor does not have to be calibrated before every measurement and therefore it is easier to use.

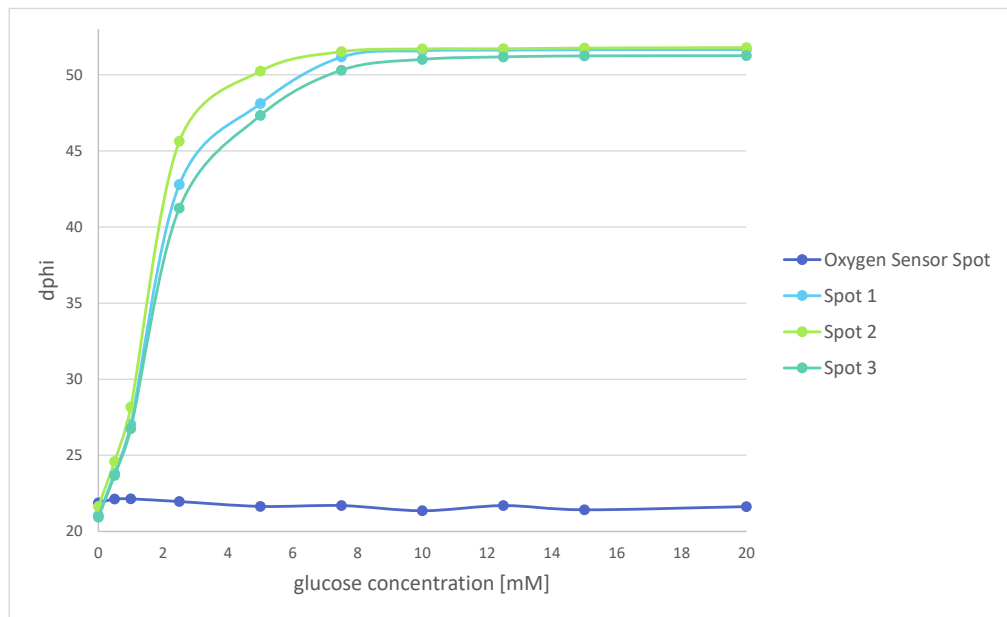
Sensors with the same composition were prepared next to each other and measured the same way, then the sensors were stored in the fridge for ten days and subsequently measured again. This was done with sensors having polyHEMA as diffusion barrier layer and with sensors having ethylcellulose as diffusion barrier layer on PMMA slides.



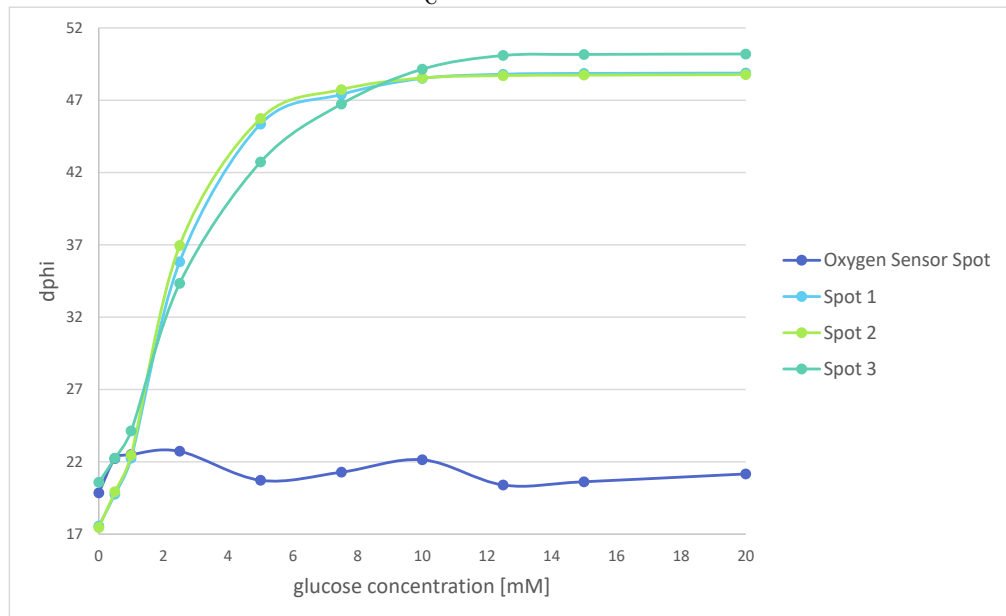
a



b



c



d

Figure 5.21: Reproducibility of Sensors with 14 polyHEMA Diffusion Barrier Layers Printed Next to Each Other;
a: Difference in Oxygen Partial Pressure of Same Sensors Next to Each Other,
b: Difference in Oxygen Partial Pressure of the Same Sensors after Ten Days;
c: Phase Angles of the Same Sensors Printed Next to Each Other;
d: Phase Angles of the Same Sensors after Ten Days

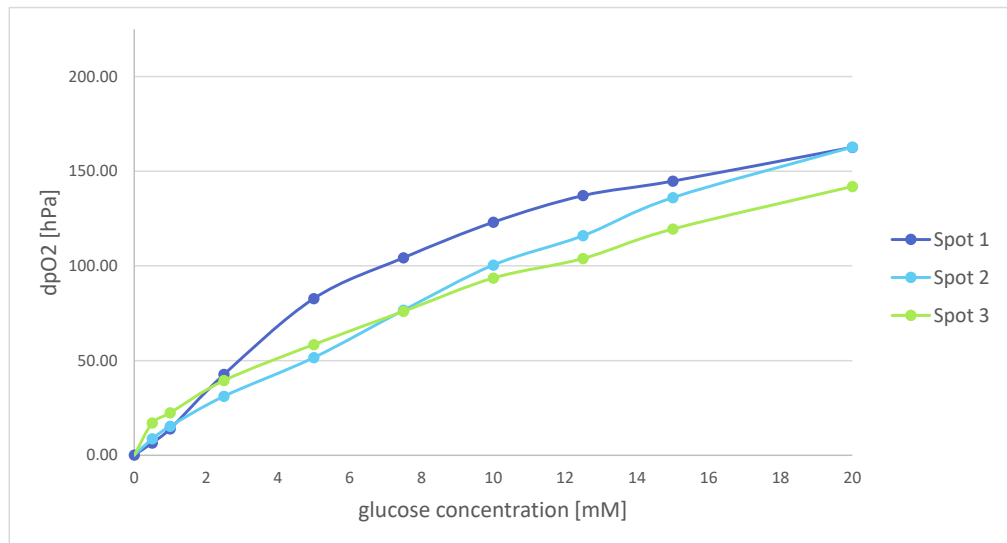
In the diagrams above, the sensors were generally reproducible regarding the difference in the oxygen partial pressure. The signal between the sensors only differentiated at 2.5 mM and 5 mM glucose. After ten days the difference in the partial pressure changed for spot number

four but stays still quite reproducible.

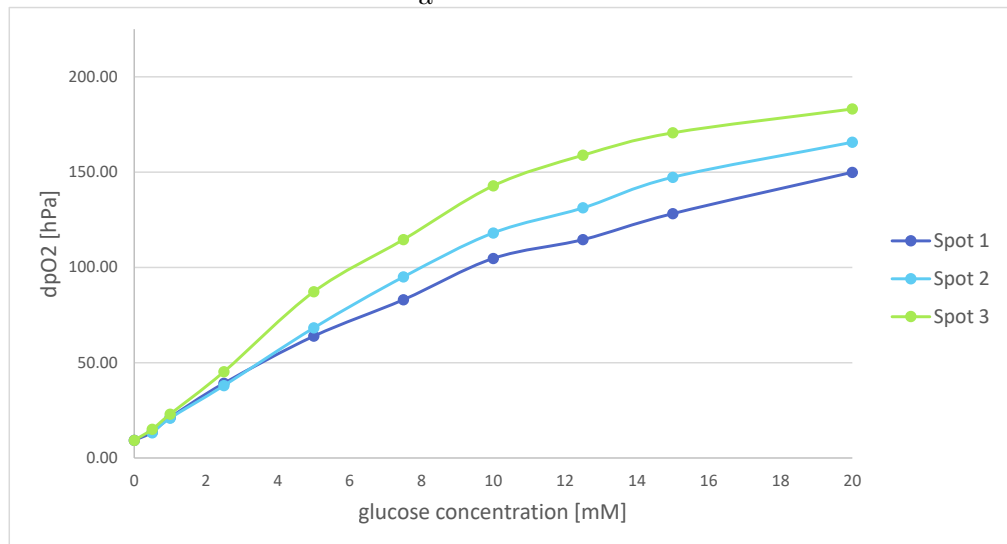
When looking at the raw data, sensors printed with the same parameters in the same batch next to each other looked quite reproducible, but after 10 days the phase angle of the sensors decreased by about 2 dphi. The reason for this could be the migration of oxygen sensor particles into different layers or the separation of the different layers.

The sensors showed reproducibility as far as sensors are printed with the same parameters in the same batch next to each other, but the measured phase angle changed after 10 days and so each sensor has to be calibrated before each single measurement.

The same measurements were performed with sensors with ethylcellulose as diffusion barrier layer.



a



b

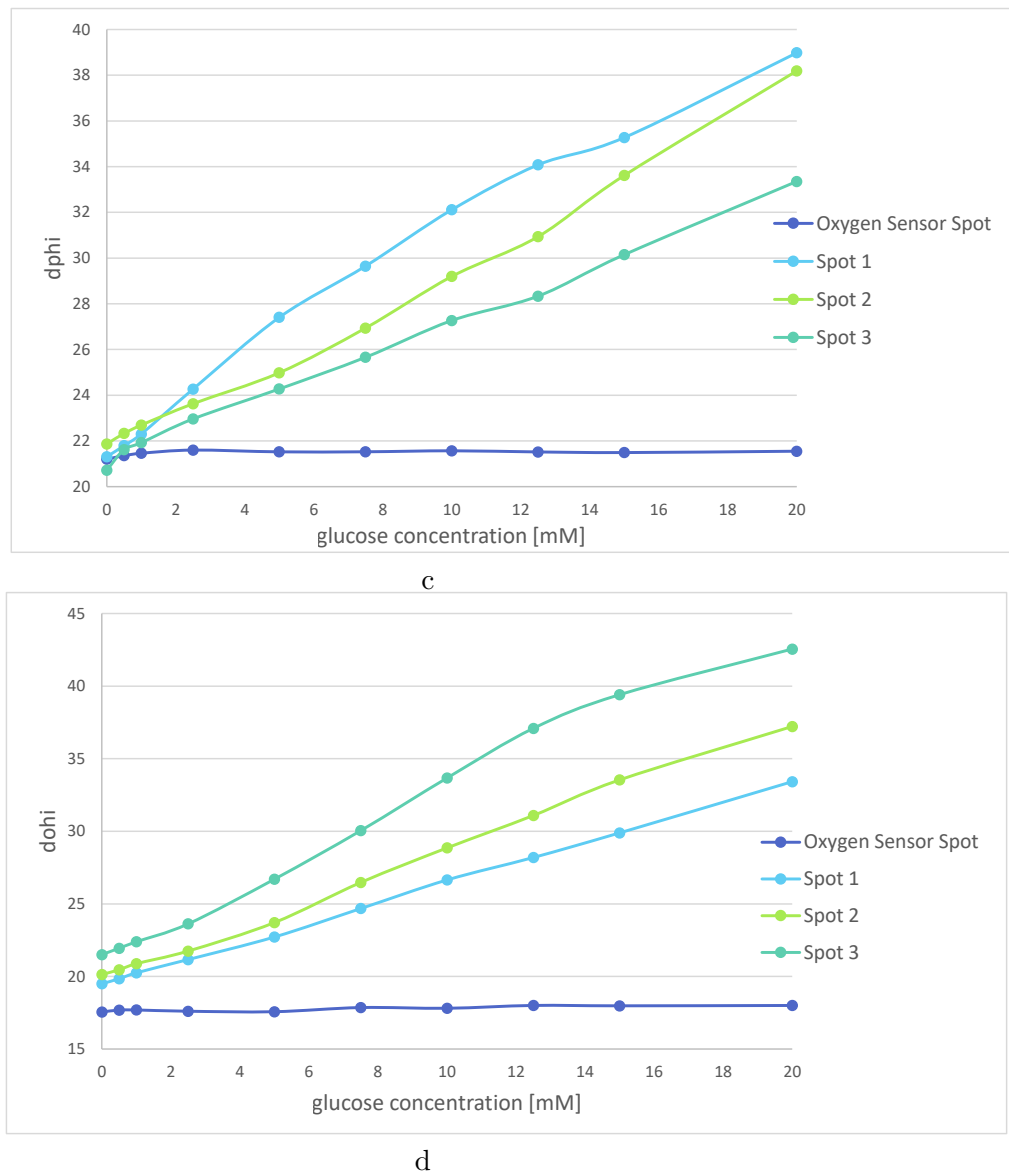


Figure 5.22: Reproducibility of Sensors with Ethylcellulose as Diffusion Barrier Layer Printed Next to Each Other;

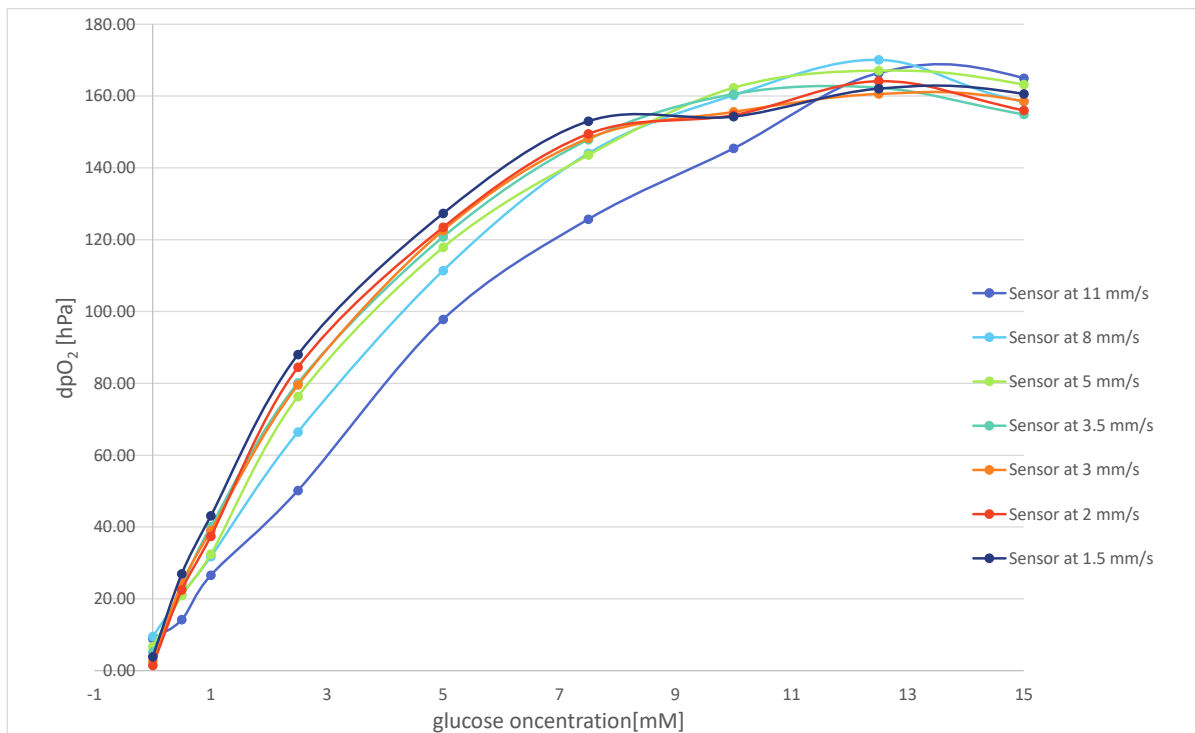
- a: Difference in Oxygen Partial Pressure of Same Sensors Next to Each Other,
- b: Difference in Oxygen Partial Pressure of the Same Sensors after Ten Days;
- c: Phase Angles of the Same Sensors Printed Next to Each Other;
- d: Phase Angles of the Same Sensors after Ten Days

Sensors with ethylcellulose as diffusion barrier show poor reproducibility concerning the same sensors printed with the same parameters in the same batch next to each other. As ethylcellulose is a much stronger diffusion barrier for glucose than polyHEMA, small differences in the dispensed volume make a difference. The difference in the oxygen partial pressure also changes significantly with time. After 10 days the partial pressure at higher glucose concentrations rises up to 30 hPa. This can also be observed in the shift of the phaseangle. Spot 4 had a dphi of 33

on the first day but after 10 days it rose up to 43 dphi. In 0 mM glucose buffer, however, the phase angle decreases of about 2 dphi which could also be noticed for sensors having polyHEMA in the diffusion layer. For sensors with ethylcellulose as the diffusion barrier, the diffusion barrier got weaker after 10 days and the oxygen sensor particles diffused into different layers.

5.7 Flow Velocity Dependency of the Sensors

Sensors on PMMA slides were measured at different flow velocities in a 250 μL and 120 μL rhombic chamber chip.



a

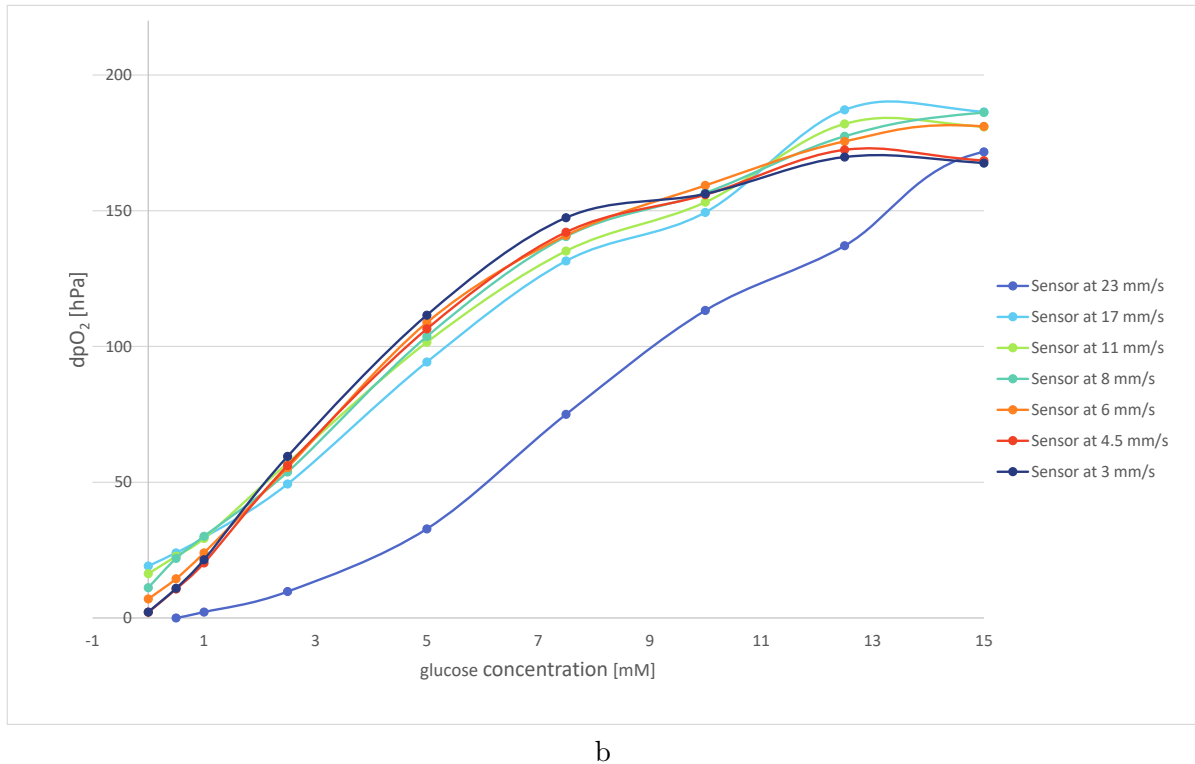


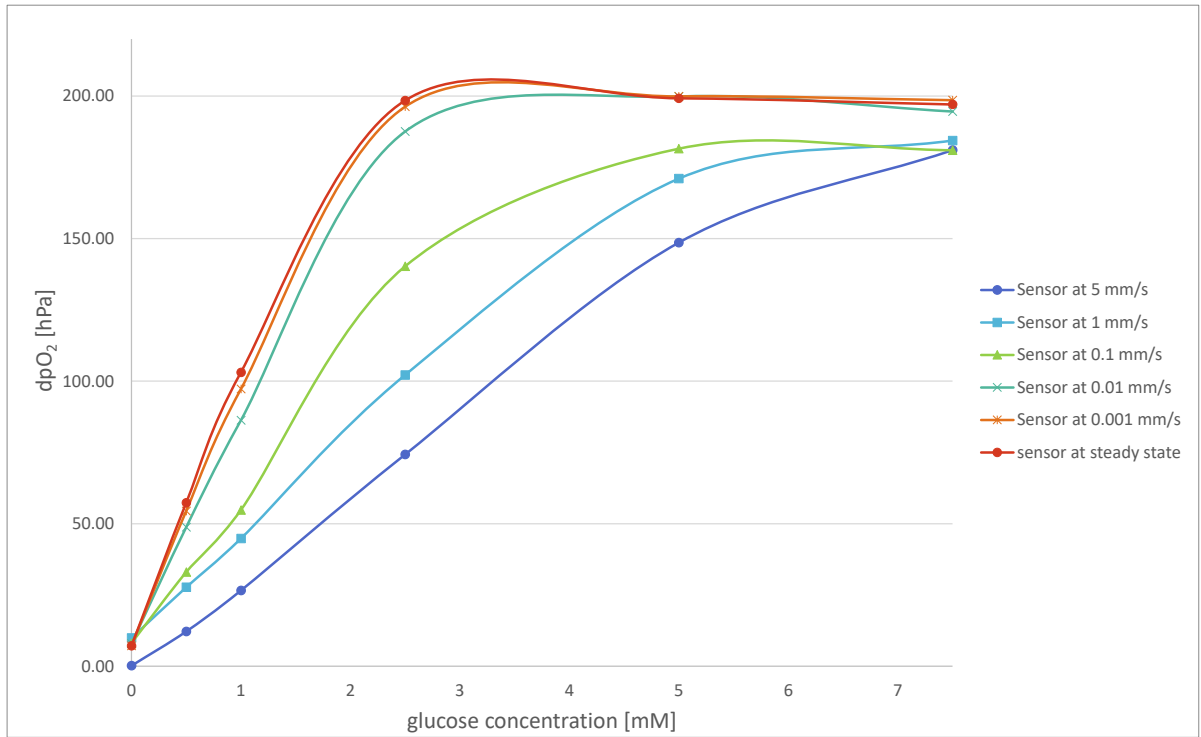
Figure 5.23: Sensors with 22 polyHema Diffusion Barrier Layers Measured at Different Flow Velocities;

a: Measured in a 250 μL Rhombic Chamber Chip,

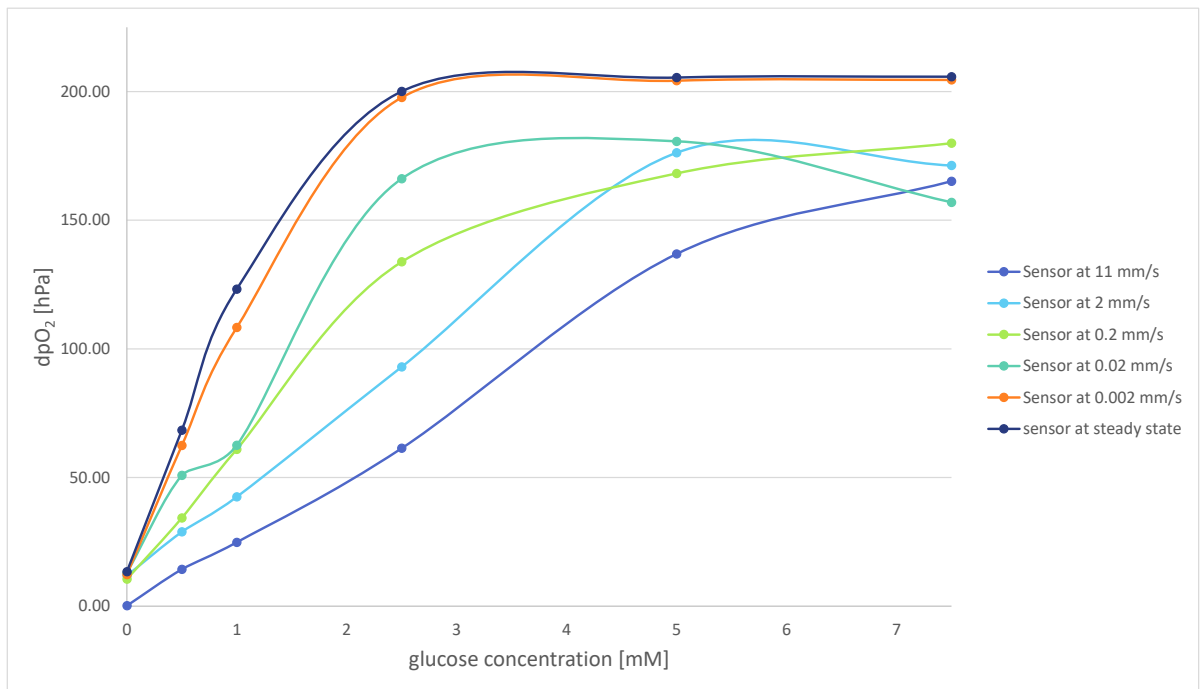
b: Measured in a 120 μL Rhombic Chamber Chip

The diagrams showing the phase angles and the standard deviation of the phase angles of the different sensors can be found in the appendix in diagrams 11.4 and 11.5. In the diagrams above, the dynamic range of the sensors change in dependency on the flow velocities. With higher flow velocities the glucose sensor is less sensitive to glucose and measurements up to higher concentrations are possible.

The same sensors were investigated at flow velocities ranging from 11 mm/s to steady state.



a



b

Figure 5.24: Sensors with 22 polyHEMA Diffusion Barrier Layers Measured at Different Flow Velocities;
a: Measured in a 250 μL Rhombic Chamber Chip,
b: Measured in a 120 μL Rhombic Chamber Chip

The diagram showing the phase angles and the standard deviation of the phase angles of the different sensors can be found in the appendix in diagrams 11.6 and 11.7. At higher flow rates the sensors are less sensitive to glucose, at lower flow velocities the phase angle changes faster with different flow rates. The size of the chip in which the sensors are measured also matters. Chips with smaller volumes are less sensitive to the change in the flow velocity.

The reason why the sensors depend on the flow velocity is still unknown. However, there are several theories, including that more glucose may diffuse through the diffusion barrier at lower flow velocities, that the enzyme consumes all the oxygen at lower flow velocities, or less oxygen reaches the oxygen sensor spot.

As the sensors are dependent on the flow velocity the dynamic range decreases to lower glucose concentrations. For this reason applications glucose measurements in steady state are only suitable for concentrations up to 2 mM glucose.

5.8 Measurements of Glucose in Bulk

The flow velocity measurements in higher volumes were performed in a beaker.

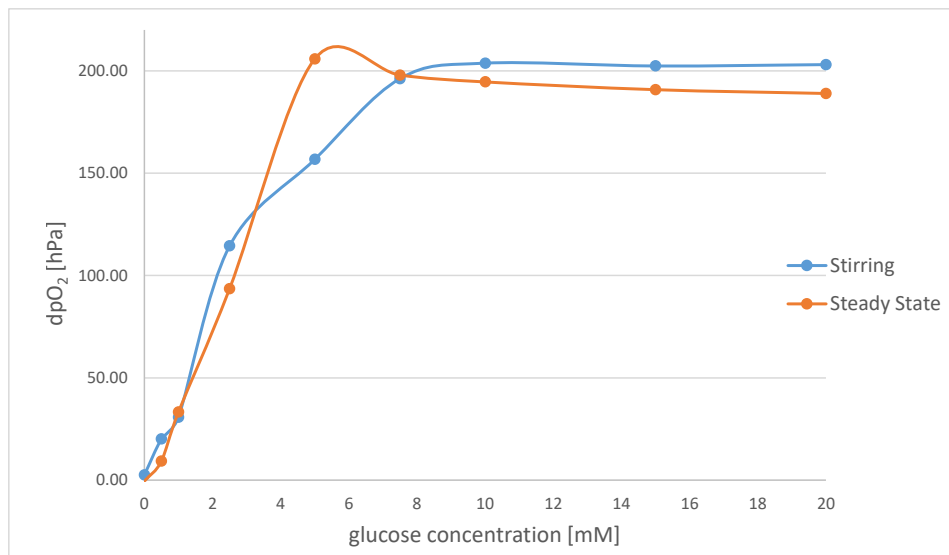


Figure 5.25: Measurement in a Beaker

The diagram showing the phase angles and the standard deviation of the phase angles of the different sensors can be found in the appendix in diagram 11.8. As seen in the diagram the difference in the partial pressure of oxygen changes for the sensor in a stirring beaker up to 7.5 mM glucose, while at steady state the oxygen is consumed already at 5 mM glucose. At steady state there is no exchange of oxygen at the sensor spot and therefore all the oxygen is consumed faster than in a stirring beaker.

6 Conclusion and Outlook

While working at this master thesis different glucose sensors were successfully prepared using the microdispenser. Profiles of every sensor were established by measuring with the profilometer. Measurements in rhombic chamber chips were performed with different glucose buffer solutions. The first sensors showed a big coffee ring effect, which inhibited the reproducible preparation of sensors. The sensors had a length of 1.4 mm and a height of 32 μm . Oxygen sensor spots were printed small enough so that the whole spot was measured and as a consequence the coffee ring had no influence. The diameter of the oxygen sensor was 600 μm and the fibre had a diameter of 1 mm.

The coffee ring effect in the enzyme layer was decreased by printing smaller droplets on top of one big one. In the diffusion layer the coffee ring effect could not be reduced and the diffusion layer was printed as 4x4 matrix to achieve a fully covered enzyme layer.

To decrease the coffee ring effect in the diffusion layer, a spraying add-on was installed, but reproducible layers could not be prepared. The spraying add-on might work for lower viscosity inks, but using lower viscosity inks would increase the number of required layers and the waiting time between each dispensed layer. As a consequence producing glucose sensors would be an extremely time-consuming procedure.

Printing on different support materials had no influence on the coffee ring effect, plasma etched polymer slides even showed stronger coffee ring behaviour. The sensors presented good adhesion on every material and could be measured with different glucose buffers. In general, the characterisation of these sensors had no influence on the dynamic range but the dispensing of the cocktails with different solvents might have swollen the surface of the different polymer slides.

The dynamic range can be tuned by dispensing multiple diffusion barrier layers on top of each other. It is possible to measure up to 1.5 mM glucose with only a few diffusion layers but it is also possible to measure up to 12.5 mM glucose with higher diffusion layers. Using a different diffusion barrier, in this thesis ethylcellulose was used, is theoretically achievable, but such prepared sensors did not turn out to be reproducible.

Sensors consisting of a polyHEMA diffusion barrier layer were reproducible regarding the sensor production, but showed little storage stability.

The prepared sensors had a strong flow velocity dependency. Measurements at steady state are only possible for very low glucose concentrations.

The sensors prepared are suitable for high flow velocity measurements in rather big chambers. Further reducing the size of the sensors and the size of the chamber would decrease the

dependency on the flow velocity and so the sensors could measure higher concentrations at lower flow velocities. Glucose Monitoring in higher volumes is also possible, but the liquid has to be stirred.

With some modifications of the sensor could be used in microfluidic applications, for example the monitoring of the glucose consumption of cells in microfluidic chambers.

Using the microdispenser enables reproducible fast-printed sensors.

7 References

1. Gonzalez-Macia, L., Morrin, A., Smyth, M. R. & Killard, A. J. Advanced printing and deposition methodologies for the fabrication of biosensors and biodevices. *The Analyst* **135**, 845 (2010).
2. Krebs, F. C. Polymer solar cell modules prepared using roll-to-roll methods: Knife-over-edge coating, slot-die coating and screen printing. *Processing and Preparation of Polymer and Organic Solar Cells* **93**, 465–475 (Apr. 2009).
3. Krause, C., Werner, T. & Wolfbeis, O. S. Multilayer Potassium Sensor Based on Solid-State Coextraction. *Analytical Science* **14**, 163–167 (Feb. 1998).
4. Mayr, T., Abel, T., Kraker, E., Koestler, S., Haase, A., Konrad, C., Tscherner, M. & Lamprecht, B. An optical sensor array on a flexible substrate with integrated organic opto-electric devices. *Eurosensor XXIV Conference* **5**, 1005–1008 (Jan. 1, 2010).
5. Crouch, E., Cowell, D. C., Hoskins, S., Pittson, R. W. & Hart, J. P. Amperometric, screen-printed, glucose biosensor for analysis of human plasma samples using a biocomposite water-based carbon ink incorporating glucose oxidase. *Analytical Biochemistry* **347**, 17–23 (Dec. 1, 2005).
6. Sayago, I., Terrado, E., Lafuente, E., Horrillo, M., Maser, W., Benito, A., Navarro, R., Urriolabeitia, E., Martinez, M. & Gutierrez, J. Hydrogen sensors based on carbon nanotubes thin films. *Synthetic Metals* **148**, 15–19 (Jan. 3, 2005).
7. Ehgartner, J., Sulzer, P., Burger, T., Kasjanow, A., Bouwes, D., Kruehne, U., Klimant, I. & Mayr, T. Online analysis of oxygen inside silicon-glass microreactors with integrated optical sensors. *Sensors and Actuators B: Chemical* **228**, 748–757 (June 2016).
8. Chung, W.-Y., Sakai, G., Shimanoe, K., Miura, N., Lee, D.-D. & Yamazoe, N. Preparation of indium oxide thin film by spin-coating method and its gas-sensing properties. *Sensors and Actuators B: Chemical* **46**, 139–145 (Feb. 15, 1998).
9. Setti, L., Piana, C., Bonazzi, S., Ballarin, B., Frascaro, D., Fraleoni-Morgera, A. & Giuliani, S. Thermal Inkjet Technology for the Microdeposition of Biological Molecules as a Viable Route for the Realization of Biosensors. *Analytical Letters* **37**, 1559–1570 (Dec. 27, 2004).
10. Li, J., Rossignol, F. & Macdonald, J. Inkjet printing for biosensor fabrication: combining chemistry and technology for advanced manufacturing. *Lab Chip* **15**, 2538–2558 (2015).

11. Setti, L., Fraleoni-Morgera, A., Ballarin, B., Filippini, A., Frascaro, D. & Piana, C. An amperometric glucose biosensor prototype fabricated by thermal inkjet printing. *Biosensors and Bioelectronics. Selected Papers from the Eighth World Congress on Biosensors, Part II* **20**, 2019–2026 (Apr. 15, 2005).
12. Li, M., Tian, J., Al-Tamimi, M. & Shen, W. Paper-Based Blood Typing Device That Reports Patient's Blood Type "in Writing". *Angewandte Chemie International Edition* **51**, 5497–5501 (May 29, 2012).
13. Guan, L., Tian, J., Cao, R., Li, M., Cai, Z. & Shen, W. Barcode-Like Paper Sensor for Smartphone Diagnostics: An Application of Blood Typing. *Analytical Chemistry* **86**, 11362–11367 (Nov. 18, 2014).
14. Maejima, K., Tomikawa, S., Suzuki, K. & Citterio, D. Inkjet printing: an integrated and green chemical approach to microfluidic paper-based analytical devices. *RSC Advances* **3**, 9258 (2013).
15. Yu, W. W. & White, I. M. Inkjet Printed Surface Enhanced Raman Spectroscopy Array on Cellulose Paper. *Analytical Chemistry* **82**, 9626–9630 (Dec. 2010).
16. Newman, J., Turner, A. & Marrazza, G. Ink-jet printing for the fabrication of amperometric glucose biosensors. *Analytica Chimica Acta* **262**, 13–17 (June 1, 1992).
17. Paul, K. E., Wong, W. S., Ready, S. E. & Street, R. A. Additive jet printing of polymer thin-film transistors. *Applied Physics Letters* **83**, 2070–2072 (Sept. 8, 2003).
18. Liu, R., Ding, H., Lin, J., Shen, F., Cui, Z. & Zhang, T. Fabrication of platinum-decorated single-walled carbon nanotube based hydrogen sensors by aerosol jet printing. *Nanotechnology* **23**, 505301 (2012).
19. Gruber, P., Marques, M. P., Sulzer, P., Wohlgemuth, R., Mayr, T., Baganz, F. & Szita, N. Real-time pH monitoring of industrially relevant enzymatic reactions in a microfluidic side-entry reactor (mikroSER) shows potential for pH control. *Biotechnology Journal*, 1600475 (Feb. 2017).
20. Park, T. & Shuler, M. Integration of Cell Culture and Microfabrication Technology. *Biotechnology Progress* **19**, 243–253 (Apr. 4, 2003).
21. Piner, R. D., Zhu, J., Xu, F., Hong, S. & Mirkin, C. A. "Dip-Pen" Nanolithography. *Science* **283**, 661–663 (Jan. 29, 1999).
22. Tang, Q. & Shi, S.-Q. Preparation of gas sensors via dip-pen nanolithography. *Sensors and Actuators B: Chemical* **131**, 379–383 (May 2008).
23. Hu, Y., Das, A., Hecht, M. H. & Scoles, G. Nanografting De Novo Proteins onto Gold Surfaces. *Langmuir* **21**, 9103–9109 (Sept. 2005).
24. Liu, M. & Liu, G.-Y. Hybridization with Nanostructures of Single-Stranded DNA. *Langmuir* **21**, 1972–1978 (Mar. 2005).

25. Lakowicz, J. R. *Principles of fluorescence spectroscopy* 3rd ed. 954 pp. (Springer, New York, 2006).
26. Broekaert, J. A. C. *Analytical atomic spectrometry with flames and plasmas* 364 pp. (Wiley-VCH, Weinheim, 2002).
27. Hulanicki, A., Glab, S. & Ingman, F. Chemical Sensors Definitions and Classifications. *Pure Appl. Chem.* **63**, 1247–1250 (1991).
28. Clark, L. C. & Lyons, C. Electrode systems for continuous monitoring in cardiovascular surgery. *Annals of the New York Academy of sciences* **102**, 29–45 (1962).
29. Wang, J. Electrochemical Glucose Biosensors. *Chemical Reviews* **108**, 814–825 (Feb. 2008).
30. Malitesta, C., Palmisano, F., Torsi, L. & Zambonin, P. G. Glucose fast-response amperometric sensor based on glucose oxidase immobilized in an electropolymerized poly(o-phenylenediamine) film. *Analytical Chemistry* **62**, 2735–2740 (Dec. 1, 1990).
31. Cass, A. E., Davis, G., Francis, G. D., Hill, H. A. O., Aston, W. J., Higgins, I. J., Plotkin, E. V., Scott, L. D. & Turner, A. P. Ferrocene-mediated enzyme electrode for amperometric determination of glucose. *Analytical chemistry* **56**, 667–671 (1984).
32. Wu, J. & Qu, Y. Mediator-free amperometric determination of glucose based on direct electron transfer between glucose oxidase and an oxidized boron-doped diamond electrode. *Analytical and Bioanalytical Chemistry* **385**, 1330–1335 (July 19, 2006).
33. Toghiani, K. E. & Compton, R. G. Electrochemical non-enzymatic glucose sensors: a perspective and an evaluation. *Int. J. Electrochem. Sci* **5**, 1246–1301 (2010).
34. Pletcher, D. Electrocatalysis: present and future. *Journal of Applied Electrochemistry* **14**, 403–415 (1984).
35. Burke, L. Premonolayer oxidation and its role in electrocatalysis. *Electrochimica Acta* **39**, 1841–1848 (Aug. 1, 1994).
36. Chou, C.-H., Chen, J.-C., Tai, C.-C., Sun, I.-W. & Zen, J.-M. A Nonenzymatic Glucose Sensor Using Nanoporous Platinum Electrodes Prepared by Electrochemical Alloying/Dealloying in a Water-Insensitive Zinc Chloride-1-Ethyl-3-Methylimidazolium Chloride Ionic Liquid. *Electroanalysis* **20**, 771–775 (Apr. 2008).
37. Dawson, K., Baudequin, M. & O’Riordan, A. Single on-chip gold nanowires for electrochemical biosensing of glucose. *The Analyst* **136**, 4507 (2011).
38. Tong, G.-X., Liu, F.-T., Wu, W.-H., Shen, J.-P., Hu, X. & Liang, Y. Polymorphous [small alpha]- and [small beta]-Ni(OH)₂ complex architectures: morphological and phasal evolution mechanisms and enhanced catalytic activity as non-enzymatic glucose sensors. *CrystEngComm* **14**, 5963–5973 (2012).
39. Reitz, E., Jia, W., Gentile, M., Wang, Y. & Lei, Y. CuO Nanospheres Based Nonenzymatic Glucose Sensor. *Electroanalysis* **20**, 2482–2486 (Nov. 1, 2008).

40. Liu, D., Luo, Q. & Zhou, F. Nonenzymatic glucose sensor based on gold–copper alloy nanoparticles on defect sites of carbon nanotubes by spontaneous reduction. *Synthetic Metals* **160**, 1745–1748 (Aug. 2010).
41. Liu, M., Liu, R. & Chen, W. Graphene wrapped Cu₂O nanocubes: Non-enzymatic electrochemical sensors for the detection of glucose and hydrogen peroxide with enhanced stability. *Biosensors and Bioelectronics* **45**, 206–212 (July 15, 2013).
42. Steiner, M.-S., Duerkop, A. & Wolfbeis, O. S. Optical methods for sensing glucose. *Chemical Society Reviews* **40**, 4805 (2011).
43. Oliver, N. S., Toumazou, C., Cass, A. E. G. & Johnston, D. G. Glucose sensors: a review of current and emerging technology. *Diabetic Medicine* **26**. bibtex: oliver_glucose_2009, 197–210 (2009).
44. Sierra, J. F., Galbán, J. & Castillo, J. R. Determination of Glucose in Blood Based on the Intrinsic Fluorescence of Glucose Oxidase. *Analytical Chemistry* **69**, 1471–1476 (Apr. 1997).
45. Sanz, V. Fluorometric sensors based on chemically modified enzymes Glucose determination in drinks. *Talanta* **60**, 415–423 (June 13, 2003).
46. Trettnak, W., Leiner, M. J. & Wolfbeis, O. S. Optical sensors. Part 34. Fibre optic glucose biosensor with an oxygen optrode as the transducer. *Analyst* **113**, 1519–1523 (1988).
47. Papkovsky, D. B. Luminescent porphyrins as probes for optical (bio)sensors. *Sensors and Actuators B: Chemical* **11**, 293–300 (Mar. 1, 1993).
48. Pasic, A., Koehler, H., Klimant, I. & Schaupp, L. Miniaturized fiber-optic hybrid sensor for continuous glucose monitoring in subcutaneous tissue. *Sensors and Actuators B: Chemical* **122**, 60–68 (Mar. 8, 2007).
49. Rossi, L. M., Quach, A. D. & Rosenzweig, Z. Glucose oxidase–magnetite nanoparticle bioconjugate for glucose sensing. *Analytical and Bioanalytical Chemistry* **380**, 606–613 (2004).
50. Endo, T., Ikeda, R., Yanagida, Y. & Hatsuzawa, T. Stimuli-responsive hydrogel–silver nanoparticles composite for development of localized surface plasmon resonance-based optical biosensor. *Analytica Chimica Acta* **611**, 205–211 (Mar. 24, 2008).
51. Ertekin, K., Cinar, S., Aydemir, T. & Alp, S. Glucose sensing employing fluorescent pH indicator: 4-[(p-N,N-dimethylamino)benzylidene]-2-phenyloxazole-5-one. *Dyes and Pigments* **67**, 133–138 (Nov. 2005).
52. Badugu, R., Lakowicz, J. R. & Geddes, C. D. Boronic acid fluorescent sensors for monosaccharide signaling based on the 6-methoxyquinolinium heterocyclic nucleus: progress toward noninvasive and continuous glucose monitoring. *Bioorganic & Medicinal Chemistry* **13**, 113–119 (Jan. 3, 2005).

53. Aslan, K., Lakowicz, J. R. & Geddes, C. D. Tunable plasmonic glucose sensing based on the dissociation of Con A-aggregated dextran-coated gold colloids. *Analytica Chimica Acta* **517**, 139–144 (July 26, 2004).
54. D’Auria, S., Herman, P., Rossi, M. & Lakowicz, J. R. The Fluorescence Emission of the Apo-glucose Oxidase from *Aspergillus niger* as Probe to Estimate Glucose Concentrations. *Biochemical and Biophysical Research Communications* **263**, 550–553 (Sept. 24, 1999).
55. *Harper’s illustrated biochemistry* (ed Murray, R. K.) 26. ed. OCLC: 249611100 (Lange Medical Books/McGraw-Hill, New York, NY, 2003). 693 pp.
56. Wilson, R & Turner, A. Glucose oxidase: an ideal enzyme. *Biosensors and Bioelectronics* **7**, 165–185 (1992).
57. Carraway, E. R., Demas, J. N., DeGraff, B. A. & Bacon, J. R. Photophysics and photochemistry of oxygen sensors based on luminescent transition-metal complexes. *Analytical chemistry* **63**, 337–342 (1991).

8 List of Figures

2.1	Scheme of a Knife Coating Printer	3
2.2	Scheme of Screen Printer	3
2.3	Spay Coating without and with a Mask	4
2.4	Scheme of the Spin Coating Procedure	5
2.5	Scheme of a Thermal Inkjet Printer	6
2.6	Scheme of a Piezoelectric Inkjet Printer	6
2.7	Scheme of an Electrostatic Inkjet Printer	7
2.8	Scheme of an Acoustic Inkjet Printer	7
2.9	Scheme of Aerosol Jet Printer	8
2.10	Steps of a Dispensing	9
2.11	Tappet lift - Time Diagram of one Dispensing Step	9
2.12	Scheme of the Microdispenser Spray Add-On	10
2.13	The Process of Microcontact Printing	11
2.14	Scheme of Dip-Pen Nanolithography	12
2.15	Scheme of the Nanografting Printing Process	12
2.16	Jablonski Diagram	15
2.17	Luminescence Quenching through Complex Formation	16
2.18	Dynamic Quenching Mechanism	17
2.19	Emission and Shifted Excitation Signal	18
2.20	Conformations of Glucose: a: D-Glucose, b: L-Glucose, c: α -D-Glucose, d: β -D-Glucose	23
3.1	Picture of a FireStingO2, Phase Fluorimeter	25
3.2	Structure of the Oxygen Sensor Particles	27
3.3	Layout of a 250 μl Rhombic Chamber Chip, the Chip is 800 μm Deep	28
3.4	Layout of a 120 μl Rhombic Chamber Chip, the Chip is 500 μm Deep	28
4.1	Picture of the Adhesive Tape, the Rhombic Chamber Chip and the Polymerslide with the Sensors	31
4.2	Picture of how one Side of the Adhesive Tape is Peeled off	31
4.3	Picture of the Adhesive Tape Fixed on the Rhombic Chamber Chip	32
4.4	Picture of how the Cover of the Adhesive Tape is Peeled off the Rhombic Chamber Chip	32

4.5	Picture of the Final Sensor Chip; the Chips consist of Oxygen and Glucose Sensors in Alternative Order, Beginning with an Oxygen Sensor	33
4.6	The Setup of the Computerised Numerical Control and the Microdispenser . .	34
5.1	Composition of the Glucose Sensor	38
5.2	Profilometer Measurements of a Sensor	39
5.3	Profilometer Measurements of the Diffusion Barrier Layers Sprayed as Tracks with Different Properties, a: Parameters 1 b: Parameters 2	41
5.4	Profilometer Measurements of the Diffusion Barrier Layer Sprayed as Circles .	42
5.5	Profilometer Measurements of the Oxygen Layer and the Enzyme Layer on Glass and Silanised Glass	44
5.6	Profilometer Measurements of the Oxygen Layer and the Enzyme Layer on PMMA and Plasma Etched PMMA	45
5.7	Profilometer Measurements of the Oxygen Layer and the Enzyme Layer on PS and Plasma Etched PS	46
5.8	Profilometer Measurements of the Oxygen Layer and the Enzyme Layer on Topas and Plasma Etched Topas	47
5.9	Profilometer Measurements of the Oxygen Layer and the Enzyme Layer on PC and Plasma Etched PC	48
5.10	Profilometer Measurements of Sensors with Different Numbers of Diffusion Barrier Layers	50
5.11	Pictures of the Different Layers and a Finished Chip	52
5.12	Oxygen Calibration and Stern-Volmer Two-Site Model	53
5.13	Response Curve of a Sensor	54
5.14	Sensors on Glass and Silanised Glass Exposed to Various Glucose Concentrations in Phosphate Buffer pH 7.2	55
5.15	Sensors on PMMA and Plasma Etched PMMA Exposed to Various Glucose Concentrations in Phosphate Buffer pH 7.2	55
5.16	Sensors on PS and Plasma Etched PS Exposed to Various Glucose Concentrations in Phosphate Buffer pH 7.2	56
5.17	Sensors on Topas and Plasma Etched Topas Exposed to Various Glucose Concentrations in Phosphate Buffer pH 7.2	56
5.18	Sensors on PC and Plasma Etched PS Exposed to Various Glucose Concentrations in Phosphate Buffer pH 7.2	57
5.19	Dynamic Range of Different Sensors with Different Numbers of polyHEMA Diffusion Barrier Layers on PMMA Slides	58
5.20	Dynamic Range of Different Sensors with Different Concentrations of Ethylcellulose in the Diffusion Barrier Layers on PMMA Slides	59

5.21	Reproducibility of Sensors with 14 polyHEMA Diffusion Barrier Layers Printed Next to Each Other;	
	a: Difference in Oxygen Partial Pressure of Same Sensors Next to Each Other,	
	b: Difference in Oxygen Partial Pressure of the Same Sensors after Ten Days;	
	c: Phase Angles of the Same Sensors Printed Next to Each Other;	
	d: Phase Angles of the Same Sensors after Ten Days	61
5.22	Reproducibility of Sensors with Ethylcellulose as Diffusion Barrier Layer Printed Next to Each Other;	
	a: Difference in Oxygen Partial Pressure of Same Sensors Next to Each Other,	
	b: Difference in Oxygen Partial Pressure of the Same Sensors after Ten Days;	
	c: Phase Angles of the Same Sensors Printed Next to Each Other;	
	d: Phase Angles of the Same Sensors after Ten Days	63
5.23	Sensors with 22 polyHema Diffusion Barrier Layers Measured at Different Flow Velocities;	
	a: Measured in a 250 μL Rhombic Chamber Chip,	
	b: Measured in a 120 μL Rhombic Chamber Chip	65
5.24	Sensors with 22 polyHEMA Diffusion Barrier Layers Measured at Different Flow Velocities;	
	a: Measured in a 250 μL Rhombic Chamber Chip,	
	b: Measured in a 120 μL Rhombic Chamber Chip	66
5.25	Measurement in a Beaker	67
11.1	Measured ϕ Values of Sensors with PolyHEMA as Diffusion Barrier Layer and Different Amount of Layers	83
11.2	Measured ϕ Values of Sensors with Different Amount of Ethylcellulose in the Diffusion Barrier Layer	84
11.3	Measuring Curve of a Sensor	84
11.4	Sensor with PolyHEMA as Diffusion Barrier Layer Measured at Different Flow Velocities in a 250 μL Rhombic Chamber Chip	85
11.5	Sensor with PolyHEMA as Diffusion Barrier Layer Measured at Different Flow Velocities in a 120 μL Rhombic Chamber Chip	85
11.6	Sensor with PolyHEMA as Diffusion Barrier Layer Measured at Different Flow Velocities in a 250 μL Rhombic Chamber Chip	86
11.7	Sensor with PolyHEMA as Diffusion Barrier Layer Measured at Different Flow Velocities in a 120 μL Rhombic Chamber Chip	86
11.8	Measurement of Sensors in Higher Volumes	87

9 List of Tables

2.1	Types of Luminescence	14
2.2	Classes of Enzymes	24
3.1	Printer Parts	25
3.2	Devices for measurement	25
3.3	Sonifier parts	26
3.4	Polymers used	26
3.5	Dyes and Enzymes	26
3.7	Phosphate Buffer	27
3.6	Polymer Slides	27
4.1	Settings of the Sonifier to homogenise the oxygen sensor cocktail	29
4.2	Settings of the Sonifier to Homogenise the Enzyme Layer Cocktaill	30
4.3	Used Parameters of the Profilometer	30
4.4	Microdispenser Settings	34
4.5	Microdispenser Parameters	35
4.6	Printing Parameters of the Microdispenser	36
5.1	Parameters of the Microdispenser	40
5.2	Parameters of the Microdispenser	42
5.3	Phase Angle Values of Sensors exposed to Air Saturated pH 7.2 Phosphate Buffer	54
10.1	List of Abbreviations	79

10 List of Abbreviations

GOx	Glucose Oxidase
PVC	polyVinylchloride
PDMS	Polydimethylsiloxane
polyHEMA	polyHydroxyethylmethacrylate
PMMA	polyMethylmethacrylate
PS	polyStyrene
PC	polyCarbonate

Table 10.1: List of Abbreviations

11 Appendix

11.1 CNC Control

```

                                spot_schwammkopf[115]
%
(for you to change)

#<correction_y>      =      28.9      (correction in x axis in mm)
#<correction_x>      =      5.2      (correction in y axis in mm)
#<correction_z>      =      0.3      (correction in z axis in mm)
#<squares_per_line>  =      3        (number of squares in y
direction)
#<lines>             =      1        (number of lines)
#<square_length_y>   =      12       (number of spots per square
edge)
#<square_length_x>   =      12       (number of spots per square
edge)
#<dist_squares_y>    =      12       (distance of squares in line)
#<dist_squares_x>    =      9.4      (distance between lines)
#<spot_distance>     =      0.3      (distance between spots in
square)
#<repeat_all>        =      1        (repeat all including cleaning
process)
#<wait_all>          =      0        (waiting time between
repetitions)

(try not to change those. if you do, be careful! If you have questions ask
Fipsotron)

#<repeat_count>=1
#<move_speed>=2000
#<wait_pass> = 0.1 (wait between passes)
#<wait_trigger> = 0.02 (wait trigger)
#<repeat_clean> = 6 (cleaning steps)
#<wait_clean> = 0.06
#<repeat_all> = 1
#<wait_all> = 0

(program starts here)

O109 if [#<correction_y> GE 0]
O108 if [#<correction_x> GE 0]
O107 if [#<correction_z> GE 0]
O106 repeat [#<repeat_all>]
#<counter>=0
#<counter_x>=0
g4 p#<wait_all>
G90                                (absolute mode)
G40                                (toolradius correction off)
G21
g54 g0 z30
g54 g0 x-20 y[#<correction_y>]
g54 g0 z5
O105 repeat [#<repeat_clean>]

```

Seite 1

```

spot_schwammkopf[115]
g54 g0 y[#<correction_y>]+30]
g54 g0 y[#<correction_y>]
0105 endrepeat
g54 g0 x[#<correction_x>] y[#<correction_y>] z[#<correction_z>]
0100 repeat [#<lines>]
0101 repeat [#<squares_per_line>]
g90 x[#<counter_x>*#<dist_squares_x>+#<correction_x>]
g90 z[#<correction_z>]
0102 repeat [#<repeat_count>]
#<line_counter>=1
0103 repeat [#<square_length_x>]
g90 y[#<counter>*#<dist_squares_y>+#<correction_y>]
0110 if [#<line_counter> EQ 2]
g91 G1 y[#<spot_distance>/-2] f#<move_speed>
0110 endif
0104 repeat [#<square_length_y>]
g4 p#<wait_pass>
s1m3
g4 p#<wait_trigger>
s1m5
g4 p#<wait_pass>
g91 G1 y#<spot_distance> f#<move_speed>
0104 endrepeat
0111 if [#<line_counter> EQ 1]
#<line_counter> = 2
0111 else
#<line_counter> = 1
0111 endif
g91 x#<spot_distance>
0103 endrepeat
0102 endrepeat
#<counter>=[#<counter>+1]
0101 endrepeat
#<counter>=0
#<counter_x>=[#<counter_x>+1]
0100 endrepeat
(g28)
(g91 z-22)
(g91 g1 x6 f100)
(f#<move_speed>)
g90 x0 y0 z35
0106 endrepeat
0107 else
(MSG, You would have crashed! Do not set correction z lower than 0!)
0107 endif
0108 else
(MSG, You would have crashed! Do not set correction x lower than 0!)
0108 endif
0109 else
(MSG, You would have crashed! Do not set correction y lower than 0!)
0109 endif
%
```

11.2 Phase Angle Measurements of the Different Sensors

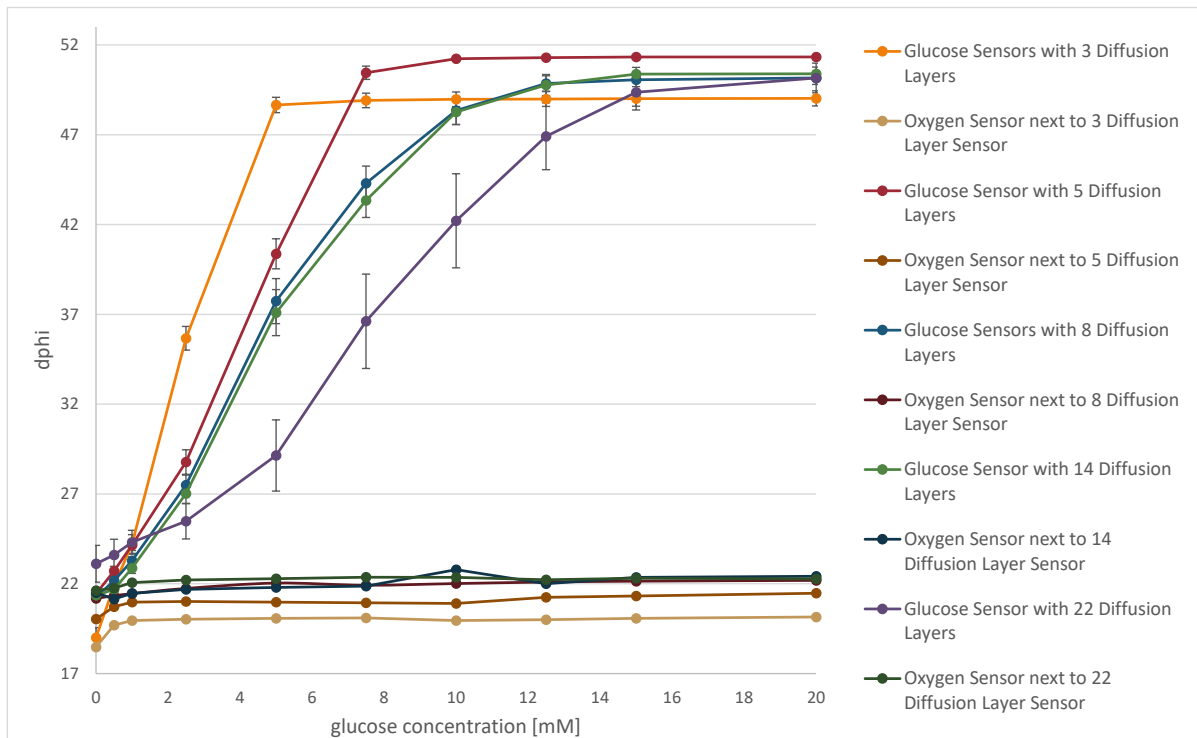


Figure 11.1: Measured $d\phi$ Values of Sensors with PolyHEMA as Diffusion Barrier Layer and Different Amount of Layers

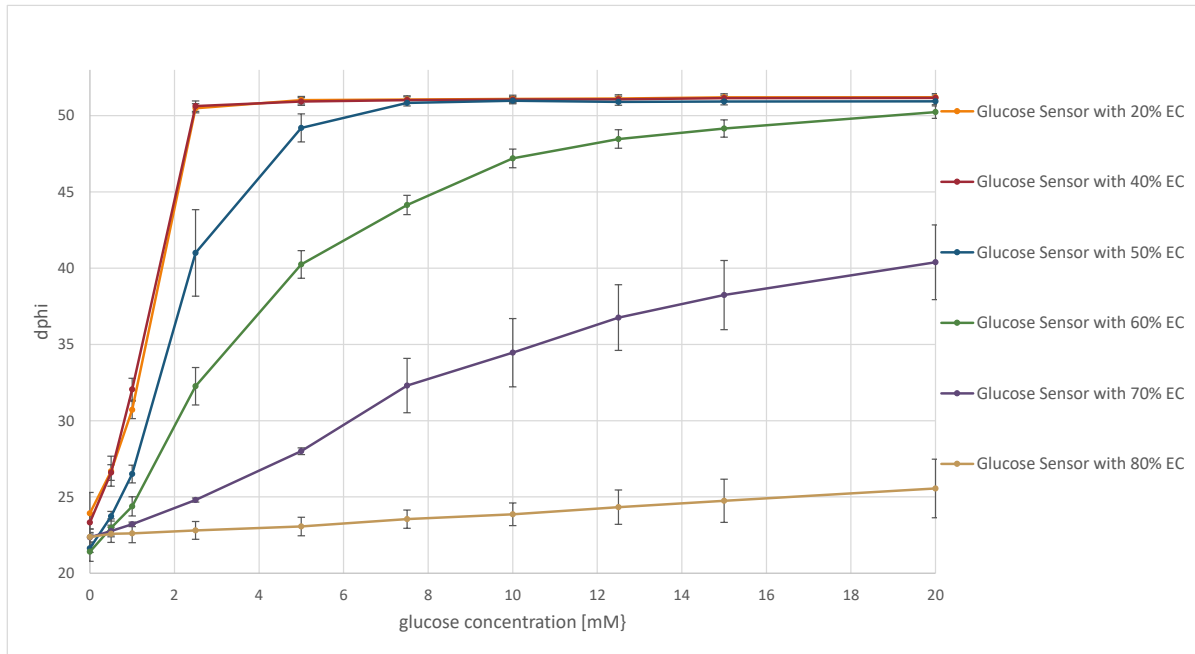


Figure 11.2: Measured dphi Values of Sensors with Different Amount of Ethylcellulose in the Diffusion Barrier Layer

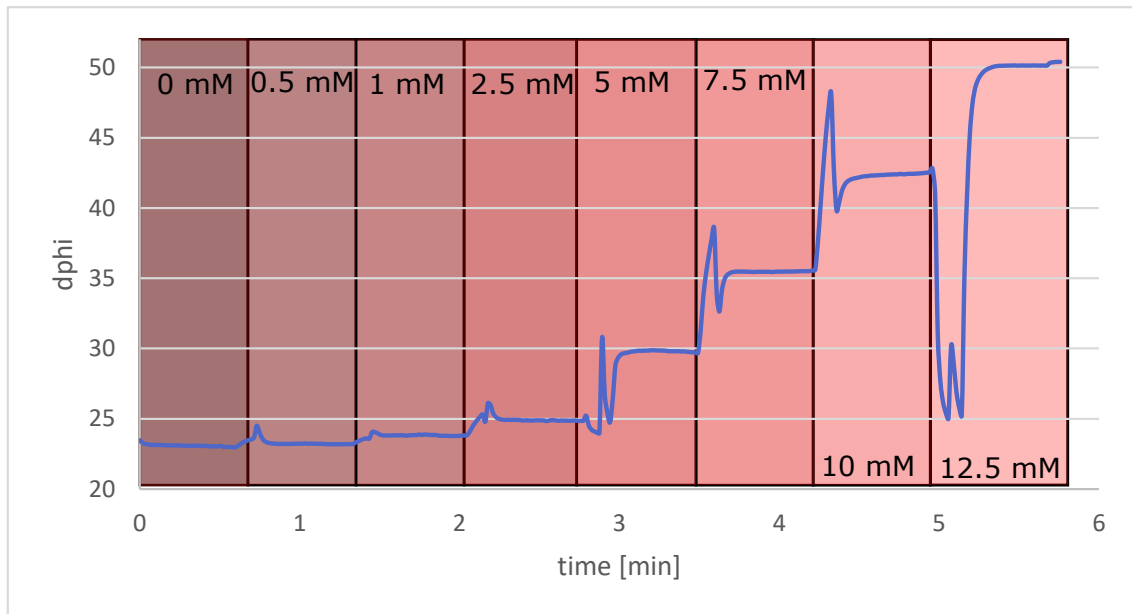


Figure 11.3: Measuring Curve of a Sensor

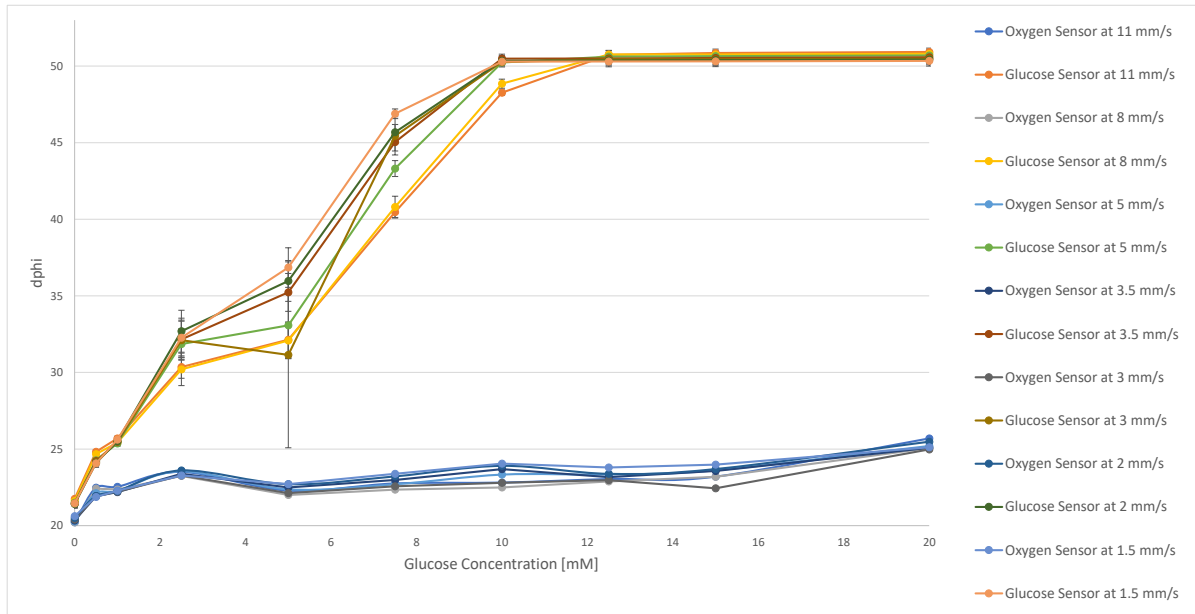


Figure 11.4: Sensor with PolyHEMA as Diffusion Barrier Layer Measured at Different Flow Velocities in a 250 μ L Rhombic Chamber Chip

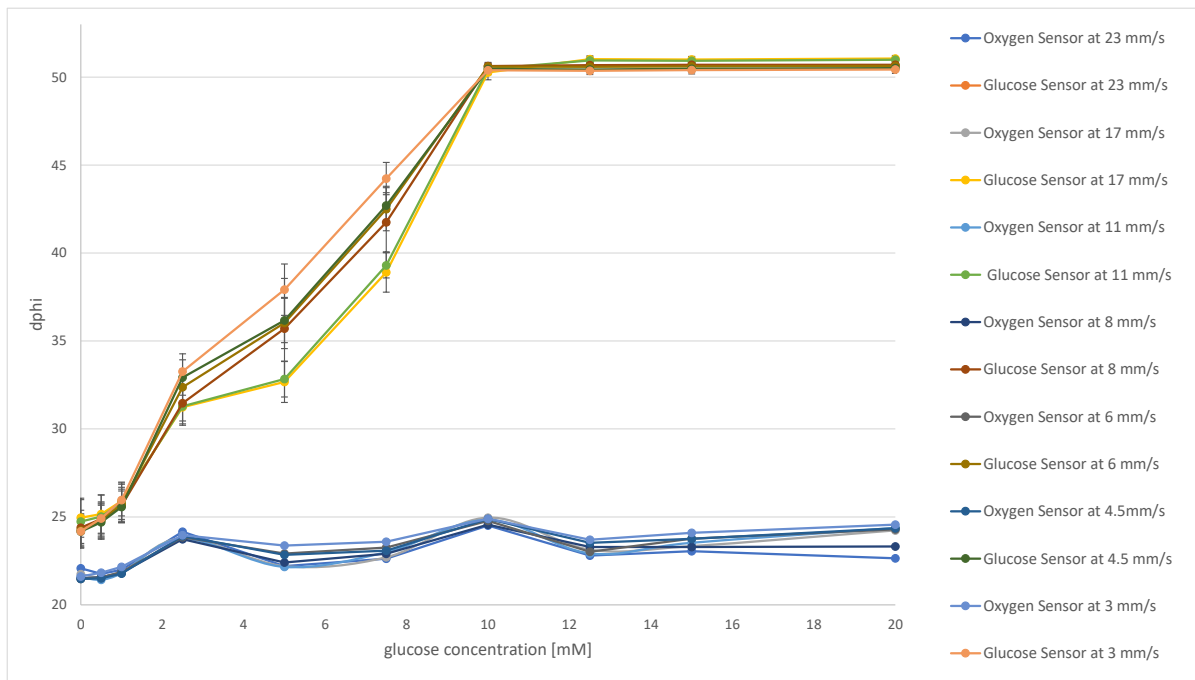


Figure 11.5: Sensor with PolyHEMA as Diffusion Barrier Layer Measured at Different Flow Velocities in a 120 μ L Rhombic Chamber Chip

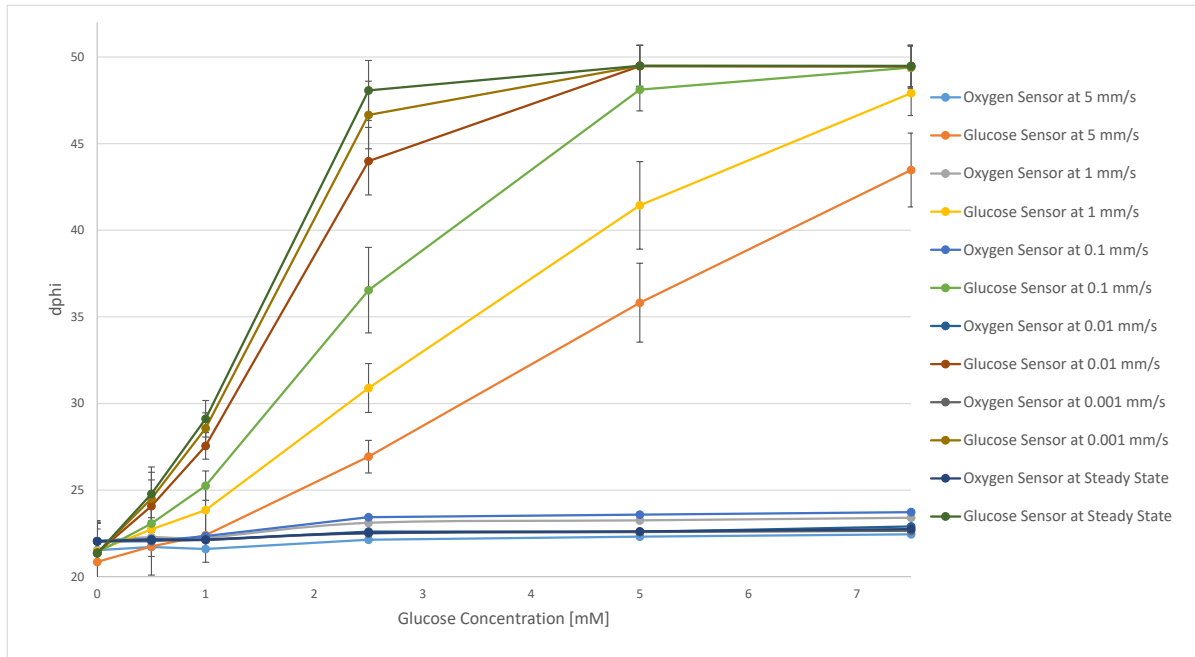


Figure 11.6: Sensor with PolyHEMA as Diffusion Barrier Layer Measured at Different Flow Velocities in a 250 μL Rhombic Chamber Chip

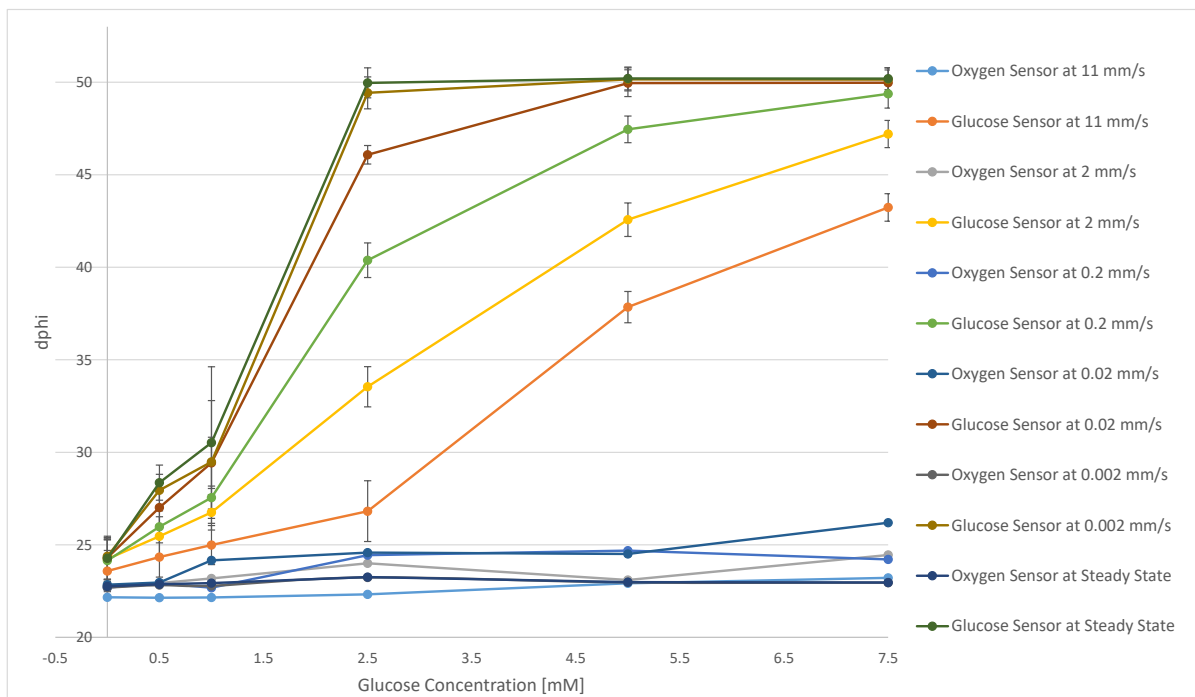


Figure 11.7: Sensor with PolyHEMA as Diffusion Barrier Layer Measured at Different Flow Velocities in a 120 μL Rhombic Chamber Chip

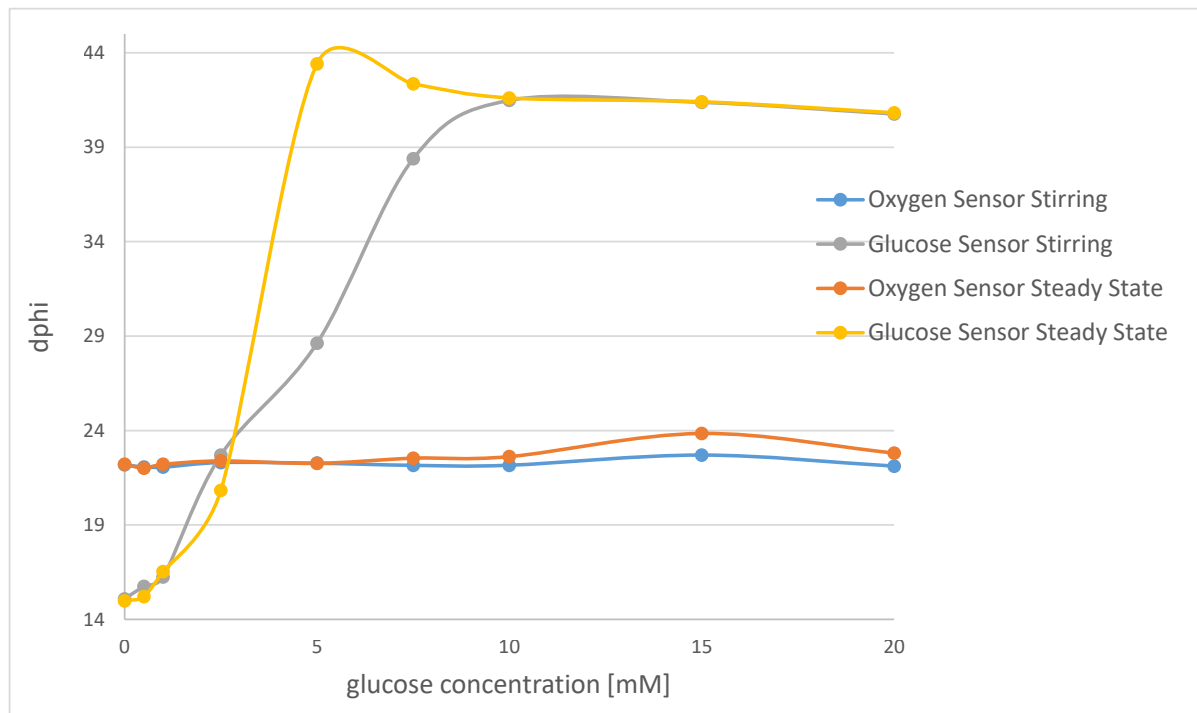


Figure 11.8: Measurement of Sensors in Higher Volumes